◉ NTNU

Norwegian University of Science and Technology

Bachelor Thesis
Project number: 70341108

Utilizing a liquid aluminium bath to recycle Waste Electric and Electronic Equipment while up-concentrating/recovering rare earth elements. Fundamental testing.

Resirkulere elektrisk og elektronisk avfall med flytende aluminium og oppkonsentrere/gjennvinne sjeldne jordartsmetaller. Fundementale forsøk

---

Author:
Eystein Vada
Eskil Christensen

Supervisor:
Dr. Robert Fritzsch
Prof. Ragnhild E. Aune

May 19, 2019

Abstract

Electric and Electronic Equipment (EEE) has changed the world. A rapid development of technology and increasing wealth makes the obsoletion of EEE faster than before. This has lead to a dramatic increase in Waste Electric and Electronic Equipment (WEEE). In 2021 it is estimated that 52.2 million tonnes of WEEE will be produced. WEEE is today the fastest growing waste stream, and if it is not handled properly, it is hazardous to the environment.

Rare Earth Elements (REEs) are a group of elements vital for the function of electronics. One of the REEs, neodymium (Nd), is extensively used in NdFeB magnets contained in speakers, electric motors and wind turbines, to name a few. There is no lack of Nd in the earth's crust, but as the richest ores deplete, the environmental impact and price of REEs increases. The focus of this thesis is to give a better understanding of the problems and possibilities, regarding the recovery of Nd from WEEE.

A literature study has been conducted, and the main processes of recycling WEEE today, pyro- and hydrometallurgy, have been investigated with regards to REEs. The study shows that REEs are generally not recycled. Many processes are able to separate and recover REEs, but they have not yet been implemented. Mechanical processes are used as a part of the recycling process, to separate metallic from non-metallic fractions. Mechanical processes can be labour intensive and inefficient in terms of recovery rate. In pyrometallurgy, very few processes can recover REEs in their metallic forms, but rather as oxides. An energy intensive process in then needed to reduce the Rare Earth Oxides. Hydrometallurgy dissolves metals and then separates them by precipitation. The chemical reagents can have a big environmental impact and have a considerable cost.

Experiments conducted in this thesis investigates the possibility of utilizing a liquid aluminium bath to recycle WEEE while up-concentrating/recovering REEs. Smartphones, Printed Circuit Boards (PCBs) and NdFeB magnets have been submerged in aluminium, and the results have been analyzed in regards to Nd concentration present in different phases. The phase observed with the highest Nd concentration was found to have close to 20 mol% Nd. This was achieved by submerging NdFeB magnets for 36 minutes at 770 °C with a total concentration of 5 mol% Nd in the system. From the experiment using smartphones, a phase containing 2.40 mol% Nd has been observed, which is higher than the concentration of Nd in the system. Experiments using PCBs has shown that the glass fiber found in some PCBs can pose a problem, as it hinders more PCBs to be added to the melt.

Sammendrag

Elektriske og elektroniske apparater har forandret hvordan vi lever. På grunn av en rask teknologisk utvikling og økende økonomisk handelekraft hos forbrukere, har levetiden til elektronikk og elektroniske apparater blitt betraktelig kortere. Dette har ført til at elektrisk og elektronisk avfall har blitt den raskest voksende avfallstypen i verden. I 2021 er det forventet at verden vil produsere 52.2 millioner tonn med elektrisk og elektronisk avfall. Elektrisk og elektronisk avfall kan forurense miljøet dersom det ikke blir tatt hånd om på en forsvarlig måte.

Sjeldne jordarter er en gruppe grunnstoffer som har blitt en viktig del av vår hverdag, i form av økt bruk i ny teknologi. En av de mest brukte sjeldne jordartene er neodym (Nd). Neodym er brukt i permanente magneter, som er essensielle for blant annet høytalere, elektriske motorer og vindturbiner, for å nevne noen bruksområder. Forekomsten av Nd i jordskorpen er relativt høy, men på grunn av at metallet ikke finnes lokalt i høye konsentrasjoner blir det utvunnet som et biprodukt av andre metaller. Denne studien vil prøve å gi en bedre forståelse av problemer og muligheter knyttet til gjenvinning av Nd fra elektronisk avfall.

Det er gjort en litteraturestudie på prosesser brukt til resirkulering av elektronisk avfall. Av disse er pyrometallurgi, hydrometallurgi og mekaniske metoder de mest brukte i dag. Sjeldne jordarter blir i dag stort sett ikke resirkulert, selv om mange av prosessene tillater dette. Mekaniske prosesser blir brukt til å pulverisere elektrisk avfall for så å skille metaller fra ikke-metaller. Mekaniske prosesser blir ofte benyttet som det første steget i pyro- og hydrometallurgi. Pyrometalliske prosesser bruker varme og mye energi til å gjennvinne de sjeldne jordartsmetallene. Selv om pyrometalliske prosesser bruker mye energi på å gjennvinne de sjeldne jordartsmetallene, er dette som regel som oksider. Å redusere oksidene til metaller er en energikrevende prosess. Hydrometallurgi bruker kjemikalier til å løse opp metaller fra elektronisk avfall og å separere de ved hjelpe av utfelling. Kjemikaliene brukt i hydrometallurgi kan ha en negativ effekt på miljøet og de er kostbare.

I oppgaven er det utført forsøk på å resirkulere elektrisk og elektronisk avfall med flytende aluminium (Al), og å oppkonsentrere/gjennvinne sjeldne jordartsmetaller. Smarttelefoner, kretskort og permanente magneter har blitt løst i flytende Al og resultatet har blitt analysert. En fase ble oppkonsentrert til 20 mol%, fra smeltens totale Nd-konsentrasjon på 5 mol%. Dette ble oppnådd etter 36 minutter ved 770 °C. En fase på 2.40 mol% Nd ble funnet når seks smarttelefoner ble løst i Al. Dette er er en oppkonsentrering av Nd fra smeltens totale Nd-konsentrasjon. Glassfiber kan gjøre resirkuleringen av kretskort vanskelig, da glassfiberen flyter på aluminiumsoverflaten og hindrer videre tilsatts av kretskort.

Preface

You are about to read "Utilizing a liquid aluminium bath to recycle waste electric and electronic equipment while up-concentrating/recovering are earth elements. Fundamental testing". This thesis gives an overview of methods used for recycling of Waste electric and electronic equipment with focus on rare earth elements. It also contains an experimental part where liquid aluminium is used to up-concentrate rare earth elements from neodymium magnets and waste electric and electronic equipment.

The reasons for choosing this as our bachelor thesis comes from several places. The generation of waste electric and electronic equipment is a dawning problem that society has not focused on solving. It is clear to us that the world's growing need for materials can not be sustained by the mining of new materials. Both the generation of waste products, and the need for more materials is rising. How will this problem be solved?

The thesis was written to fulfill the graduation requirements of a bachelor's degree in materials technology at The Norwegian University of Science and Technology (NTNU). We have been engaged in researching and writing this thesis from January to May 2019. Our research question was formulated together with our supervisors, Dr. Robert Fritzsch and Prof. Ragnhild E. Aune. The research has been difficult, but extensive work on the topic has allowed us to answer that question. Both our supervisors, Dr. Robert Fritzsch and Prof. Ragnhild E. Aune, has been available and very helpful in this work.

A popular science article was written to fulfill the requirements of the bachelor thesis, the article is available in appendix K.

Eystein Vada	Eskil Christensen
May 19, 2019	May 19, 2019
Trondheim, Norway	Trondheim, Norway

Contents

1   Introduction

Waste Electrical and Electronic Equipment (WEEE) and e-waste are the two most frequently used terms for discarded Electronic and Electronic Equipment (EEE). WEEE can be made out of over 1000 different materials and substances [1], and the variation in the composition makes it difficult to recycle. The materials and substances in WEEE can be separated into three main groups; metals, ceramics and organic materials. Drastic technological advancements over a short period of time along with increased wealth, giving people the opportunity to upgrade and buy the newest electronics, has made WEEE the fastest-growing waste stream in the world. In 2016 the world produced 44,7 million tonnes of WEEE, this is expected to rise to 52,2 million tonnes by 2021, Figure 1. One of the problems regarding WEEE, is that it has not received the attention it deserves. Only 41 countries have an official e-waste statistics as of 2017, meaning that approximately only 20 % of the worlds WEEE are documented to be collected and recycled [2].
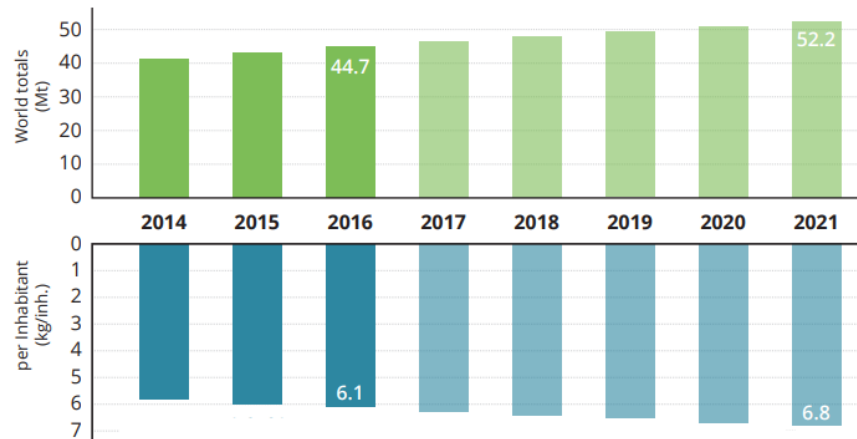
Figure 1: *Production of WEEE in the world from 2014 to 2021. Values for 2017-2021 are estimates [2]*

In the mid-1990s more than 90% of WEEE was landfilled, incinerated or recovered without pre-treatment [3]. Today it is known that WEEE pollutes ground water, acidifies the soil, generates toxic fumes and gases, if incinerated, and releases carcinogenic substances into the air [4]. The favoured option is to reduce the amount of WEEE produced, which ends up in the waste chain. Nevertheless, as the world's technological demand grows, the EEE waste-stream also grows. One way to reduce the WEEE produced and still satisfy the demand for EEE is to minimize the resources in every component, which is an easy answer that is difficult to accomplish. The more realistic, but less favored option is to increase the lifetime, reuse and/or recycle WEEE. Recycling is not the ideal way to handle WEEE, but because of the significant technological improvements, the reuse of old electronics is a challenge. Burning of WEEE for energy recovery and disposal at landfills is the least favorable way to handle WEEE [4].

Some of today's recycling of WEEE happens due to laws prohibiting disposal of WEEE at landfills in developed countries. This is quite contrary to less developed countries, where the lack of laws governing waste disposal enables informal handling of WEEE. In less developed countries the value of the materials and components recycled exceeds the labor expenses of disassembling the WEEE. While informal recycling is not considered proper handling of WEEE, it at least enables reuse of components and recycling of some materials [5]. While some of today's recycling is done due to laws probithing disposal, WEEE is mainly recycled for economic reasons, recovering the precious metals (PMs) such as as gold (Au) silver (Ag), platinum (Pt), and palladium (Pd), mainly found in the Printed Circuit Boards (PCBs). Precious metals can make out as much as 80% of the value of the materials in PCBs from computers and smartphones, and 50% of PCBs from TVs and DVD-players [6]. Rare Earth Elements (REEs) contributes only to a small part of the material value, due to the small quantities used in PCBs. PCBs contribute to the total amount of WEEE with only 3-5 wt%. PCBs contain a large amount of engineering plastics, if recycled, will add a higher economic and environmental value to the process [7]. Different PCBs can use different laminates. PCBs marked with FR2,

1

FR stands for Flame retardant, uses paper reinforced resin where as FR4 uses glass fiber reinforced resin [8]. Most of the used extraction processes applied today require crushed PCBs to extract the Precious Metals (PMs), as this is the most economic profitable operation. PCBs can contain different toxic elements, such as flame retardants and heavy metals. The Flame Retardants (FR) can generate toxic substances at high temperatures, which is a challenging part of using pyrometallurgical methods to recycle the PCBs. The heavy metals lead (Pb), chromium (Cr), mercury (Hg), arsenic (As) and cadmium (Cd) exhibits significant effects on humans, such as reduced birth weight, lung function and other health issues[9].

In industry, different metallurgical processes are used to recover metals from PCBs. Commonly used processes for this can be summarized as the pyrometallurgical and hydrometallurgical routes. Both of these routes have their advantages and disadvantages. Significant amounts of research on the recycling of WEEE and mainly PCBs has been accomplished in the recent years. Some of this research is trying to improve already existing processes,including their different stages, while some are trying to invent new processes.

REEs are a group of elements defined by International Union of Pure and Applied Chemistry (IUPAC) as yttrium (Y), scandium (Sc) and the 15 lanthanides; lanthanum (La), cerium (Ce), praseodymium (Pr), neodymium (Nd), promethium (Pm), samarium (Sm), europium (Eu), gadolinium (Gd), terbium (Tb), dysprosium (Dy), holmium (Ho), erbium (Er), thulium (Tm), ytterbyium (Yb) and lutetium (Lu) [10]. Despite the name, there are many elements which are less abundant in the earth's crust. For example, the platinum group metals (PGMs) are much rarer in terms of how many parts per million (ppm) that occurs in the earth's crust [11]. The rarity of the REEs comes from their tendency to be finely dispersed in the earth's crust, and are only found in ores with low concentration. Unlike the rarer PGMs, which tends to be located at concentrated deposits at very few locations. Therefore, REEs are mainly mined as a coproduct of other metals. Production of heavy Rare Earth Oxides (REOs) is found to consume over 20 times more primary energy compared to steel, and further processing from REO into REE will increase the energy consumption even more [12]. Less than 1 % of end of life REEs are recycled [13], and the price for some of the REEs are expected to have an annual price increase of up to 15%, due to the increasing demand and supply-shortage [7]. One of the most used REE is Nd which is used for it's magnetic abilities to create permanent magnets.

Permanent magnets are materials used to generate a magnetic field without the need for electric power. This makes them a key material in high performance, minimization and high efficiency of appliances and electronic apparatuses[14]. High performance magnets are replacing electromagnets and therefore the demand for high performance magnets are expected to increase in the future. Permanent magnets can be divided into two groups, REE permanent magnets, like NdFeB magnets and non-REE permanent magnets, like ferrites and Fe-Ni[15].

It is estimated that 35% of NdFeB magnets are used in computers, 25% in audio systems, 15% in wind turbines, 15% in automobiles, 5% in household appliances and 5% for MRI machines[16]. NdFeB magnets from wind turbines, MRI machines and automobiles are easily recycled, because of their large size they are easily separated. NdFeB magnets in computers, audio systems and household appliances are difficult to extract, caused by the small amounts used in each product and it's complex assemble. To reduce the oxidation of NdFeB magnets there are added numerous dopant elements and a coating [17].

Globally, solid waste management costs are estimated to increase from 205.4 billion dollars annually in 2016 to 375.5 billion dollars in 2025 [18]. One way to reduce the cost is to recycle more of the solid waste, where WEEE is the fastest-growing waste stream. Recycling of solid waste is by some referred to as urban mining [19], [20], [21]. The concept of urban mining concerns all the activities and processes in the recycling of materials, energy and components from products, buildings, infrastructure and, in particular, waste [19]. Most of the PMs and REEs in urban mines are found in WEEE and waste catalysts [9], making recycling of WEEE a good source for PMs and REEs. In some waste streams the concentration of REEs, and some PMs, are higher than in their primary ores. Therefore, WEEE represents an opportunity as secondary ores with a high recovery value [19], [22]. Mining rates are at a historical maximum for most metals, but the average ore grade has decreased [23]. The decreasing ore grade can lead to an imbalance between supply and demand, making today's practice unsustainable and increasing the importance of metal recovery.

2   Objective

The general objective in the present work is to gather information about the processes concerning the recycling of WEEE, as well as the possibilities to utilize a liquid aluminium bath to recover neodymium from WEEE.

The project specific objectives are:

- To identify the difficulties in utilizing an aluminium bath to melt/recycle WEEE.

- To examine what happens to PCBs and smartphones when submerged in molten aluminium.

- To examine the effect of an electromagnetic field on the submersion of PCBs in molten aluminium.

- To investigate the possibility of selective phase separation in regards to Nd.

3   Background

This chapter presents methods and processes used for today's recycling of WEEE and will also include some novel techniques.

3.1   Mechanical Methods

Different mechanical methods are used to separate WEEE into their components. Some of which includes desoldering, disassembling and shredding [24]. There are different approaches for the disassembling of WEEE. Either a selective approach, where WEEE is disassembled into it's components for re-use, or a simultaneous disassembly, where all the parts are disassembled simultaneously by heat to remove the soldering [25]. With simultaneous disassembly, there is a risk that the components will no longer function as intended. However, both simultaneous and selective dissasembly will make it easier to separate components containing hazardous or precious materials [24].

3.1.1   Communition

Crushing and shredding, also known as communition, is done to liberate the metallic fraction from the non-metallic fraction in PCBs, to prepare for further metallurgical processes. Communition is traditionally done with a low speed and high torque shear shredder [26]. It can also be done by using a swing hammer mill [27].

While being deemed necessary to process PCBs, the loss of material during communition is substantial, with up to 40% of the PMs are lost. In addition to this, dangerous particles, gasses, small particles of different metallic elements, Bromine Flame Retardants (BFR) and dioxins are released [4].

3.1.2   Separation Methods

To further separate metallic fractions from one another and from non-metallic fractions, techniques that exploit certain material traits are used. Different fractions have different density, electric and magnetic properties. In WEEE different fractions can consist of polymers ($< 2,0 g/cm^3$), light metals ($\sim 2,7 g/cm^3$), glass ($\sim 2,6 g/cm^3$) and heavy metals ($> 7 g/cm^3$). These fractions can be separated by the use of gravity separation methods. There are several methods used for gravity separation, all of which exploit the different densities of the fractions.

Separation of ferromagnetic metals from non-ferromagnetic metals can be done by magnetic separation [28]. The attractive magnetic forces are different for ferromagnetic and non-ferromagnetic metals, making it possible to separate the two fractions by balancing attractive magnetic forces with gravitational, frictional or inertial forces.

A common method for separating materials is by the use of the differences in electric conductivity. There are different techniques to do this, such as corona-electrostatic separation, triboelectric separation and by using eddy currents.

The roll-type corona-electrostatic separator is a commonly used machine for separating metals and plastics from WEEE. A grounded rotating roll electrode and other active electrodes are connected to a DC high voltage supply. The granular mixture is fed on the surface of the rotating roll at a certain speed and pass through the electric field that generates between the roll electrode and active electrodes. After an intense ion bombardment, non-conductive particles are charged and pinned to the surface of the rotating roll electrode by the electric image force while the conductive particles are charged by electrostatic induction and are attracted towards the electrostatic electrode [29].

The triboelectric separator consists of two electrodes, one of them being grounded. The voltage of the other electrode is in the order of 10^4 V. The electrodes may be covered by insulating material that prevents the particles from recharging in case of direct contact with the electrodes. At the bottom of the device there are several recycle bins used for collecting the different fractions [30].

Eddy currents uses electromagnetic forces to separate metals from non-metals. A voltage is induced in a conductor if it is subjected to a time-varying magnetic flux. This results in currents flowing in the conductor, called Eddy currents. Eddy currents will produce magnetic forces between any conducting material and the magnet producing this current. This is used to separate metals from non-metals [31].

3.1.3   Separation of Rare Earth Elements by Mechanical Methods

One example from the WEEE recycling industry used a two-step communition process to obtain a particle size of $< 20mm$. Ferrous fractions were separated using magnetic separation. The non-ferrous fraction were further separated using sieves, flotation and electrostatic separation. This resulted in 5 fractions:

- 1) Ferrous scrap, 50 wt%, destined for material recovery.

- 2) Dust fraction, 5-8 wt%, destined for landfill.

- 3) Plastic materials, 30-35 wt%, destined for incineration

- 4) Copper grains, 3.5-6 wt%, destined for further refining.

- 5) Aluminium grains, 2.5-4 wt%, destined for further refining

Researchers studied the last four fractions more closely and found that almost all of the REEs are accumulated in the dust, a fraction that ends up in a landfill. In addition to what is lost in the dust fraction, Figure 2 shows that almost all of the remaining REEs are accumulated in the plastic fraction, which is incinerated and not refined further [32].
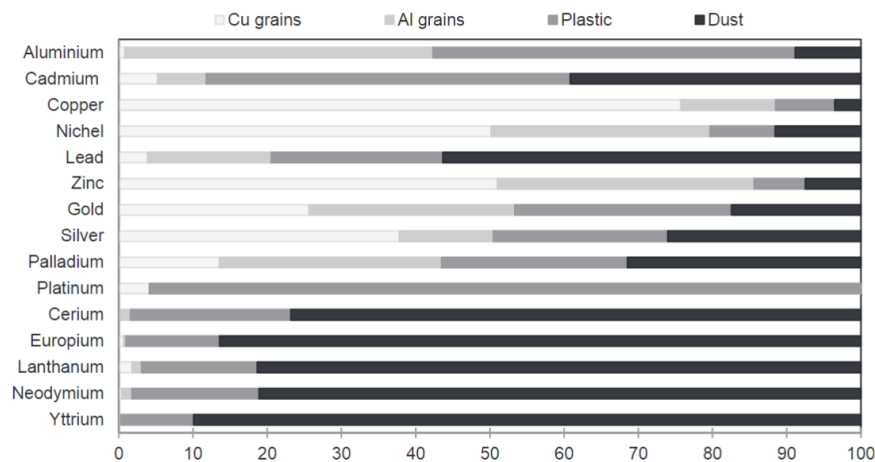
Figure 2: *Which fraction of the mechanically separated WEEE different elements accumulated. All fractions except from ferrous scrap is represented here [32].*

Along with losing close to 100% of the REEs in the communition process much of the PMs are also lost in this process. Most of the Nd comes from NdFeB magnets which are brittle, when the magnets are shredded they will tend to convert into small particles and dust [33]. Other studies have also found high losses of REEs and PMs, one study conducted by Bacher *et al.* [34], on mobile phones, found that communition lost 60% Au, 80% Pd and over 70% of Nd when compared to hand dismantling. One recycling plant in Belgium (Aparec) focusing on End of Life (EOL) LCD-TVs lost 74% of Au content of PCBs. A similar plant in Japan (Hitachi) lost only 10% Au. One of the differences between these recycling plants is that in Japan the PCB was dismantled from the TVs before communition, due to Japanese legislation[35].

Duan *et al.* reported a method using a hammer mill with a water medium to crush PCBs and a gravity separator to separate the metal. This process generated a metallic concentrate of 92.36 % and a metal recovery of 97.12 % [36]. The study does not mention which metals were recovered, but with a high metal recovery rate and water as medium, less was lost to the dust fraction.

3.2 Pyrometallurgy

3.2.1 Fundamental Understanding of Pyrometallurgical Methods

Pyrometallurgical methods such as incineration, smelting in plasma arc furnace or blast furnace, melting, drossing, sintering and high temperature gas phase reactions are used in different steps of WEEE recycling. Pyrometallurgical processes require energy in the form of heat, usually by combustion or electrical heating. [37].

Incineration is the process of combustion of organic materials. This is done partially to reduce both volume and mass of the waste and to recover energy from high calorific waste [38]. For WEEE, there are two ways the concept of incineration can be applied.

- Low-tech process utilizing open combustion

Essentially an uncontrolled process with the intention to recover valuable metals from the waste. An example is power cables, which are burned to remove the insulation and facilitate the recovery of copper. PCBs are burned to liberate the metal rich electronic components (ECs), which releases toxins [39], [40].

- Temperature controlled incineration

PCBs start burning at relatively low temperatures (400°C). Nevertheless, due to release of CO the temperature should be kept above 800°C [41]. At a pilot-scale incinerator in China, the remnants of disassembled PCBs were burned at 800°C and then the gas from the burning was treated at 1100°C. In this experiment most of the metal was enriched in the residue, but not all of it [42].

Smelting is the process used to convert ores into metals. Different chemicals are used as reducing agents, however in the case of WEEE recycling, the plastic components of the WEEE, such as PCBs, casings and insulation, are rich in carbon and can be utilized as a reducing agent, as is done at Umicore's smelter in Hoboken, Belgium [43]. The most common reducing agent used in industry is coke, which is almost pure carbon. The reduction of metal oxide with carbon is shown in reactions (Rx.1) and (Rx.2)

$$MO + C \rightleftharpoons M + CO \tag{Rx.1}$$

$$MO + CO \rightleftharpoons M + CO_2 \tag{Rx.2}$$

In reaction (Rx.1) and (Rx.2) M is a metal and MO is the metal oxide. In these reactions metal oxide is reduced into its metallic form, by use of carbon as the reducing agent. Reaction (Rx.2) can be broken down into reaction (Rx.3) and (Rx.4)

$$MO \rightleftharpoons M + \frac{1}{2}O_2 \tag{Rx.3}$$

$$\frac{1}{2}O_2 + C \rightleftharpoons CO \tag{Rx.4}$$

Not all reactions are spontaneous and some requires energy. The energy required can be calculated using Gibbs equation, (1). Where $\Delta G°$ is the change in Gibbs free energy, $\Delta H°$ is the change in enthalpy, T is temperature in kelvin and $\Delta S°$ is the change in entropy.

$$\Delta G° = \Delta H° - T\Delta S° \tag{1}$$

In ordinary environmental temperatures $\Delta G°$ for reaction (Rx.3) is always positive, meaning the reaction requires energy. ΔG °for reaction (Rx.4) will always be negative, thus a spontaneous reaction. The energy released from reaction (Rx.4) may not be sufficient to drive reaction (Rx.3) at low temperatures [44]. The energy required for reduction to metallic state differs between elements and is also temperature dependant, as shown in Table (1).

A comprehensive diagram showing the stability of compounds over different temperatures was introduced by Harold Ellingham in 1944. Figure 3 shows an Ellingham diagram for some elements.

Table 1: *Changes in Gibbs free energy for reduction of some selected metals and oxidation of carbon at 298K and 2000K*

Reaction	$\Delta G°(298K)[kJmol^{-1}]$	$\Delta G°(2000K)\ [kJmol^{-1}]$
$\frac{2}{3}Al_2O_3 \rightarrow \frac{4}{3}Al + O_2$	+1054	+691
$2MgO \rightarrow 2Mg + O_2$	+1138	+643
$\frac{2}{3}Fe_2O_3 \rightarrow \frac{4}{3}Fe + O_2$	+744	+314
$SnO_2 \rightarrow Sn + O_2$	+520	+42
$2HgO \rightarrow 2Hg + O_2$	+118	-381
$2Ag_2O \rightarrow 4Ag + O_2$	+22	-331
	Formation of CO_2	
$C(s) + O_2(g) \rightarrow CO_2(g)$	-394	-396
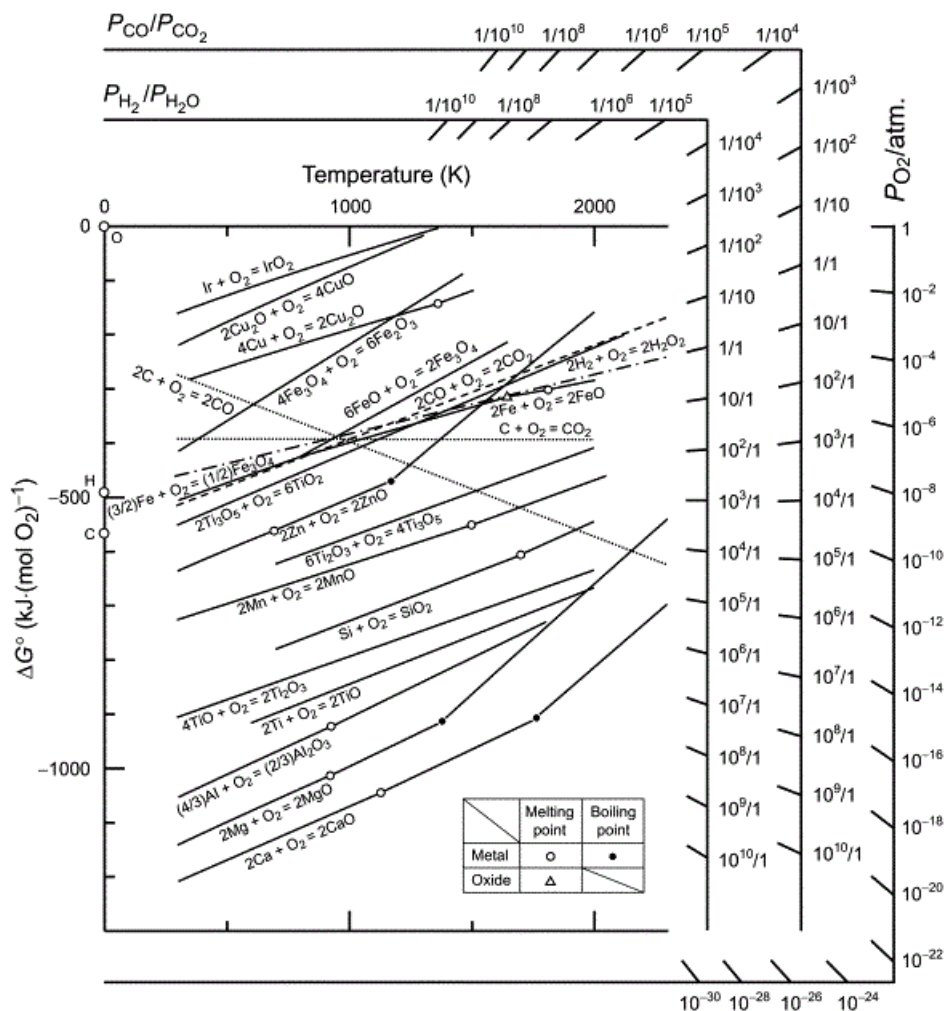
Figure 3: *Ellingham diagram, with change in Gibbs free energy as a function of temperature for some elements [45]*

The Ellingham diagram is helpful to understand the equilibrium in heterogeneous systems including metal, its oxide, and gas phase. As can be seen from from figure 3, for some elements coke is sufficient as reducing agent at low temperatures, but for iron (Fe) the temperature needed is about 900 °C. Other metals require different reducing agents.

3.2.2   Methods for the Separation of Rare Earth Elements from NdFeB Magnets

This chapter has until now discussed general methods for WEEE recycling, and the rest will contain pyro-metallurgical methods especially used to separate REEs from NdFeB magnets contained in WEEE. Some possible routes within pyro-metallurgical REE recyling of NdFeB magnets are suggested and can be divided into 5 groups [46]:

- 1. Roasting processes

- 2. Liquid metal extraction

- 3. Molten salt extraction

- 4. Molten slag extraction

- 5. Direct melting

3.2.3   Roasting

The general aim of roasting is to change the state or form of REEs so that they can be more effectively dissolved using hydrometallurgy. A commonly used roasting process is oxide roasting. Oxide roasting converts all metallic compounds into it's oxide form, which can then be treated by hydrometallurgical leaching processes. The reason for using oxide roasting is to make the leaching process faster or more selective [47].

One suggested method is chlorination roasting. This process uses molten metal halides, such as magnesium chloride ($MgCl_2$), ammonium chloride (NH_4Cl) or chlorine (Cl_2) to chlorinate the REEs at high temperatures creating rare earth chlorides ($RE - Cl_3$). The formed $RE - Cl_3$ can then be separated from the Fe residue in the magnets by high temperature distillation [48].

During sulfide roasting the aim is to react only the REEs with sulfates and leave Fe and metals as water insoluble oxide. The magnetic material is dissolved using sulfuric acid (H_2SO_4). The resulting mixture is then heated to a temperature where the rare earth sulfates ($RE - SO_4$) are thermally stable but the iron sulfide $FeSO_4$ is not. $FeSO_4$ will then decompose into iron oxide (Fe_2O_3), which is less soluble in the solution and will fall out as solid particles [49].

3.2.4   Liquid Metal Extraction

Some options for the recovery of REEs from NdFeB magnets have been identified by the use of molten metal extraction [50]. In general this technique uses different metals in their liquid state to extrac Nd by diffusion. Research has shown that Magnesium (Mg) and possibly the other alkaline earth metals calcium (Ca) and Barium (Ba) can do this [51]. Using Mg as an extractant, Mg-REE alloys will form, leaving Fe and boron (B) unreacted in its solid state. The Mg can then be separated from the REEs by distillation, as Mg is more volatile than Nd. At 1300 K Nd has a vapor pressure of 10^{-6} atm while Mg has 0.73 atm [50]. This method has shown it's best results with a holding time of up to 72 hours, therefore it is considered slow. Under optimal conditions an extraction rate of 99 % was achieved [50]. However, the optimal conditions require a greater amount of Mg, as is seen in Figure 4.

Ag can also be used in a similar fashion. With Ag as the extractant Takeda et. al [52] reported a Ag-Nd alloy containing about 50 mass% Nd in a temperature range of 1000-1300 °C using a mixture from NdFeB magnets. Nd could then be separated from Ag by oxidizing the melt with air. Neodymium oxide (Nd_2O_3) would form and separate from the Ag, which stayed liquid. This yielded a 90 % extraction of Nd from the magnet scrap. One problem this study encountered was the wettability of Ag with Nd_2O_3 , which made it harder to separate Nd from Ag.
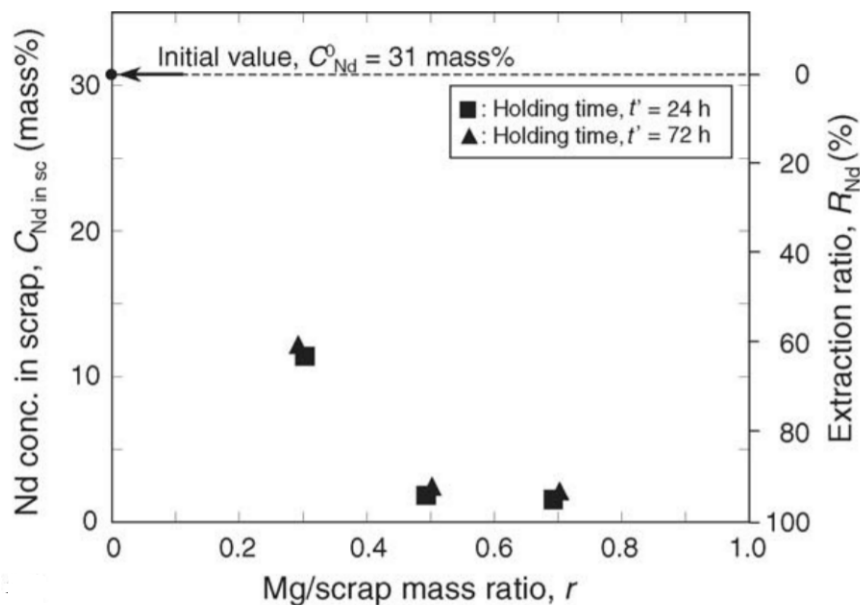
Figure 4: *The extraction rate of Nd improves with increasing Mg to scrap ratio. The initial value of Nd concentration in scrap is the concentration of Nd in the NdFeB magnets used in this specific trial* [50]

.

3.2.5   Molten Salt Extraction

Another study conducted by Hua *et al.* [53] reported a process using molten chloride salts ($MgCl_2 - KCl$) to selectively dissolve REEs from magnet scraps, leaving both the Fe and B. A recovery rate of 90 % was observed at temperature ranges from 700-1000 °C. $RECl_3$ would form and could then together with the salt mixture be processed by electrolysis to a Mg-Nd alloy. The Mg-Nd alloy can be used in a distillation processes similar to the one discussed in subsubsection 3.2.4.

Hua et. al [53] also suggested a method for recovering REOs by use of fluorides. The idea is to recover the REOs from the magnet, using molten fluorides. Molten fluorides will react with the REOs and form RE-fluorides (REF_3). REF_3 can then be used in molten salt electrolysis, to form REE. The non-oxidized NdFeB magnet scrap can then be used to create new magnets.

3.2.6   Molten Slag Extraction

Two methods using slag as a measure of extraction have been reported by Yang et. al [46]. In the glass slag method boron oxide (B_2O_3) was used to selectively oxidize and dissolve the REEs found in NdFeB magnets to form $Nd_2O_3 - B_2O_3$ slag. The slag can then be leached using hydrometallurgical methods to separate Nd as neodymium hydroxide ($Nd(OH)_3$). The study of this possibility showed that glass slag extraction of Nd using B_2O_3 is possible, but that the extraction of Nd from the slag was at the time not economically viable.

The other proposed method is with $CaO - SiO_2 - Al_2O_3$ or $CaO - CaF_2$ fluxes to extract the REEs from from the magnet scrap at 1500 °C. This process enables the separation of a phase with a high concentration of REEs and a phase with a high concentration of Fe, and shows a recovery rate of 99 %. The REEs are concentrated in the slag and needs to be hydrometallurgically treated. The Fe-rich phase can be utilized as scrap in steelmaking.

3.2.7   Direct Melting

In a study conducted by Jakobsson et. al [54], REE-rich ferrous scrap, containing 6500 ppm Nd, was directly melted to see if REEs from NdFeB magnets could be collected as REOs. REOs have a high thermal stability

and tends to end up in the slag phase. This was melted under a protective argon (Ar) atmosphere and held at 1600 °C for one hour. 2.5 wt% of the material ended up in the slag phase, while the rest stayed in it's metallic form. REO made up 33 wt% of the slag phase, while the metallic phase only contained between 16.5 and 2.6 ppm. The slag contained 10 000-50 000 higher concentration than the metallic phase. The study also showed that certain phases in the slag had a higher REO content than others, and it suggested that further physical separation of the slag could improve the concentration of REOs. A different direct melting method was researched Bian et. al [55], it used a combination of processes: Vacuum induction smelting (VIM) and hydrolysis and magnetic separation process (HMS). This was named VIM-HMS. In this process NdFeB magnets were smelted in a graphite crucible by induction furnace under vacuum (1 Pa). This saturated the mix with carbon creating a $NdFeBC_{sat}$ alloy. By rinsing this in de-ionized water the REE carbides were hydrolyzed. Further separation of the REEs from the iron in the magnet were done by magnetic separation. This yielded a 99.7 % pure REE hydroxide, with a recovery efficiency of 93 %.

Table 2: *Overview of which group the specific process belongs to, the different yields, what material has been used and a short note on the process.*

Process group	Specific process	Yield at optimum [wt%]	Material used	Background and reference
			Pyrometallurgy	
Roasting	Chlorination roasting	92% REEs separated and converted to $NdCl_3$	Pyroprocessed Light Water Reactor fuel	Aim was to ease recycling of nuclear fuel [56]
	Sulfide roasting	95-100% REEs	Automotive grade magnets	Multiple steps required [49]
	Oxide roasting	up to 99% REEs	NdFeB magnets	Conventional pre-treatment for leaching[57],[58]
Liquid metal extraction	Molten magnesium extraction	up to 99% Nd	NdFeB magnets	metallic Nd [59], [51], [50] Extracts
	Molten silver extraction	90% Nd	NdFeB magnets	Nd separated as oxide[52]
Molten salt extraction	Molten chlorides	estimated 90-95% of Nd converted to $NdCl_3$	Al-Nd inter-metallics	$NdCl_3$ can be electrolyzed in the mixture to create Nd-Mg alloy to be used in molten magnesium extraction [53]
	Molten fluorides	94.2% converted into NdF_3	NdFeB magnets	Only recovers REOs [60]
Molten slag extraction	B_2O_3	57-74% Nd	$Nd_x B_2O_3$ containing 25% Nd	Poor recovery from slag [61], [62]
	$CaO - SiO_2 - Al_2O_3$ / $CaO - CaF_2$	Close to 100%	complex magnet scrap	Recovers both REEs from slag and metal from the metallic phase [63]
Direct melting	Slag phase concentration	Slag phase containing 33% REOS	Mixed WEEE scrap containing 6500ppm REEs	More steps required to reproduce metal from slag [54]
	VIM-HMS	93% REE hydroxide	NdFeB magnets	Must be be converted into oxide for further use [55].

3.3 Hydrometallurgy

This chapter presents different hydrometallurgical methods for the leaching of metals from PCBs, focusing on the different reagents used and their efficiency.

3.3.1 General Hydrometallurgy

The term hydrometallurgy covers reactions which takes place in water or organic solvents with the aim to produce metals or compounds [64]. There are three stages to hydrometallurgy;

- 1. The metal of interest must be leached from a solid into a aqueous solution

- 2. The condition of this metal-bearing solution must be concentrated and purified

- 3. The recovery of metal from the purified aqueous solution and to reuse the solution in stage 1

Traditional leaching methods employ cyanide based chemicals or mineral acids [65]. Cyanide based chemicals are mostly used for the recovery of PMs, while mineral acids have been used for both PMs and base metals. In general, a leaching process driven by is required for effective extraction of PMs and base metals [66]. PCBs are covered with plastic or a chemical coating [67] which makes it harder to leach metal from the PCBs without any type of pre-treatment to expose metals to the leaching reagent [66]. Hydrometallurgy can be used to pre-treat PCB, as shown in an experiment conducted by Tuncuk *et al.* [66] which used sodium hydroxide (NaOH) to pre-treat PCBs to remove the chemical coating. The pre-treatment with NaOH led to a dissolution of aluminium (Al), zinc (zn), tin (Sn), Fe, Pb, Cu, nickel (Ni) as shown in Table 3.

Table 3: *The loss of metals when removing the chemical coating from PCB with NaOH. No dissolution of Ag, Au or Pd was observed [68]*

Metals	Losses [μg/g]	Insecurity
Al	911	± 0.85
Zn	27	± 0.10
Sn	21	± 0.04
Fe	10	± 0.37
Pb	4	± 0.02
Cu	0.43	± 0.00
Ni	0.11	± 0.00

3.3.2 Mineral Acid Leaching

Mineral acid, also called organic acids, is derived from an inorganic compound including H_2SO_4, hydrochloric acid (HCl) and nitric acid (HNO_3). It has a low cost, is well investigated and are flexible in process control and up-scaling. Generally, base metals like Zn, Fe, Sn and Al can be dissolved in dilute mineral acid. Cu and precious metals are only significantly dissolved in oxidizing or non-oxidizing acids in the presence of oxidants [65].

3.3.3 Cyanide-Based Leaching

Cyanide-based leaching is mostly used for the leaching of PMs. Although cyanide is highly toxic, it's high efficiency and low cost makes it a preferred leaching agent by the industry. In some regions of the world, a license for cyanide processing for new gold projects is rather unlikely as cyanide pose a environmental threat because of its toxicity [69]. There are many studies trying to find substitutes such as; thiosulfate ($S_2O_3^{2-}$) [70], [71], [72], [73], Thiourea ($SC(NH_2)_2$) [74], [75], [76], aqua regia ($HNO_3 + HCl$) [77] and iodine leaching (I^-) [78]. Table 4 compares the leaching rates, environmental impacts, research standards and economic feasibility of various different leaching reagents and bioleaching.

Table 4: *Comparative assessment of leaching rates, environmental impacts, research standards and economic feasibility of various leaching reagents. Scaled from 0 to 5, where 0 is bad and 5 is excellent. [79]*

Reagent	Economic feasibility			Environmental impact	Research standard
	Leaching rate	Reagent cost	Corrosive	Toxicity	Reliability
Cyanide	3	5	5	0	5
Aqua regia	4	4	0	3	5
Thiourea	4	4	4	4	4
Thiosulfate	2	2	5	4	2
Chloride	5	4	0	3	4
Bromide	5	2	2	3	2
Iodide	5	3	5	5	3
Bioleaching	3	2	0	0	3

It is assumed that the formation of gold cyanide ion $(Au(CN^-)_2)$ is the main cause for gold dissolution [80]. The process of dissolution of gold with oxygen reduction is shown in reaction (Rx.5). This process can take 1-2 days, but with adding 500-1000g/ton of hydrogen peroxide (H_2O_2) the duration can be reduced to 2-4 hours[80], the reaction with H_2O_2 is shown in (Rx.6).

$$2Au + 4NaCN + 2H_2O + O_2 \rightarrow 2NaAu(CN)_2 + 2NaOH + H_2O_2 \qquad (Rx.5)$$

$$2Au + 4NaCN + 2H_2O_2 \rightarrow 2NaAu(CN)_2 + 2NaOH \qquad (Rx.6)$$
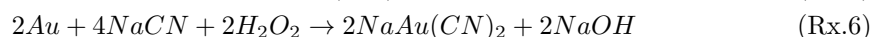
3.3.4   Multi-Stage Leaching

By leaching in multiple steps whit change to the acid or environment its possible to get better effect and to leach metals selectively. A study conducted by Silvas *et al.* [81] showed that by leaching shredded PCBs with 1 M H_2SO_4 in a ratio of 1:10 at 75 °C; 90 wt% Al, 8.6 wt% Sn, and 40 wt% Zn and 0 wt% Cu, Fe, Ni, Pb were extracted. Then with 1 M H_2SO_4 in a ratio of 1:10 and with H_2O_2 as an oxidative agent at 75 °C; 10 wt% Al, 100 wt% Cu, 40 wt% Zn and 0 wt% Fe, Ni, Pb and Sn were extracted. By removing most of the impurities found in Cu by leaching with H_2SO_4 first and in the second step add H_2O_2 to leach the Cu, Silvas *et al.* managed to selective leach Cu and get a higher concentration of Cu in the solvent.

3.3.5   Leaching of NdFeB Magnets

Nd-metal dissolves in diluted acids and will form neodymium-ions (Nd^{3+}) along with hydrogen gas (H^2) [82]. This is similar to other leaching processes, as that for Fe and B as shown by the reaction (Rx.7)-(Rx.9)

$$Nd(s) + H^+X^-(aq) \rightarrow Nd^{3+}(aq) + H_2(g) + X^-(aq) \qquad (Rx.7)$$

$$Fe(s) + H^+X^-(aq) \rightarrow Fe^{2+}(aq) + H_2(g) + X^-(aq) \qquad (Rx.8)$$

$$B(s) + H^+X^-(aq) \rightarrow B^{3+}(aq) + H_2(g) + X^-(aq) \qquad (Rx.9)$$
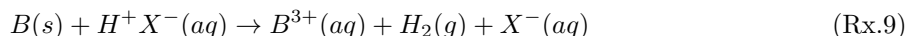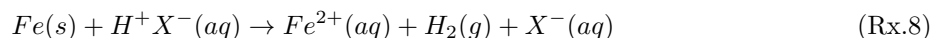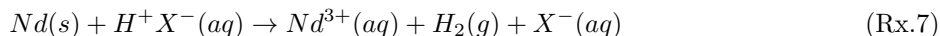
Where X is the acid. Separating Nd^{3+} from other metal ions in a leaching solution by ionic exchange, electrolysis and replacement has proven difficult, and none of those methods provided a solution with a consecration of Nd. The solution presented by Lee *et al.* [82] was to leach NdFeB magnets with H_2SO_4 and raise the pH in the solution to 0.6. This allows the Nd to precipitate completely. Fe barely precipitate at this pH, as shown in Figure 5. The precipitation product of Nd appered as NdOOH and $Nd(OH)_3$,and the finished product contained 75.41 wt% Nd
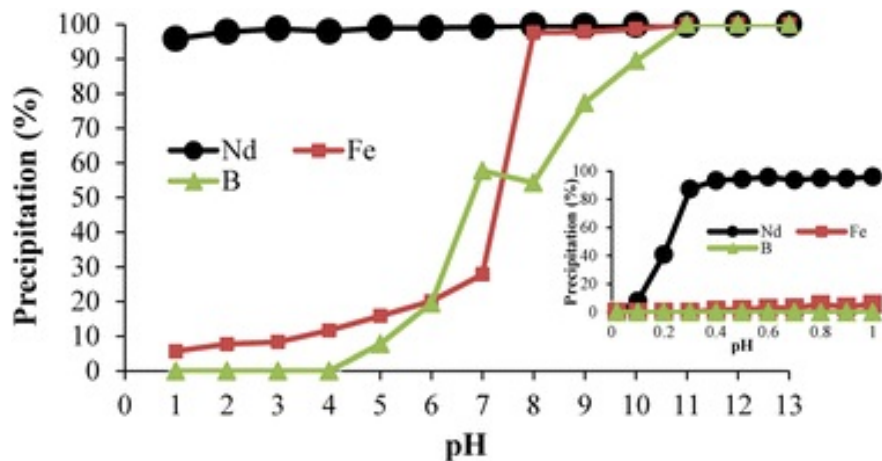
Figure 5: *The effect on precipitation of Nd, Fe and B in H_2SO_4. The main Figure shows pH from 1-13 and the minor graph shows pH from 0.1-1. Nd starts to precipitate at pH 0.1 and with a pH at 1, 95 % of the Nd has precipitated [82].*

Behera *et al.* [83] used microwave and ultrasonic to increase the efficiency of leaching with acetic acids (CH_3COOH). With ultrasound assisted leaching, 99.9 % of the Nd was leached with 90 W ultrasound power, 1 % pulp density, particle size 106-150 μm, 0.4 M CH_3COOH at 303 K.

Table 5: *Overview of different hydrometallurgical processes.*

				Hydrometallurgy				
Leaching reagent	Duration	Material used (source)	Leaching rate	Temperature	Ratio	Particle size	Background and reference
HCL + HNO_3	-	metal wire	Ag 98 % Au 97 % Pd 93 %	20 °C	0.05 g/ml	0.5 mm	Recovery of high purity precious metals from printed circuit boards and the effects of ratio metal and reagent[84].
HCl+HNO_3	0.5 hours	LCD screen	In 92 %	60 °C	2 g/ml	5 mm	Recovery of valuable materials from waste liquid crystal display panel [85]
HCL	24 hours	Red mud	Y > 80 % Nd > 80 % Dy > 80 % Sc ~ 75 % La ~ 75 % Ce ~ 75 %	25 °C	L/S : 50	~ 10 μm	Leaching of rare earths from red mud. Looking at correlation between leaching of REE and major elements and effect of leaching time, temperature and concentrations[86]
HCl + $(COOH)_2$	6 hours	sintered Nd-magnets	Nd 99 %	110 °C	-	-	Resource recovery from Nd–Fe–B sintered magnet by hydrothermal treatment. The recovered Nd is in the form of $Nd_2(C_2O_4)_3 xH2O$[87].

3.4 Biohydrometallurgy

This chapter presents biohydrometallurgy as an alternative to leaching, focusing on the different microorganisms and parameters which influence the efficiency.

3.4.1 General Biohydrometallurgy

Biohydrometallurgy, also known as bioleaching, uses living organisms to help with the dissolution of metals. Bacteria and fungi are used for a series of leaching and oxidation processes to recover certain elements, which enhances the dissolution [88]. Bioleaching sees increased interest, due to its low environmental impact, potentially low operational cost and low energy consumption [25]. Bioleaching can be conducted under mild conditions, with low to no use of toxic chemicals, where chemical leaching can create environmental problems. The method has been reported to be effective in terms of recovery rate. However, the process is slow compared to pyrometallurgical methods [89], [90]. One more issue for bioleaching is that these microorganisms are sensitive to contamination of other bacteria or fungi as well as metals that are toxic to them. The toxicity of PCBs was considered a major limitation to bioleaching of Cu.

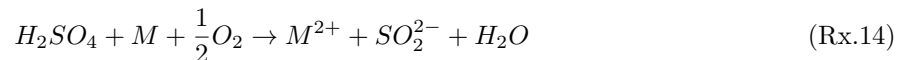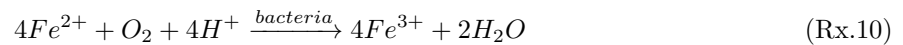Bioleaching can be divided into three different leaching methods [91]:

- Direct leaching/contact leaching: Physical contact between the bacterial cell and the mineral surface.

- Indirect bacterial leaching: A lixiviant which chemically oxidizes the mineral is generated by the bacteria.

- A combination of contact leaching and indirect leaching

Bacteria and fungi used in bioleaching are found in mine waste, mine water, cold sulfur springs, and soil [92]. The bacteria and fungi is cultivated under ideal conditions to reach desired concentration. Marra *et al.*[93] grew *A. thiooxidans* in a mineral medium containing $(NH_4)_2SO_4$, $MgSO_2 \times 7H_2O$, K_2HPO_4, KCl and Sulfur (S) for 10 days prior to the leaching. *A. thiooxidans* cells were enumerated using the spread plate method with $(NH_4)_2SO_4$, $MgSO_4 \times 7H_2O$, $CaCl_2$, KH_2PO_4, $FeSO_4$ and $Na_2S_2O_3$ for 7-10 days. The incubation and growth of bacteria and fungi is a complex and slow process. The time needed to set up and implement the process could take years to a decade [94].

A. ferooxidans helps with the bio-oxidation of metals with the oxidation of ferrous (Fe^{2+}) to ferric (Fe^{3+}), as is shown in (Rx.10). The ferric oxidizes the metal as shown in reaction (Rx.11) and (Rx.12) [95][96]. Where as *A. thiooxidans* helps with the bio-oxidation by the oxidation of sulphur(S), (Rx.13). The H_2SO_4 oxidizes the metal as shown in reaction (Rx.14) [93].

$$4Fe^{2+} + O_2 + 4H^+ \xrightarrow{bacteria} 4Fe^{3+} + 2H_2O \tag{Rx.10}$$

$$2Fe^{3+} + M \rightarrow M^{2+} + 2Fe^{2+} \tag{Rx.11}$$

$$3Fe^{3+} + M \rightarrow M^{3+} + 3Fe^{2+} \tag{Rx.12}$$

$$S + H_2O + \frac{2}{3}O_2 \xrightarrow{bacteria} H_2SO_4 \tag{Rx.13}$$

$$H_2SO_4 + M + \frac{1}{2}O_2 \rightarrow M^{2+} + SO_2^{2-} + H_2O \tag{Rx.14}$$

3.4.2 Parameters Affecting Bioleaching

The efficiency of bioleaching depends on the efficiency of the microorganism and the leaching substrate, but there are some external parameters which influence the efficiency [96], [91]:

- pH

- Nutrients

- The concentration of O_2, carbon dioxide (CO_2) and heavy metals

- Temperature

- Particle size

- Surface area

The ratio of leaching substrate and leaching agent can also have a big impact on the efficiency, as shown in Figure 6 [97].
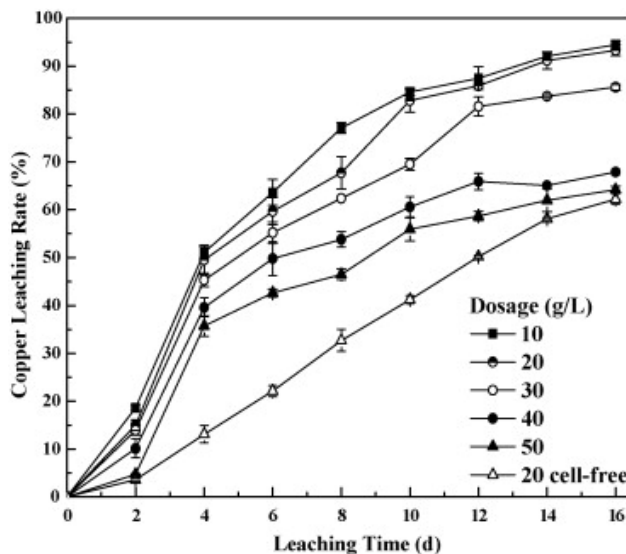
Figure 6: *Leaching rate of Cu with different dosage of PCB-powder (g/L). After 16 days the percentage extracted Cu was 95 %, 93 %, 86 %, 67 %, 64 % and 62 % for 10 g/L, 20 g/L, 30 g/L 40 g/L, 50 g/L and 20-cell free, respectively[97]*

3.4.3 Bioleaching of Copper from Printed Circuit Boards

Choi *et al.* [98] used *A.ferrooxidans* to leach Cu from shredded PCBs resulting in a extraction of 37 % and 81 % with citric acid ($C_6H_8O_7$). As well as reporting a rise in the pH after a time, giving rise to the idea that Cu also is leached out with the formation of hydroxide (OH^-) as shown in reaction (Rx.15).

$$2Cu + 2H_2O + O_2 \rightarrow 2Cu^{2+} + 4OH^-$$ (Rx.15)
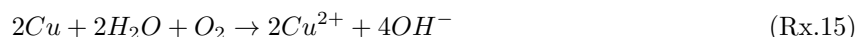
3.4.4 Bioleaching of Rare Earth Elements from Printed Circuit Boards

Marra *et al.*[93] leached PCB-dust from shredding. 92.6 % of the dust compromised of particles smaller then 0.5 mm. Using *A. thiooxidans* (DSM 9463) they managed to leach Ce > 99 %, Eu > 99%, Nd > 99 %, La ∼ 80 %, Y ∼ 80 %. The lowest pulp density was expected to have the highest leaching rate, but the highest leaching rate was reported to happen at a pulp density of 1 % (w/v).

Table 6: *Overview of different bioleaching processes.*

Bioleaching				
Microorganism	**Time**	**Leaching rate**	Ratio	**Background and referances**
Acidithiobacillus Ferrooxidans	3 days	Cu 98,6 % Zn 83.8 % Al 75.4 %	15 g/L	consumption, metal recovery and kinetics [96]
Acidithiobacillus thiooxidans	8 days	Cd 100 % Ni 100 % Zn 100 % Al 100 % Cu ~78 % Fe ~100 % Ce > 99 % Eu > 99% Nd > 99 % La ~ 80 % Y ~ 80 %	10g/L	Investigate the potential application of bioleaching for the extraction of base metals, precious metals and REEs from WEEE shredding dust [93].
Acidophilic chemolithotrophs	10 days	Co 15.1 % Ni 37.8 % Cu 54.3 % Zn 51.8 % Sc 52.0 % Y 52.6 % La 59.5 % Nd 22.1 % Sm 26.5 % Gd 27.6 %	-	Leaching of Rare Earth Elements from Coal Ashes and effects of temperature, pH and ratio has on the recovery [99].

3.5   Chelation Technology

Chelation is defined as the formation of stable metal–ligand complexes which are soluble in water [100], this means it can be classified as a form of hydrometallurgy. Chelating agents may either be organic or inorganic compounds. It is considered a green process since the chelating agent can be recovered at a high efficiency and reused [101]. Chelation already sees use in the extraction of metals, however little research has been done using chelation to recover metals from WEEE as moste of the research on chelation concerns purifying contaminated soils and water. Although, the following flowchart in Figure 7 has been proposed. The flowchart proposes dismantling as well as communion prior to the actual chelation step. This is followed by precipitation using acid and then filtering out a metal-salt solution. The recovered chelating agent can be reused after washing and drying. Jadhao *et al.* [18] reported a recovery of more than 96 % of the chelating agent but, reported a decrease in the efficiency of recycled chelating agents, shown in Figure 8.
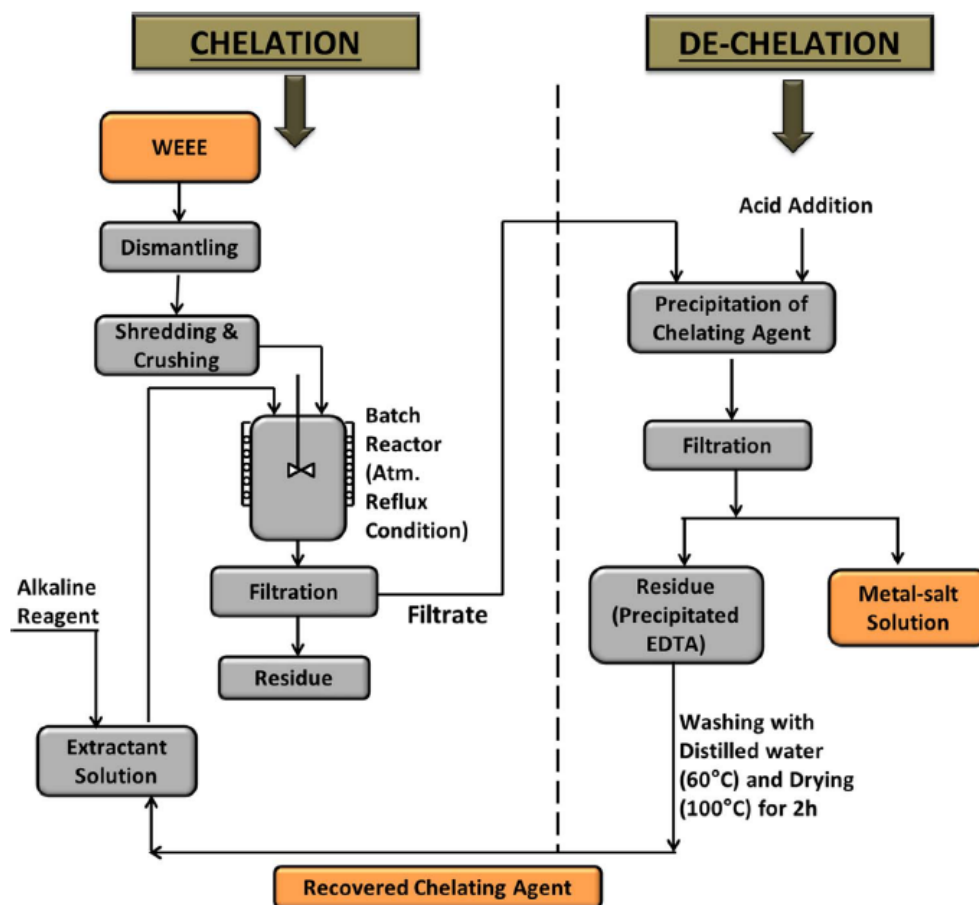
Figure 7: *Proposed flowchart for WEEE recycling by use of chelation [25].*

.
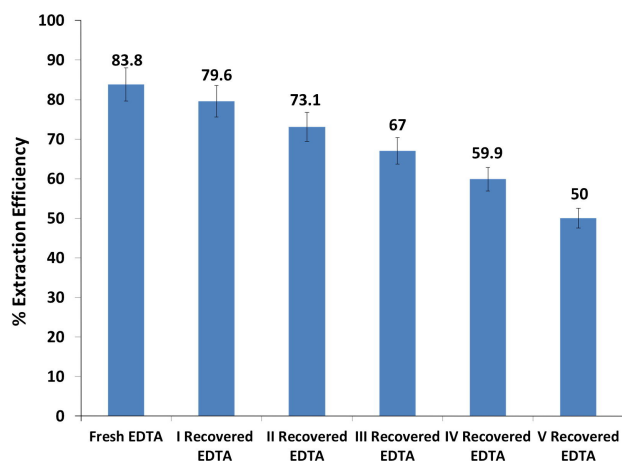
Figure 8: *Shows the rate of recovery for different chelating agent recocery cycles. Fresh EDTA achieved an extraction rate of 83.8%, one recovery cycle later the extraction rate is 79.6%. Stirring speed=700 rpm, particle size=150 µm, pH=8, 0.5M EDTA, reaction temperature=100 °C and reaction time=3 hours.*

EDTA (ethylenediaminetetraacetic acid), DTPA (diethylenetriaminepentaacetic acid), HEDTA ((hydroxyethyl)ethylenediaminetriacetic acid) and S,S-EDDS (S,S-ethylenediaminedisuccinic acid) are commonly used chelation agents. EDTA, DPTA and HEDTA are non-biodegradable in standard test [102], however S,S-EDDS is biodegradable [103]. For the chelating agent EDTA, the Cu-extraction increases with increasing reaction temperature, which can could be related to the enhanced reaction kinetics [18]. At higher temperatures molecules collide more frequently, which may lead to increased a higher extraction rate. For EDTA Jadhao *et al.* [18] considered 100 °C, 3 hours and a rotation speed of 700 rpm for optimal for Cu extraction with EDTA as the chelating agent. A 10 % increase in Cu extraction was achieved when the stirring speed was increased from 100 to 700 rpm. It is believed that a high concentration of chelating agent drives the reaction in a forward direction due to the reversible nature of the reaction [18], [104]. Page *et al.* [103] found a method for removing radioactive Thorium (Th) from REE ore. This was achieved by using a chelating agent more selective towards Th. Another example, is using a chelating agent selective to REEs to remove dilute REEs from geothermal water [105].

3.6 Ionic Liquids

Ionic liquids (ILs) are mixtures of organic and inorganic salts that are liquid at, or beneath room temperature. ILs are powerful solvents, but is still considered a green technology as the chemicals used are generally less harmful [106]. ILs possess unique and interesting characteristics, such as their eco-friendliness and diversity, which could prove valuable and interesting for future research in REE recycling processes, and to metallurgy as a whole. As molten salts, ILs consists of at least two components that can be varied, the cation and the anion. This means that the ILs can be tailored to solve specific compounds or elements. In general one or both of the ions in ILs are large, and the cation often has a low degree of symmetry. This affects the lattice strength and is what makes it liquid at room temperature [107]. A large amount of work and research is required, but several researchers have demonstrated that ILs can extract REEs [108], [109], [110], [111].

3.7   The Umicore Process

Umicore's Integrated Metals Smelter and Refinery in Belgium is one of Europe's largest WEEE recyclers. Umicore is a specialty materials group with expertise in material science, chemistry and metallurgy. They recover and sell platinum group metals (PGMs), special metals, such as selenium (Se), tellurium (Te), indium (In), secondary special metals, such as antimony (Sb), Sn, As, bismuth (Bi) and base metals.

Umicore gets it's waste from industrial waste, byproducts from the non-ferrous industry (drosses, matte, speiss, anode slimes etc.), precious metal sweeps and bullions, spent industrial catalysts, and WEEE from consumer recyclables such as PCBs and electrical components. Annually around 250,000 tonnes of waste is treated at Umicore's plant in Hoboken, Belgium.

3.7.1   Process Overview

First, samples of the waste are taken and analyzed with regards to metal content, so that it is known what it contains, to handle it more efficiently. Then, the process is divided into two parts, Precious Metal Operations (PMO) and Base Metal Operations (BMO). In Figure 9, the different routes elements take as they undergo processing are shown, and a short description of the process follows.
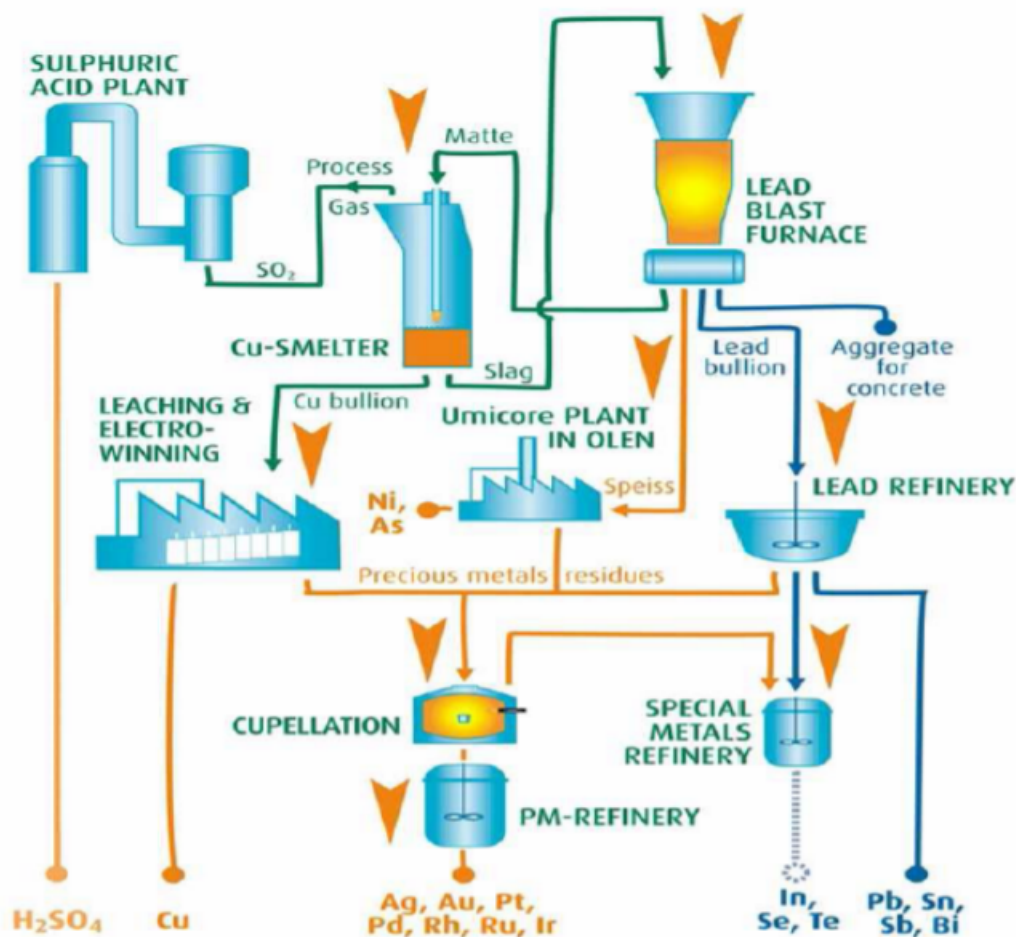
Figure 9: *Flowchart of the different processes, inputs and outputs at Umicore's smelter. The inputs are the large arrows at the top.*

The PMO uses Pb, Cu and Ni as collectors of metal. The process can roughly be divided into three steps: smelter, Cu leaching and electrowinning. The first step is using an IsaSmelt copper furnace, marked

in Figure 9 as Cu-smelter. Oxygen-rich air along with fuel is injected into the furnace through a gas lance. Coke, along with polymers from waste, is added as a reducing agent and fuel. The PMs are collected in a copper bullion, while most of the other metals end up in the Pb slag. This Pb slag is processed further in the BMO. The Cu present the copper bullion is leached out in a leaching and electrowinning plant. The residue from the bullion contains the PMs and is further refined using cupellation and silver refinery. Cupellation is a process of melting and heating where the base metals, such as Pb, forms oxides, while the PM remain molten [112], this separates and extracts the PMs from the base metals.

The BMO can also roughly be divided into three steps: lead blast furnace, lead refinery and special metals refinery, shown in Figure 9. The lead blast furnace reduces the Pb slag from PMO along with third party high Pb containing materials. This transforms the feed to impure lead bullions, nickel speiss, copper matte and depleted slag. The lead bullion contains the most metals and the Harris process is used to separate the bullion into three fractions: pure Pb, sodium antimonate ($NaSbO_3$) and special metals [113]. The special metals refinery then extracts and separates most of the metals, while Bi and Sn goes to a third party refiner. The Ni is leached out of the nickel speiss and processed into nickel sulphate ($NiSO_4$), the remnants of the speiss is sent back to the PMO for processing. The copper matte is also reprocessed and enters the stream at the IsaSmelter copper furnace. The depleted slag, which contains the REEs, is physically calibrated and used as a filler in concrete.

3.7.2   Environmental Impact

Umicore applies several techniques to minimize the environmental impact of it's operations. The S contents of the waste is converted into sulphur dioxide (SO_2) and further to H_2SO_4, this is then sold. Sprinklers are installed and spray water around the facility to prevent dust from flying off. Sensors are installed in the stack to monitor SO_2 and nitrous oxides (NO_x) emissions so that the operators can react to it. All the water from the plant is processed, this includes process water, rainwater and sprinkling water [43].

4   Theory

4.1   FactSage

CALculation of PHAse Diagrams (CALPHAD) is a method which takes thermodynamical data and lets the user create phase diagrams and survey phase equilibriums. Phase diagrams are used in materials research and engineering to understand the interrelationship between composition, microstructure and process conditions. In complex systems, computational methods such as CALPHAD are employed to model thermodynamic properties for each phase and simulate multicomponent phase behavior [114]. Initially phase diagrams were created graphically with data collected from experiments. After many years of experimental trials and data collection large databases containing thermodynamical data has evolved. These are then applied in commercial software, such as FactSage. FactSage is the fusion of two well known software packages in the computational thermochemistry, Fact-Win and ChemSage [115]. FactSage contains several databases and using the correct database ensures that the calculations done apply to the specific system. *I.e.* FactPS contains pure substances, FactOxid contains all pure oxides and oxide solutions and FactLite contains light alloy systems with focus on Mg and Al alloys [116]. Factsage shows only the phases at equilibrium, but not the different phases from start to equilibrium. The time to achieve equilibrium may be couple of hours to years in slow systems.

Typical phase rule violations for binary systems are shown in Figure 10, the explanation of the errors [117] is below the figure. The phase diagrams are thermodynamically assessed and experimentally determined, giving rise to the possibilities that some of the phase diagram can have contradictions and errors.

Figure 10: *Typical phase rule violations. The explanation of the errors is below the figure[117]*

A: A two-phase field cannot be extended to become part of a pure element side of a phase diagram at zero solute. In example A, the liquidus and the solidus must meet at the melting point of the pure element.

B: Two liquidus curves must meet at one composition at a eutectic temperature.

C: A tie line must terminate at a phase boundary.

D: Two solvus boundaries (or two liquidus, or two solidus, or a solidus and a solvus) of the same phase must meet (*i.e.*, intersect) at one composition at an invariant temperature. (There should not be two solubility values for a phase boundary at one temperature.)

E: A phase boundary must extrapolate into a two-phase field after crossing an invariant point. The validity of this feature, and similar features related to invariant temperatures, is easily demonstrated by

constructing hypothetical free energy diagrams slightly below and slightly above the invariant temperature and by observing the relative positions of the relevant tangent points to the free energy curves. After intersection, such boundaries can also be extrapolated into metastable regions of thephase diagram. Such extrapolations are sometimes indicated by dashed or dotted lines.

F: A phase boundary cannot cross the 0 at.% line except at a phase transition (melting, allotropic transformation, etc.) point of the element A.

G: The highest point of the γ phase must touch the invariant reaction line.

H: In a binary system, an invariant temperature line should involve equilibrium among three phases.

I: There should be a two-phase field between two single-phase fields. (Two single phases cannot touch except at a point. However, second-order and higher-order transformations may be exceptions to this rule.)

J: When two-phase boundaries touch at a point, they should touch at an extremity of temperature.

K: A touching liquidus and solidus (or any two touching boundaries) must have a horizontal common tangent at the congruent point. In this case, the solidus at the melting point is too "sharp" and appears to be discontinuous.

L: A local minimum point in the lower part of a single-phase field (in this case the liquid) cannot be drawn without an additional boundary in contact with it. (In this case, a horizontal monotectic line is most likely missing.)

M: A local maximum point in the lower part of a single-phase field cannot be drawn without a monotectic, monotectoid, syntectic, or syntectoid reaction occurring below it at a lower temperature. Alternatively, a solidus curve must be drawn to touch the liquidus at point M.

N: The temperature of an invariant reaction in a binary system must be constant. (The reaction line must be horizontal.)

O: A phase boundary cannot terminate within a phase field. (Termination due to lack of data is, of course, often shown in phase diagrams, but this is recognized to be artificial.)

P: The liquidus should not have a sharp peak with discontinuous slope at the melting point of a compound. (This rule is not applicable if the liquid retains the molecular state of the compound, i.e., in case of a strong association.)

Q: The compositions of all three phases at an invariant reaction must be different.

R: Initial slopes of the liquidus and solidus must have the same sign (both up or down).

S: A four-phase equilibrium is not allowed in a binary system.

T: Two separate phase boundaries that create a two-phase field between two phases in equilibrium should not cross one another.

4.1.1 Laves_C15

All Al_2RE have the laves_C15-structure A_2B , prototype Cu_2Mg [118]. The Al_2Nd is a ferromagnet and a very stable intermetallic. It has a melting temperature of 1733 K [119] and a curie temperature of 65 K [120]. The laves_C15 crystal structure is a cubic structure, shown in Figure 11. The dark atoms in the figure is the Al atoms and the R is the Nd atoms.
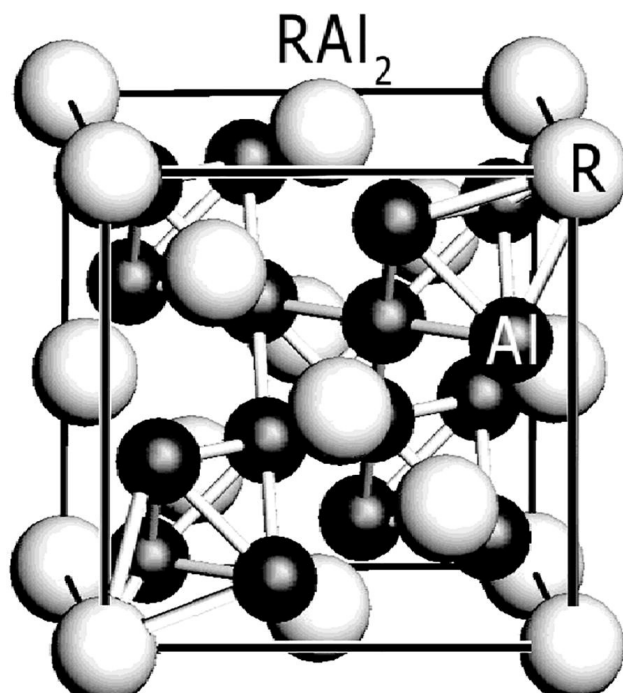
Figure 11: *The crystal unit cell of the laves_C15 crystal where R is the Nd atoms and Al is the Al atoms [121].*

4.2   Diffusion

When pure solid Fe comes in contact with pure liquid Al two intermetallic phases are formed. Near the Al, $FeAl_3$ forms and close to the Fe, Fe_2Al_5 forms [122]. The growth rate is generally high for a stationary system, but for a dynamic system the growth is dependent on the dissolution of the Fe and its saturation of Fe [123].

The interaction between solid Ni and molten Al is the formation of Al_3Ni. The intermetallic, Al_3Ni, breaks off and disperses into the molten Al [6]. Kyriakopous *et al.* [6] reported that a piece of Al_2O_3 blocked the reaction between Al and Ni, and locally slowed down the dissolution process, as shown in Figure 12.
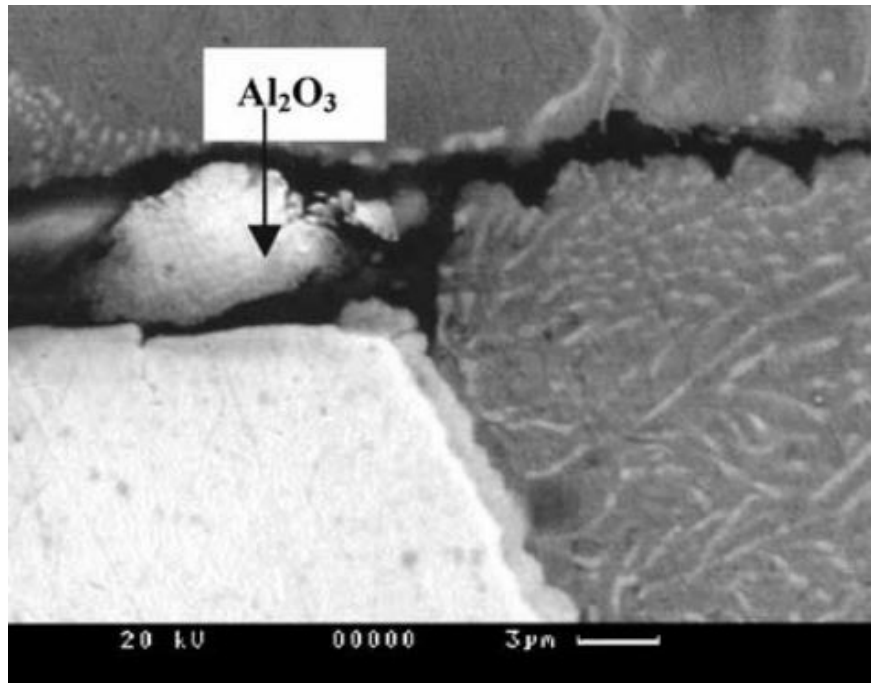

Figure 12: *Interaction of solid nickel in molten Al after 30 seconds at 700 °C. The Al_2O_3 particle blocks the reaction between Al and Ni [6].*

4.2.1   Dissolution

Additives with a higher melting point than the bath temperature, are dissolved by mass transfer trough the bondary layer between the melt and the alloying additives. The mass balance could be written as: Mol of X removed from the additive = Flow of the additive trough the boundary layer [124]. Equation (2) explains the mass balance mathematically.

$$-\frac{dr}{dt}A\rho_m = kA(c_M - c_{M_b})$$

$$-dr\rho_m = k(c_M - c_{M_b}dt$$

$$t = \frac{\rho_m(R - r)}{k(c_M - c_{M_b})} \tag{2}$$

Where $\frac{dr}{dt}A$ is the volume of a spherical shell and A is the contact area, R is the radius of the additive added in and r is the radius of the additive after a time t, ρ_m is the number of mol additives in kmol/m^3, k is the mass transfer coefficient, c_M is the concentration of the additives in the melt at equilibrium with the pure solid in kmol/m^3, c_{M_b} is the concentration of X in the bulk melt. To achieve full dissolution of the additives

27

the radius r of the additive, and the concentration of the additives in the bulk, c_{M_b}, must be equal to 0. With this, equation (2) can be rewritten to equation (3) [124].

$$t_d = \frac{\rho_m R}{k \times c_M} \tag{3}$$

4.3   Electromagnetism

Placing the liquid Al inside a electromagnetic coil will have two known effects.

First, it will induce eddy-currents within the material, which generates heat due to ohmic loss, also known as induction heating.

Secondly, it will generate Lorentz forces, pushing the melt towards areas with lower field strength, [125].

Because of the high surface tension of liquid Al, PCBs will float on top of the liquid Al, and the metallic fraction of the PCBs will oxidize. It is a working hypothesis by R. Fritzsch [126], where the electromagnetic field of a single phase, low frequency, induction coil influences the wetting behaviour of Al. The electromagnetic field, and the induced Lorentz forces, hereby disturbs the surface tension and generate a pressure within the metal which pushes the metal towards the not wetted surface. This should improve the ability of the Al to submerge PCBs and other recyclable materials

4.3.1   Lorentz Forces

Lorentz force is the principle behind electromagnetic movement, such as generators. Lorentz force is acting on the liquid as a reactive force, inducing a velocity in the liquid. When a liquid metal is crossing magnetic field lines, flux variation occurs, which leads to local electromotive forces [127]. The induced electric current that arises can be calculated as shown in equation 4.

$$J^* = \sigma(u \times B) \tag{4}$$

σ is the electric conductivity [S/m] of the liquid, u is the local velocity [m/s] of the liquid and B is the magnetic flux density [T].

Lorentz force can then be calculated as the cross product of the induced electric current J^* and the magnetic flux density B, shown in equation 5. The induced Lorentz forces will stir the melt and help with the mixing.

$$F_L = (J^* \times B) \tag{5}$$

4.3.2   The Electromagnetic Coil

Measurements of the magnetic field strength were done in four different places without a crucible. Figure 13 shows where the measurements were taken, and table 7 shows the magnetic field strength in different height at different places inside the coil.
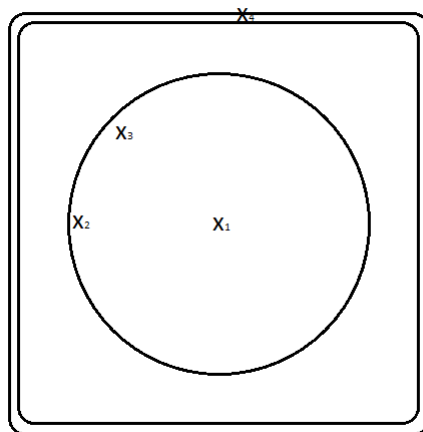

Figure 13: *Overview of where the field was measured. X_1 was measured in the center, X_2 and X_3 was measured on the inner wall of the isolation and X_4 was measured in the gap between the isolation and the coil. Results in Table 7*

.

Table 7: *Measurements of the magnetic field strength inside the coil in militesla [mT]. Measurements are done with a gaussmeter. X_4 measures the peak value of the magnetic field inside the coil.*

Spot	Bottom	Center	Top
X_1	28,8	33,7	31,5
X_2	35,2	34	27,5
X_3	34,2	34,5	27,6
X_4		50,0	

Figure 14 shows the coil used in most of the experiments.

Figure 14: *The electromagnetic coil seen from above. The inside of the coil is isolated for preventing the Al to solidify too fast.*

4.3.3   Calculations of Magnetic Fields

Equation (6) gives the peak of the magnetic flux density in an ideal system. Ideal system means that the geometry of the coil, the material and the current is optimal.

$$B_{inf} = \frac{\mu_0 \mu_r N_c I_c}{l_c} \tag{6}$$

Where B_{inf} is the magnetic flux density [T] of the infinite coil looking at a finite length l_c [m], N_c is the number of turns of the coil, I_c is the current in the coil [A], μ_0 is the permeability of free space [$\frac{H}{m}$] and $\mu_r = \frac{\mu}{\mu_0}$, where μ is the permeability of the material inside the coil [$\frac{H}{m}$].

If there is a electric conductive material inside the coil the material will induce a magnetic field to oppose the magnetic field from the coil. This effect will reduce the magnetic flux density in the coil and around the work piece [128]. The electromagnetic penetration depth [m] into the coil and the work piece is given by:

$$\delta_c = \sqrt{\frac{\rho}{\pi \mu_0 \mu_r f}} \tag{7}$$

Where ρ is the electronic resistivity of the material and f is the frequency of the current in the coil. The resistivity changes with the temperature of the material and its physical state [128].

Equation 7 gives a correlation between penetration depth and frequency, which is the only parameter that can easily be changed.

4.4   Magnetic Separation

Separating particles from a conducting liquid with the use of magnetic fields, is possible if the particle has a lower electric conductivity (σ_p) than the melt (σ_l). The concept is shown in figure 15. The particles move trough the melt in the opposite direction of the lorentz forces, because of a pressure gradient created by the Lorentz forces. The particles will accumulate in depths roughly corresponding to the hydrodynamic boundary layer and the penetration depth of the magnetic field [129]. A mathematical description for magnetic separation was made by Leenov and Kolin [130].
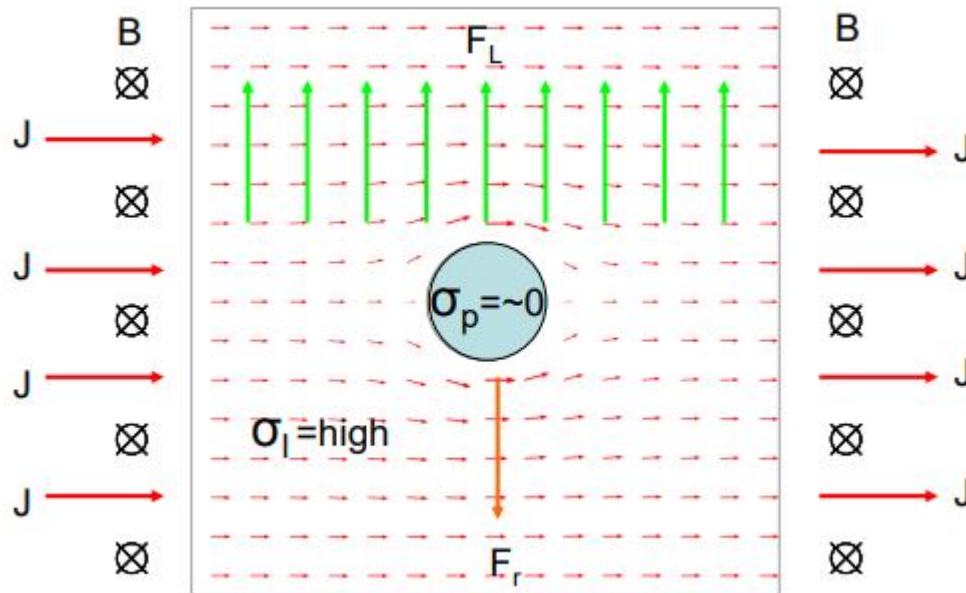
Figure 15: *The Lorentz forces (F_L) and the reaction force (F_r) acting on a non-conducting particle in a curl free magnetic field [129].*

In a magnetic field with curls, the end effect will produce electromagnetic, or Magneto-Hydro-Dynamic, stirring. This stirring effect results in fast separation of particles towards the wall of the crucible. The end effect also occurs at the ends of the work piece, Figure 16 shows the end effect in a coil with a work piece. The risk of re-entrainment of collected particles is significant [129]

Figure 16: *The end effect in coils [131].*

5   Experiments

5.1   Introduction

In all experiments conducted the aim has been to dissolve and up-concentrate Nd in certain phases within molten Al. The principle concept has been:

- If it would mix

- At what rate it would mix

- If Nd could be up concentrated in certain phases

- Identify what governed this process

These questions has lead to the development of six trails. Figure 17 is a flowchart of the process that lead to the different trials.
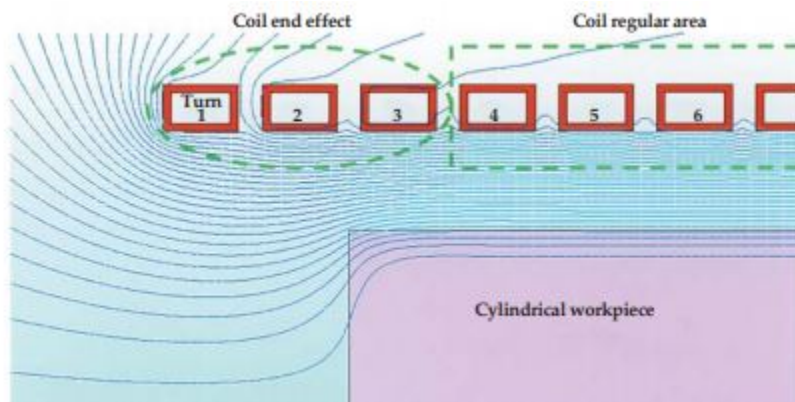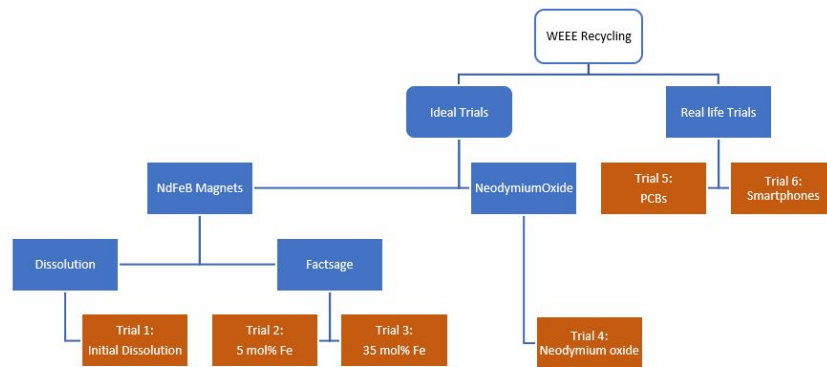

Figure 17: *Flowchart describing how the different trials were designed.*

NdFeB magnets were submerged in liquid Al. The melt was held at elevated temperatures over different periods of time, with and without stirring, creating a fundamental understanding of the kinetics.

PCBs extracted from computer motherboards were investigated in a similar manner to that of the NdFeB magnets. Tests on PCBs are more closely linked to reality, than using pure NdFeB magnets. Challenges met in this experiment would resemble what can be expected in the real world.

Due to a much lower average radius of particles than the NdFeB magnets, powdered neodymium oxide (Nd_2O_3) was interesting to experiment with. Would it dissolve in liquid Al and how fast would it dissolve?

Smartphones of different kinds were submerged in liquid Al, to investigate the kinetics and the general ability to dissolve, without any sort of pre-treatment.

A risk assesment was conducted for the experimental work. This is included in appendix A.

5.2   Materials

Table 8 summarizes all the materials used in the experiments. Table 9 summarizes all the equipment used in the experiments. Following is a description of where the materials and equipment were obtained and a short description of how they are used.

Table 8: *This table presents the materials used in the experiments. * The purity of the Fe was not ensured, but was marked "pure". ** No datasheet was provided for Zn-coated NdFeB magnets, they were assumed to be of similar composition as magnets from supermagnete.de. The composition is available in appendix B. *** Model list is available in the text following this table.*

Materials	Purity	Usage	Provided by
Al	99.99%	All materials are submerged in Al	Norsk Hydro AS
Fe	Pure*	Adjust composition	IMA
Nd	99.1%	Adjust composition	Alfa Aesar
Nd_2O_3	99%	Trial 4	Alfa Aesar
Ni-coated NdFeB magnets	See appendix B	Trial 1, 2 and 3	Supermagnete.de
Zn-coated NdFeB magnets	**	Trial 1, 2 and 3	Clas Ohlson
PCBs	-	Trial 5	IMA
Smartphones	***	Trial 6	Friends and family

Table 9: *This table presents the equipment used in the experiments. * Two different types of crucibles were used. For experiments conducted in the muffle furnace the crucible measured h=185 mm and d=130 mm. For crucibles used in the induction furnace, the crucible graphite had a outer shell, the crucible measured dimensions h=265 mm and d=95 mm. ** Provider not available.*

Equipment	Type/Model	Usage	Provided by
Muffle furnace	3.5 kW, flap door	Melting Al	Nabertherm
Induction Furnace	75kW/IF75	High temperature experiments	Inductotherm
Electromagnetic coil	Induction coil	Provide stirring	IMA
Mechanical stirrer	Metal rod with 4 arms	Provide stirring	IMA
Crucibles	Refractory ceramic crucible*	Experiment vessel	IMA
Argon gas	Instrument argon 5.0/99.999%	Protective atmosphere	AGA AS
Thermocouple	K-type	Temperature measurements	-**
Fume hood	Steel cover connected to pipe	Provide better ventilation	NTNU
Boron Nitride	ZYP Coating	Non-stick coating	Pyrotek

The Al used, was provided by Hydro Aluminium AS facilities in Karmøy, Norway, with a purity of 99.99 %. It was cut into appropriate size to fit the different crucibles, as well as the correct amounts for the trails. NdFeB magnets came from two different sources. Supermagnete's Ni-coated magnets (article no. Q-08-08-04-N) and Clas Ohlson's Zn-coated neodymium magnets (article no.s :31-566 & 31-1467). Magnets were demagnetized prior to tests by heating to the stated curie temperature of 310°C. Magnets obtained from Clas Ohlson had to be dismantled from a steel plate. Ni-coated magnets had previously been chemically analyzed and Zn-coated magnets were assumed to be of similar composition, see appendix B for chemical analysis of Ni-coated magnets. PCBs from computer motherboards were of different specifications, all components directly fastened to the PCBs were not removed. The PCBs had to be cut to fit the crucible, and measured roughly 5x5 cm. 6 smartphones were obtained from friends and family for the experiments. These were of the following models: Apple iPhone 7, Samsung Galaxy S5, Samsung Galaxy S3, Samsung Galaxy S Advance GT-i9070, Sony Xperia Z2 and Sony Xperia Z3. Nothing was removed or added to any phone. The Nd_2O_3 powder was supplied by Alfa Aesar. The Nd_2O_3 powder was packaged in Al foil, with roughly 10 g in each package. Lumps of metallic neodymium were used in experiments adjust the molar concentration of the elements. This was provided by Alfa Aesar. Pure Fe had the same application as the metallic Nd, this was provided by the institute and it's origin is not known. As a heat source for the experiments two

types of furnaces were used. Nabertherm muffle furnace capable of delivering 3.5 kW effect and an induction furnace capable of delivering 75 kW effect, the latter will be referred to as IF75. Lorentz forces created by the electromagnetic coil was used to stir the melt. In experiments where electromagnetic stirring was not used, a mechanical stirrer was used instead. Different crucibles were used in the experiments, for experiments conducted in the muffle furnace refractory ceramic crucibles with dimensions h=185 mm and d=130 mm were used. The crucibles were coated with boron nitride, the boron nitride was supplied by Pyrotek, and made by ZYP Coatings. The boron nitride coating was supplied by Pyrotek, For experiments conducted in the IF75 induction furnace refractory ceramic crucibles with a graphite outer shell were used, these had dimensions h=265 mm and d=95 mm. To adequately ventilate fumes generated from trails on PCBs and smart phones a fume hood was built. The fume hood consisted of a cover connected to a 60 cm long pipe, all in stainless steel. Argon gas was provided by AGA, and had a purity of 99.999 %, the gas was used to purge the atmosphere in which the trails took place, to prevent oxygen in the system. A gas lance was used to inject the gas. Thermocouples were used to measure temperature during the trails. For experiments in the muffle furnace a handheld device was used. For experiments conducted in the IF75 the thermocouple was connected to a computer which logged the temperature. Quartz tubes connected to a rubber pipette filler was used to collect samples of molten metal during the trails.

5.3 Experimental Setup and Procedure

The different parameters in each experiment did not allow the use of the same setup every time. The temperature requirements forced experiments to be conducted in two separate laboratories. All of the different changes in parameters are summarized in Table 10. Schematic overviews of the setups used can be seen in Figure 18 and 19.

5.3.1 Experiments Conducted in the Muffle Furnace

This general procedure was followed for experiments conducted in the muffle furnace. Pure Al was put into a refractory ceramic crucible crucible with the dimensions h=185 mm and d=130 mm. The crucible was inserted into a muffle furnace (A, B and C in Figure 18), which during the experiments was heated to between 750 °C and 1000 °C before the material to be submerged was added. During each experiment samples were collected using a quartz tube connected to a rubber pipette (F and G in Figure 18). The quartz tube was lowered approximately 2 cm into the liquid and a sample was extracted by suction from the pipette filler. The samples were collected from the centre of the of the melt in various time intervals. The homogeneity of the melt was secured by either using a mechanical stirrer (E in Figure 18) or an induction coil (K in Figure 18). For experiments with induction coil mixing that would produce fumes a fume hood was used (I in Figure 18). When a protective atmosphere was used the gas was injected by a gas lance (D and J in Figure 18) Temperature was measured using a thermocouple connected to a hand held multimeter. A schematic drawing of the overall experimental setup is presented in Figure 18, and the details of each experimental run is summarized in Table 10.

Figure 18: *Setup used for experiments conducted in the muffle furnace. A: molten Al, B: refractory ceramic crucible, C: Nabertherm muffle furnace, D: gas lance, E: mechanical stirrer, F: rubber pipette filler, G: quartz tube, H: refractory ceramic crucible, I: fume hood, J: gas lance K: induction coil and L: Ca-wool insulation*

5.3.2 Experiments Conducted in the Induction Furnace

This general procedure was followed for experiments conducted in the induction furnace. Pure Al was put into a refractory ceramic crucible crucible clad with graphite with the dimensions h=265 mm and d=95 mm (B in Figure 19). The crucible was inserted into an induction furnace (A in Figure 19), which during the experiments was heated to between 900°C and 1400 °C before the material to be submerged was added. During each experiment samples were retrieved using the quertz tube. The homogeneity of the melt was

secured by Lorentz' forces from the induction furnace. A fume hood was placed over the top of the furnace, as can be seen in Figure 19. A protective atmosphere was used, and the gas was injected by a gas lance (D in Figure 19). Temperature was logged using a thermocouple connected to a computer. A schematic drawing of the overall experimental set-up is presented in Figure 19, and the details of each experimental run is summarized in Table 10.
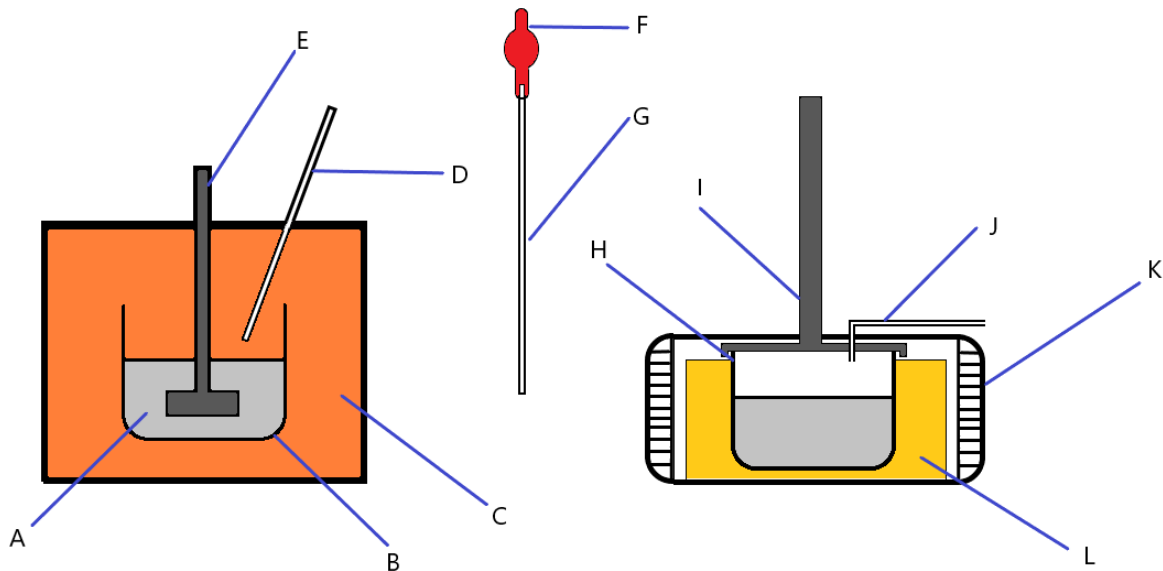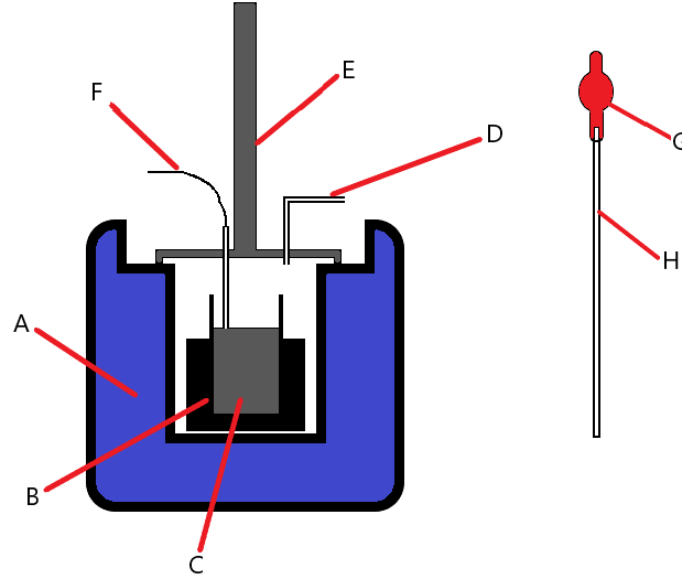

Figure 19: *Setup used for experiments conducted in the induction furnace. A: induction furnace, B: graphite clad refractory ceramic crucible, C: molten Al, D: gas lance, E: fume hood, F: thermocouple, G: rubber pipette filler and H: quartz tube*

Table 10: *Different parameters used in trials. From left to right: Amount of aluminium used in each trail. What material was submerged into the molten aluminium. How long this was held and at which temperature. Injection of argon gas into the crucible. Which oven was used; here MF is Nabertherm muffle furnace and IF75 is induction furnace. Which mechanism was used to mix. The last row is if a fume hood was used or not.*

Parameters of experiments								
	Al (g)	**Material**	**Time** [h]	**Temp.** [C]	**Ar** [L/min]	**Oven**	**Mixing**	**Fume hood**
Trial 1	531.0	143.2 g Nd-Fe-B	0.6	770-645	0.1-0.5	MF	Coil	-
Trial 2	300.5	49.2 g Nd-Fe-B & 75.2 g Nd	6	800	0.3	MF	Rod	-
Trail 3	300.3	409,7 g Nd-Fe-B* & 8.4 g Nd	2.2	900-1400	0.5	IF75	-	Yes
Trial 4	300.0	Nd_2O_3	0.5	800-900*	0.4	MF	Rod	-
Trial 5.1	2046.0	5 PCBs	<0.25	800	0.1-0.5	MF	Coil	Yes
Trial 5.2	2008.0	3 PCBs	<0.25	800	0.1-0.5	MF	-	Yes
Trail 6	1221.0	6 Smartphones	0.5	800-950	0.5	IF75	-	Yes

5.4   Analysis

Scanning Electron Microscopy (SEM) (ultra 55 limited edition, LVFESEM, Zeiss) with an Energy-Dispersive X-ray Spectroscopy (EDS) (Octane pro-a, EDAX, AMETEK) was used to study the microstructure, size and shape of the intermetallic phases, as well as for securing the chemical characterization of the produced samples. The highest resolution in the SEM was achieved by secondary electron (SE) images obtained at ultra-high-resolution mode with 15 kV accelerating voltage. Light Optical Microscopy (LOM) (Axio AX10, inverted light microscope, Zeiss) was used to give some indication to which areas of a sample that would be interesting to investigate further. Images from SEM and have been used for segmentation by computer, to tell at what level the different phases were present. EDS analysis was used to calculate the total contents of certain samples.

6   Result and Discussion

6.1   Processes

The first part of this thesis takes a closer look at processes for the recovery of REEs from WEEE. Some of the processes described are already in use and some have the potential to see use in the future.

6.1.1   Mechanical Methods

Most existing recycling routes utilizes some level of manual disassembly, to remove hazardous parts. Manual disassembly is a major cost element, but also a step that upgrades the value of the waste. Not much information was found concerning REE recovery with mechanical methods. It could be that the price of REEs are not yet at the point where, for example, manual disassembly of NdFeB magnets is economically viable. However REE prices has seen large fluctuations in both directions [7], so this could change in the future. After disassembly, communition is used to easier separate the different fractions within the WEEE, one example showed the loss of close to all REEs to the dust fraction [32]. Mechanical methods can certainly separate different waste fractions, however, today there is no viable mechanical path to separate REEs from WEEE. REEs mostly end up in the dust fraction after communition and no further mechanical methods are used to separate REEs. The dust fraction can be called upconcentrated in the sense of REEs, as the content is more concentrated in REEs, and therefore a preferred material in other steps of recycling of REEs. Mechanical methods show almost a complete loss of REEs to the dust fraction, with that in mind, communition should be avoided. However, there is done research on using water as a medium during communition, this has shown a metal recovery of 97 % [36]. With concerns to REE recovery, methods like this should be more widely researched to see if REEs could more efficiently be recovered. Close to every example of WEEE recycling covered in literature utilized some form of communition or separation as a step in the process. This creates dust, which leads to a considerable loss in concern to REEs, which is not taken into the calculation of the recovery rate. All of the processes benefit from a more concentrated material, and the dust created from communition could prove a good feed material for further processing. Dust has a large surface-to-volume ratio, which in turn makes it an ideal material for all processes that aims to dissolve metals in the dust fraction.

6.1.2   Pyrometallurgical Methods

Conventional pyrometallurgical methods used to treat WEEE does not focus on REE recovery. For the most part REEs end up in low concentrations in the slag phase after pyrometallurgical processing. This slag phase can be used as a filler in concrete, which makes the recovery of these REEs difficult. Potential pyrometallurgical methods for REE recovery has been looked into, many of these methods are efficient, giving a yield close to 100 %. Of these, most processes does not produce metallic REE, but rather as REOs. For most uses of REE, it has to be converted from oxide to metallic, which is a highly energy intensive process [132].

However, liquid metal extraction, using Mg to extract Nd from NdFeB magnets, is capable of producing metallic Nd. The method has been reproduced several times and shows similar results [50], [59], [51]. The only material used in liquid metal extraction with Mg is NdFeB magnets. Having a waste stream of only NdFeB magnets in the recycling of WEEE is hard to achieve, as there are no good mechanical way to separate NdFeB magnets from the other components. The process is, on the other hand, a promising recovery method for the discarded NdFeB magnets and scrap from factories. With a disassembly focused on extracting magnets, this could be possible, however, this is not an economically viable option today.

6.1.3   Hydrometallurgical Methods

Hydrometallurgy sees use today in recovery of metals. Compared to pyrometallurgical methods, hydrometallurgy is a slow process, and can today not be a continuous process to treat WEEE.

The proportion between leaching reagent and WEEE scrap is connected to the leaching efficiency. This makes the leaching reagent a big expense for a recovery plant, which utilizes leaching as the method to

recover metal from WEEE. This could shift the focus from recovering all metals to only focusing on the PMs. Making leaching a unsuited process for the entire WEEE recycling process.

6.1.4 Biohydrometallurgical Methods

Bioleaching is closely related to leaching, but the amount of chemical reagents used is lower as bacteria recycle the chemical reactants. This makes bioleaching more economical viable than ordinary leaching, which uses more leaching reagents. Bioleaching is generally slower than leaching, but if the incubation time for the bacteria is included in the bioleaching process, the process would be much slower than leaching

Fungi and bacteria are living organisms, they are susceptible to toxic elements and changing conditions. With the heterogeneity of WEEE in terms of composition this might prove problematic as elements toxic to these organisms may be introduced. The time needed to implement the process is long [94], with varying metal prices, this could be an economical risk.

6.1.5 Ionic Liquids and Chelation

Both ILs and chelation are relatively new methods, which are promising in regards to environmental friendliness and cost. ILs resembles hydrometallurgy, but without the use of acids, and the danger to the environment acids introduce. Chelation requires acids to de-chelate the metal ions, so in that regard, chelation is less preferred. As both of these methods aims to dissolve metals, they would require the same type of pre-treatment as hydrometallurgy. Communition will increase the surface-to-volume ratio of the WEEE, making the dissolution time shorter. Mechanical separation would be used to lower the need for reagents, as the fractions unsuited for the process would be removed. ILs and chelation both possess the interesting ability to be tailored to fit one metal or compound, to selectively leach it. This mean ILs and chelation could be implemented in any stage of the recycling process, to isolate certain elements at the most efficient stage of the process.

The future is likely to see more strict laws governing the emissions from the WEEE recycling industry, if those laws prohibit certain processes used today, ILs and chelation might see more use.

However, more research is required to make ILs and chelation an option in WEEE recycling.

6.1.6 Recycling of WEEE with Liquid Aluminium

Recycling WEEE with liquid Al may prove useful in several areas. By submerging waste into liquid Al, the organic fraction is removed, in addition to this, melting of the metals may improve the homogeneity. This may aid recycling, as furnaces able to melt Al are more available than furnaces able to melt Cu. An option could be a decentralized process step with molten Al, where the volume and heterogeneity of the WEEE is lowered, making the transport to a more advanced central facility for further separation easier. The toxicity of samples and gases created in these experiments has not been evaluated, and should be taken into consideration as the health impact of combustion of PCBs is large. This could make it difficult to have decentralized processing plants as it would require an advanced emission control.

6.2   Phase Diagrams

Factsage has been used to model 5 phase diagrams of the Al-Nd-Fe-system. The phase diagrams are binary with a constant mol% of Fe, temperatures ranging from 400 K to 1500 K and 0-20 mol% Nd, Figure 20-26. The phase diagrams show the phases at equilibrium, but the time to reach equilibrium is not calculated, so the samples from the different trials are not necessary at equilibrium. Gases and gaseous phases have not been accounted for in the modelling, which can alter the phase diagrams. Trace elements in the NdFeB magnets or their coating are not included in the phase diagrams.

Figure 20: *Phase diagram for the Al-Nd-Fe-system with the concentration of Nd ranging from 0-20 mol% with a constant concentration of 5 mol% Fe, temperatures ranging from 400-1500 K.*
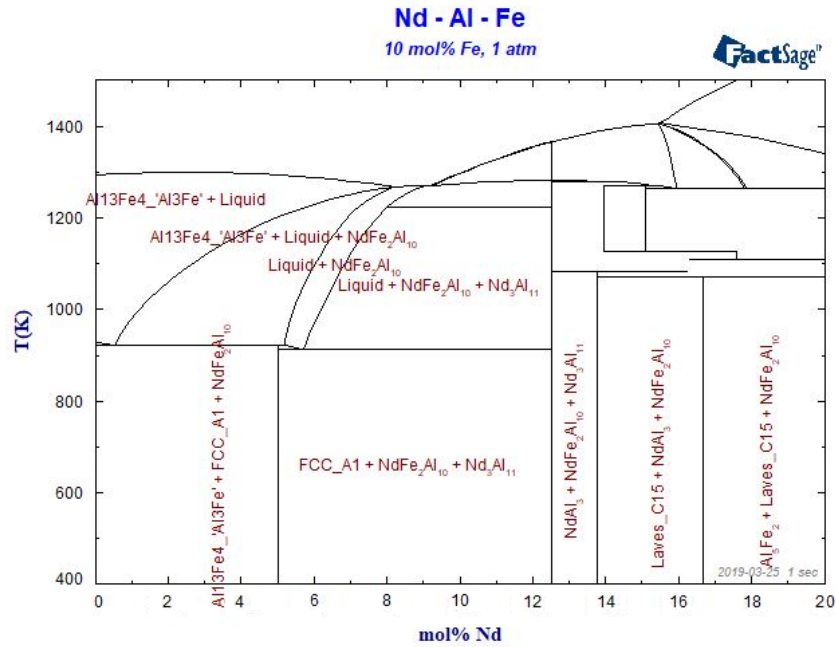
Figure 21: *Phase diagram for the Al-Nd-Fe-system with the concentration of Nd ranging from 0-20 mol% with a constant concentration of 10 mol% Fe, temperatures ranging from 400-1500 K.*
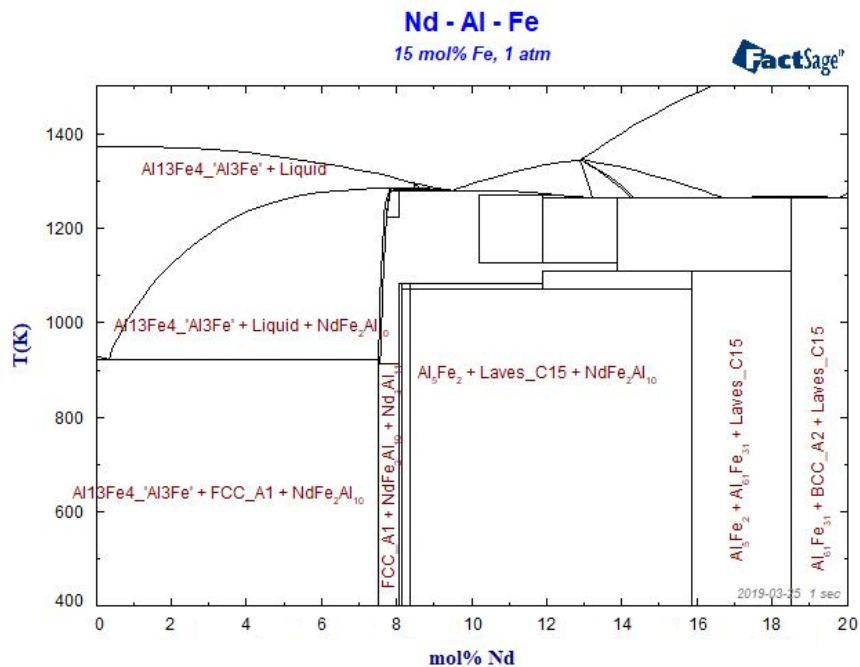
Figure 22: *Phase diagram for the Al-Nd-Fe-system with the concentration of Nd ranging from 0-20 mol% with a constant concentration of 15 mol% Fe, temperatures ranging from 400-1500 K.*
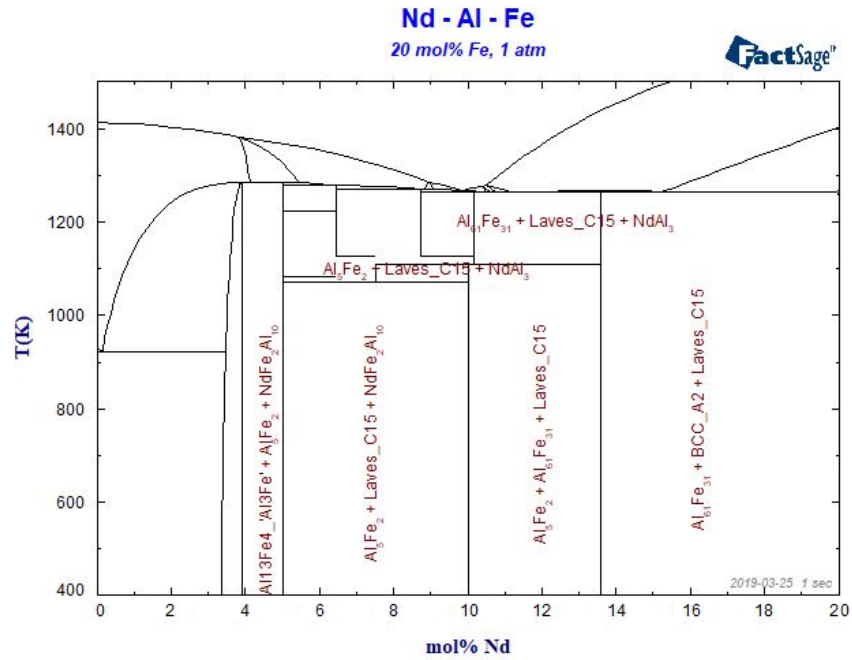
Figure 23: *Phase diagram for the Al-Nd-Fe-system with the concentration of Nd ranging from 0-20 mol% with a constant concentration of 20 mol% Fe, temperatures ranging from 400-1500 K.*
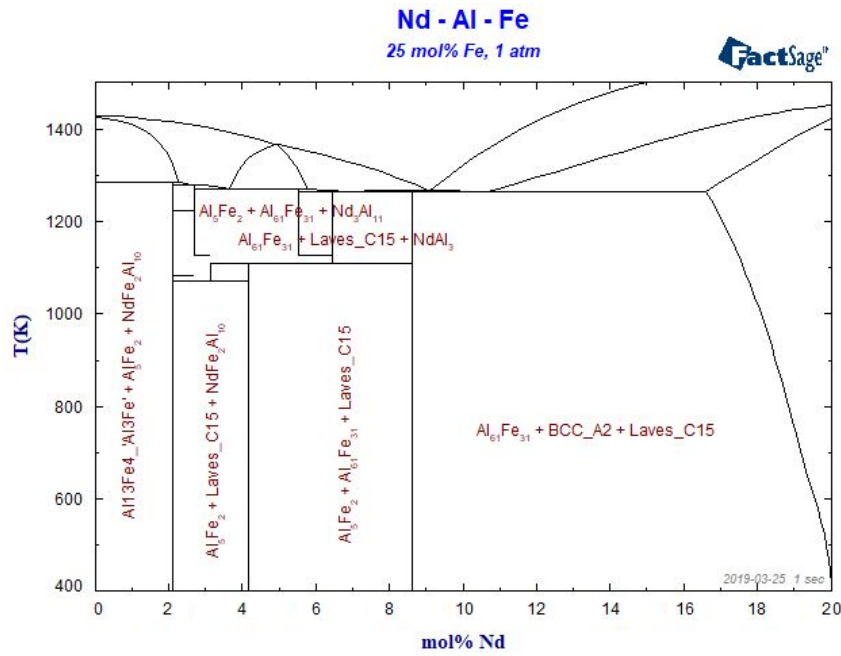
Figure 24: *Phase diagram for the Al-Nd-Fe-system with the concentration of Nd ranging from 0-20 mol% with a constant concentration of 25 mol% Fe, temperatures ranging from 400-1500 K.*
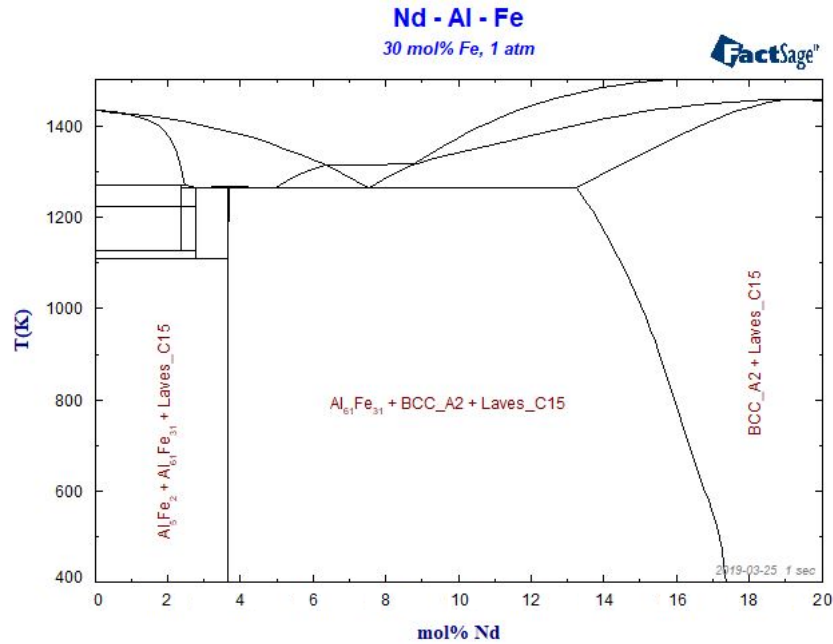
Figure 25: *Phase diagram for the Al-Nd-Fe-system with the concentration of Nd ranging from 0-20 mol% with a constant concentration of 30 mol% Fe, temperatures ranging from 400-1500 K.*
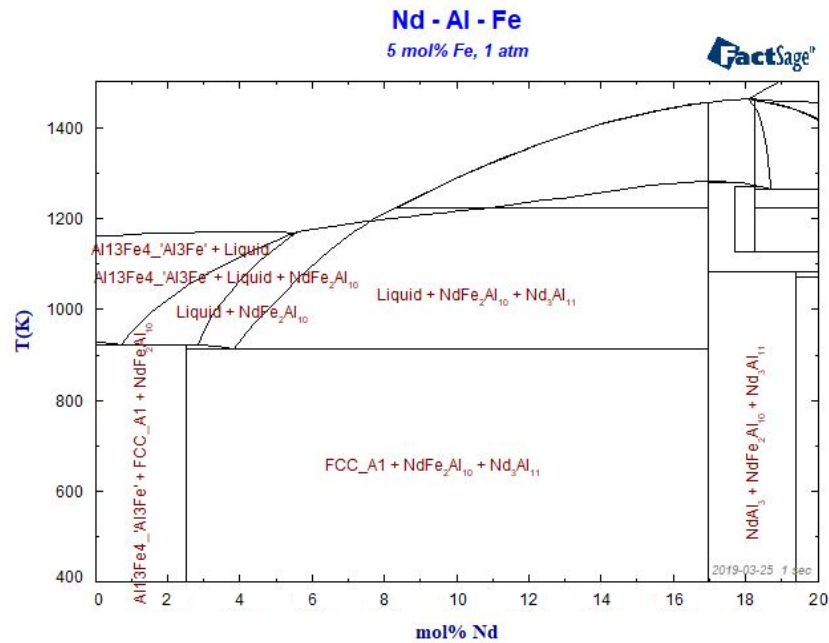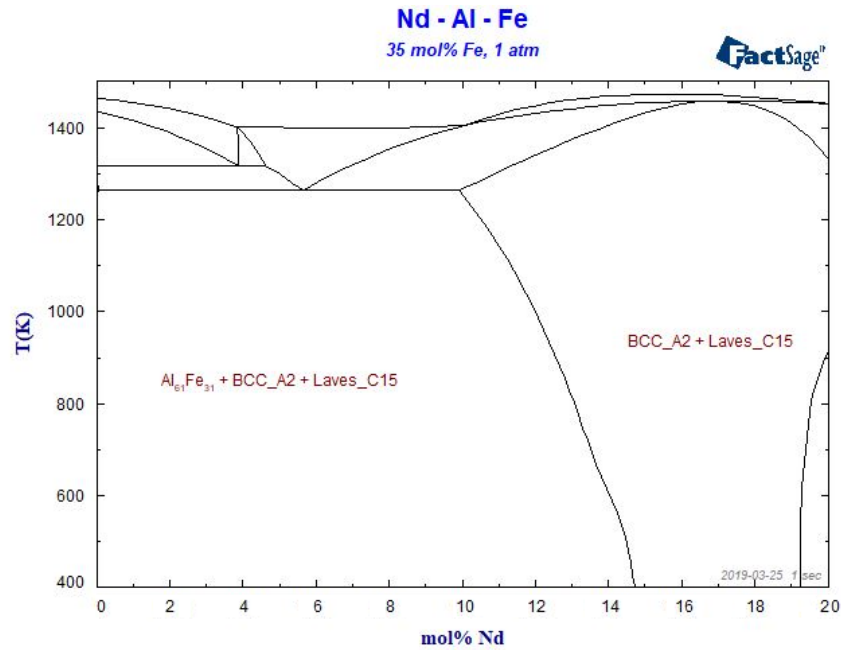

Figure 26: *Phase diagram for the Al-Nd-Fe-system with the concentration of Nd ranging from 0-20 mol% with a constant concentration of 35 mol% Fe, temperatures ranging from 400-1500 K.*

There are some areas in the phase diagrams which violates the rules according to Okomoto *et al.* [117], but as his rules are for binary two-component phase diagrams, the same rules can not be applied on binary three-component phase diagrams. Still, it is advised to be skeptical to the phase diagrams in Figures 20-26.

The phase diagrams seem to change drastically with a 5 mol% increase of Fe. It looks like an increase in

Fe concentration decreases the need for a high Nd concenctration to form Nd-rich phases. In Figure 20 the phase with the highest Nd concentration, is the $NdAl_3$ phase which forms when there is at least 17 mol% Nd. This is a lot when comparing to the amount Nd found in a smart phone. Some of the Nd is lost to less Nd-rich phases, $NdFe_2Al_{10}$ and Nd_3Al_{11}.

The phase diagram with 10 mol% Fe, Figure 21, shows that to achieve the same phases, $NdAl_3$, $NdFe_2Al_{10}$ and Nd_3Al_{11}, the concentration of Nd does not need to be higher than 12.5 mol%, which is a significant decrease comparing to the phase diagram with 5 mol% Fe, Figure 20. At 14 mol% Nd a new phase is formed, the Laves_C15 structure. The Laves_C15 structure has a high concentration of Nd, as it has a 2 to 1 ratio Al to Nd. Additional to the Laves_C15 structure, there are formed two phases containing Nd. However, at a higher Nd concentration less of these phases are formed.

In the phase diagram with 15 mol% Fe, Figure 22, the Laves_C15 structure is formed when there is less then 9 mol% Nd present. In addition to the Laves_C15 structure there is formed a phase containing Nd.

The phase diagram with 20 mol% Fe, Figure 23, the Laves_C15 structure is formed with 5 mol% Nd present, and at 10 mol% Nd present there are no other phases containing Nd.

In the phase diagram with 25 mol% Fe, Figure 24, the Nd concentration required to form the Laves_C15 structure has decreased compared to previous phase diagrams. It is only required roughly 4 mol% Nd to form the the Laves_C15 structure without any other phases containing Nd.

At 30 mol% Fe, Figure 25, the Laves_C15 structure is formed without any additional phases containing Nd. This means all the Nd present in the system directly forms the Laves_C15 phase.

The increase to 35 mol% Fe has no effect on the formation of the Laves_C15, as shown in Figure 26.

There is, according the phase diagrams, not a concern if the melt has a high Fe concentration, as the Fe seems to enable the formation of Nd-rich phases at low Nd concentration. It would rather seem that the desired Fe concentration would be between 30-35 mol% Fe for the formation of Nd-rich phases and the Laves_C15 structure.

To the authors' knowledge no research has been done on how the Nd-Al Laves_C15 structure might be leached, but according to Jin *et al.* [119], the Laves_C15 structure is a very stable intermetallic, which could be of interest if the next step is to recover the Nd by leaching. It is therefore believed that it is possible to up-concentrate Nd with Al as Nd-Al Laves_C15 and recover it.

6.3 Trial 1: Dissolution of NdFeB Magnets

The goal for this trial was to see if the NdFeB magnets would dissolve in molten Al. If to calculate the dissolution of NdFeB magnets, it would contain too many assumptions, as there was not enough information available.

In the initial tests the magnets didn't completely dissolve, but it made it possible to see the process of magnets dissolving.

6.3.1 Sample 1.K

Figure 27 shows a magnet that is not dissolved. The light gray area in the picture is the magnet, the magnet's coating is the bright boundary around the magnet and the dark gray is the Al matrix.

The thickness of the Ni coating is between 8 μm and 12 μm. Figure 27 shows that the corner is affected more than the rest of the magnet. In Figure 27, the Ni-coating is intact except for at one point, where the Al is in contact with the NdFeB magnet beneath the Ni-coating. This may be caused by a defect in the coating, which in turn can speed up the dissolution process of the NdFeB magnet.
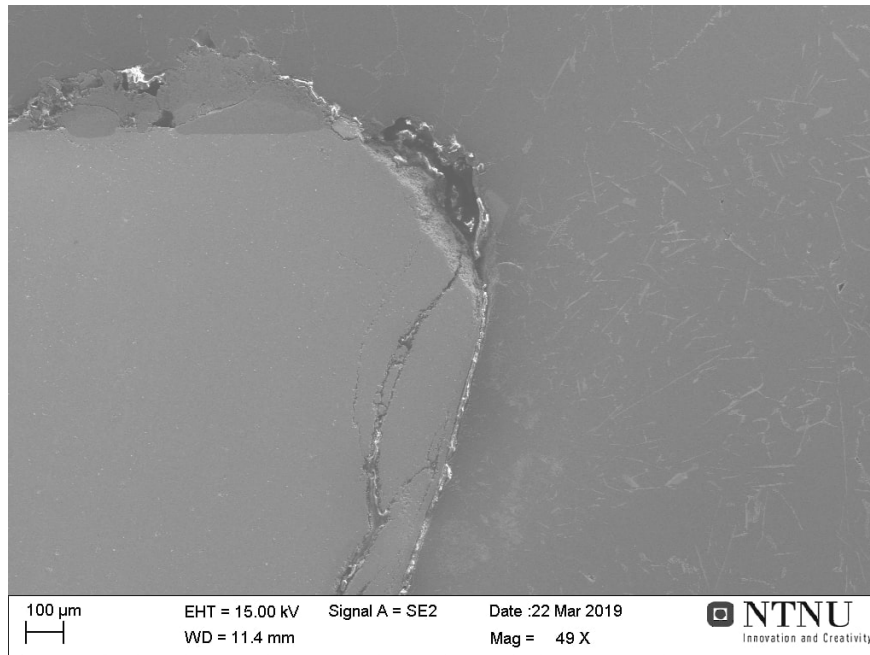
Figure 27: *The light gray area in the picture is the magnet, the magnet's coating is the bright boundary around the magnet and the dark gray is the Al matrix. The picture is taken at 49x magnification with SEM SE.*

The analysis has shown 3 different phases present in 1K, as seen in Figure 28, their composition is presented in Table 11.
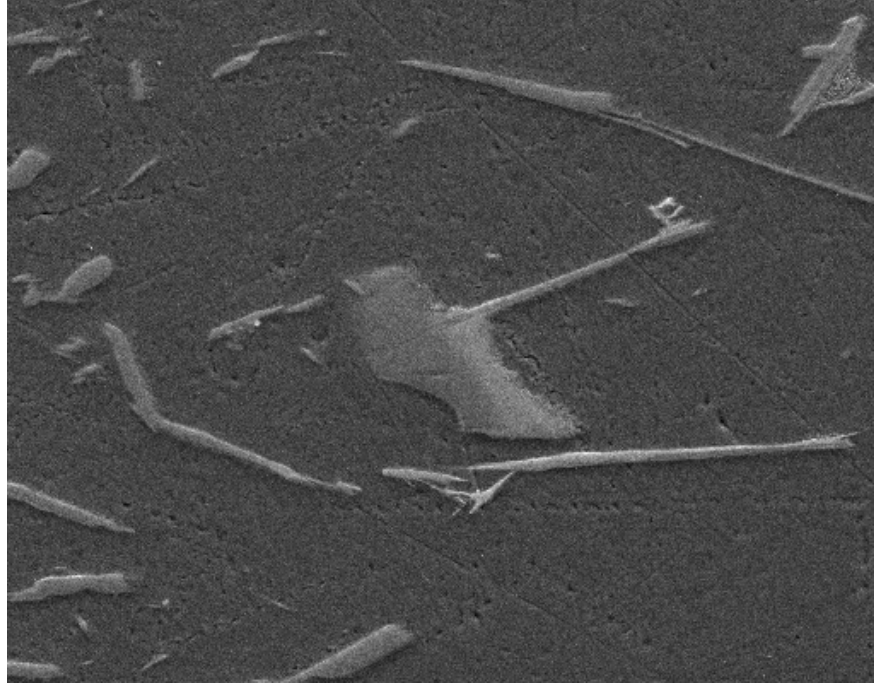
Figure 28: *Phases present in sample 1.K. The Fe-rich phase is the dark gray intermetallic, the matrix is the darkest phase and the Nd-rich phase is the brightest.*

Table 11: *The composition of the 3 phases and intermetallics present in sample 1.K, Figure 28. All numbers are in mol%. The EDS report is found in appendix C.*

Element	Fe-rich phase	Matrix	Nd-rich phase
Al	77.97 %	99.80 %	76.23 %
Pr	0.01 %	0.01 %	1.84 %
Nd	0.03 %	0.02 %	6.36 %
Fe	20.62 %	0.08 %	12.80 %
Ni	1.18 %	0.04 %	2.34 %
Cu	0.19 %	0.05 %	0.44 %

The phases and intermetallics seen in Figure 28 contain Nd, Fe and Pr, which is found on the inside of the Ni-coating. This indicates that some of the NdFeB magnets have dissolved, creating intermetallics, which have floated away due to stirring, created by the magnetic field from the electromagnetic coil. The magnets in this trail was submerged for 0.6 hours and that is not enough time to fully dissolve the NdFeB magnets at 800 °C when the magnet is coated with Ni.

6.4   Trial 2: 5 mol% Iron

The goal for this trial was to see if the electromagnetic field of the coil would influence the particles in the molten Al, making it possible to use electromagnetic separation to separate Nd-rich particles from the Al matrix. It also aims to confirm the phase diagrams, indicating that increasing Fe concentration enables the formation of the Laves_C15 structure. This trial will be compared to the trial using 35 mol% Fe.

6.4.1   Sample 2.1 and 2.2

The time after the last metallic Nd was added to the melt, to the melt started to solidify, was measured to be 3 hours and 51 minutes. After the samples were cut into pieces it was discovered that the metallic Nd had not completely dissolved, as shown by Figure 29. This made the Nd concentration lower than the calculated 5 mol% Nd, while increasing the Fe concentration slightly.

Figure 29: *A piece of metallic Nd not completely dissolved during the trial, close to the bottom of the sample.*

Figure 30 shows the microstructure of sample 2.1, which was collected before the crucible was moved to the electromagnetic coil. Figure 31 shows the microstructure of sample 2.2, which was collected 1.5 minutes after the crucible was moved to the electromagnetic coil. The temperature of the melt when collecting sample 2.1 was 800 ℃, while the temperature when collecting sample 2.2 was already down to 760 ℃. According to the phase diagram, Figure 20, this should not form any new or different phases. The same four phases and intermetallics, with very similar compositions, are found in both samples. Table 12 and 13 shows the composition of the phases.
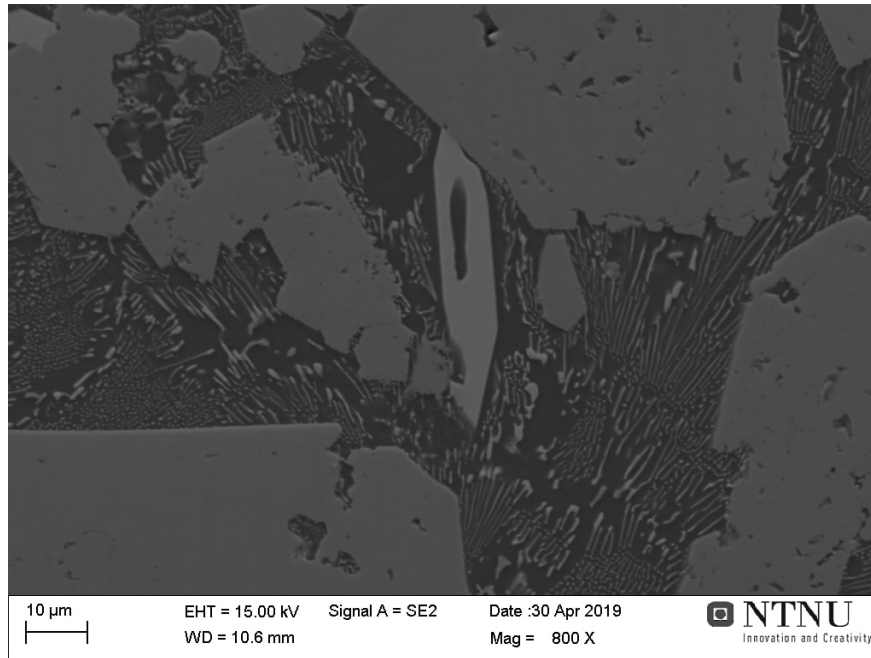
Figure 30: *The microstructure of sample 2.1, taken at 800x magnification with SEM SE*
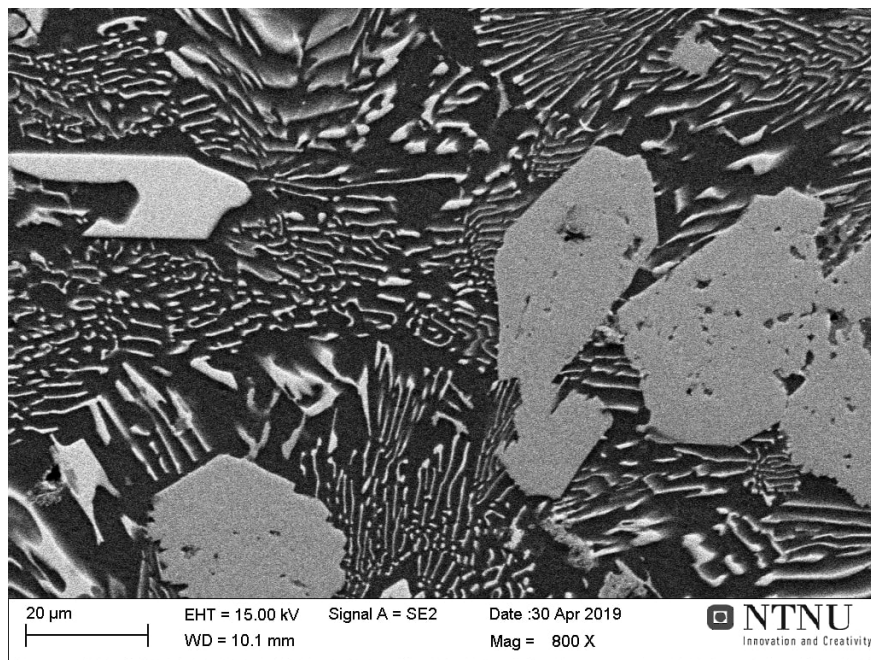
Figure 31: *The microstructure of sample 2.2, taken at 800x magnification with SEM SE*

Figure 32 shows where the different EDS, point and area, analysis were conducted, in sample 2.1. The different phases mainly compose of Al, trace amounts of Pr, with varying content of Nd and Fe. The composition is presented in table 12.
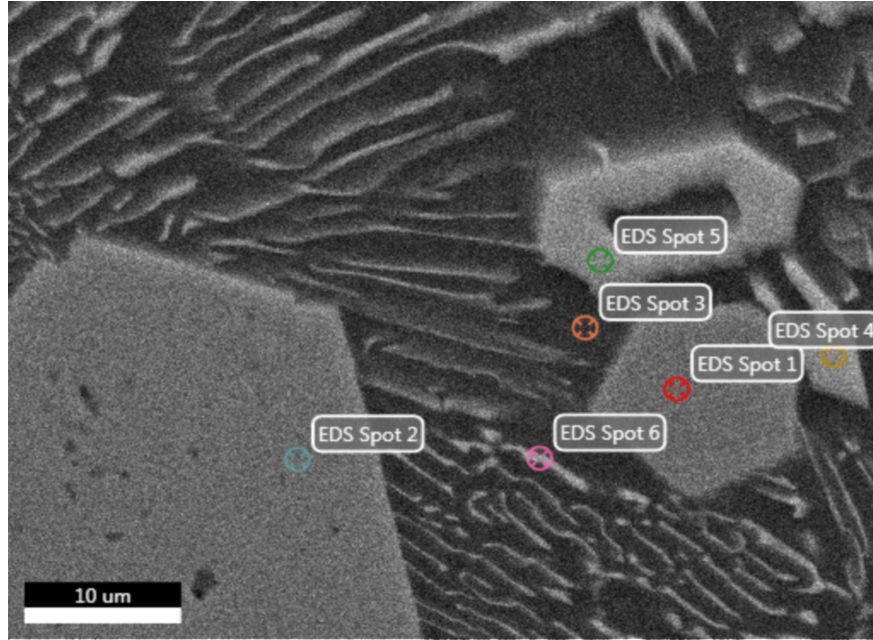
Figure 32: *Area used for the EDS analysis of sample 2.1. The figure shows where the different EDS, point and area, analysis were conducted.*

Table 12: *The composition of the different phases found in sample 2.1. All numbers are in mol%. The EDS report is found in appendix D.*

Element	Spot 1	Spot 2	Spot 3	Spot 4	Spot 5	Spot 6
Al	78.62	78.72	98.59	81.99	83.40	96.80
Pr	0.24	0.21	0.08	0.63	0.61	0.13
Nd	7.08	7.06	0.87	16.95	15.63	2.86
Fe	14.06	14.01	0.46	0.43	0.36	0.22

In sample 2.2 there are four phases and intermetallics as shown in Figure 33. The different phases mainly composes of Al with trace of Pr, and the Nd and Fe concentration varies as shown in Table 13.
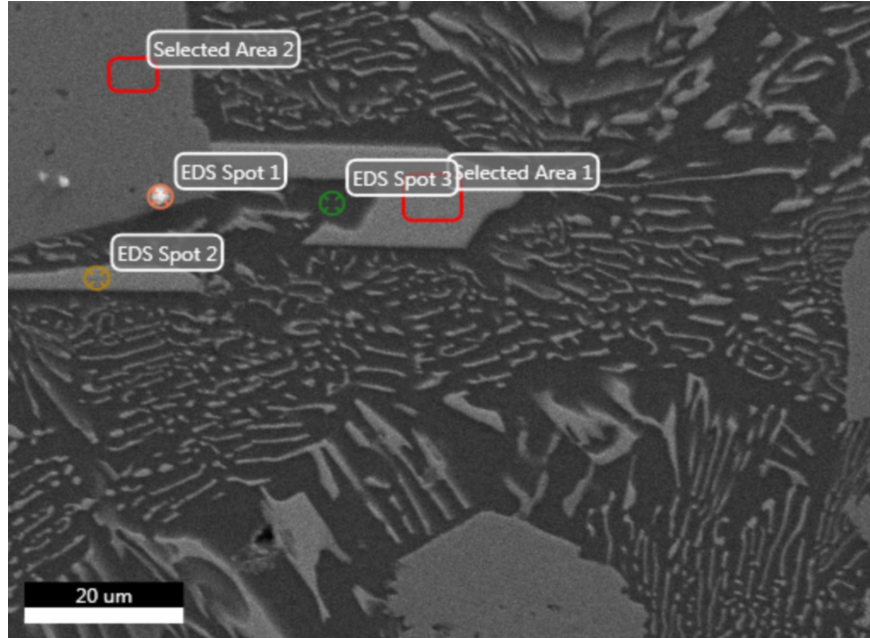
Figure 33: *Area used for the EDS analysis of sample 2.2. The figure shows where the different point and area analysis were done.*

Table 13: *The composition of the different phases found in sample 2.2. All numbers are in mol%. The EDS report is found in appendix E.*

Element	Area 1	Area 2	Spot 1	Spot 2	Spot 3
Al	79,25	78,34	87,04	79,42	79,08
Pr	0,77	0,33	0,32	0,81	0,84
Nd	19,77	7,36	4,58	19,44	19,86
Fe	0,20	13,96	8,06	0,33	0,21

Spot 1 and 2 in Figure 32, is the same phase as area 2 in figure 33. According to Table 12 and 13 the compositions of the phase is similar in both samples. This phase is rich in Fe and according to the EDS analysis Fe is mainly contained in this phase. The phase contains roughly 7 mol% Nd, but in sample 2.2, the Nd concentration is slightly higher in this phase compared to sample 2.1. This is within the margin of error, and is not believed to be an effect of the electromagnetic field of the coil.

EDS analysis of spot 3 in Figure 32, Table 12, shows a high Al concentration and the presence of the other elements is low. This is the matrix. However, EDS analysis of the matrix, spot 3 Figure 33, should show a similar composition, but it is showing the same composition as area 1 from Figure 33. This might be an error caused by the resolution of the EDS analysis, as spot 3 shows the same composition as the intermetallic in area 1, Figure 33.

Spot 4 and 5 in Figure 32 have roughly the same concentration, Table 12, as area 1 and spot 2, Table 13, in Figure 33. In sample 2.1 the phase has a slightly higher Al concentration and a lower Nd concentration than the same phase in sample 2.2. The difference in composition is within the margin of error, and is not believed to be caused by the electromagnetic field of the coil.

EDS analysis of spot 6 in Figure 32 indicates that this phase has approximately the same composition as the Al matrix, but with a higher concentration of Nd. The Nd concentration is believed to be higher and the Al concentration is believed to be lower, as the physical dimension of the phase is small and the spot analysis might include some of the Al matrix.

Spot 1 in Figure 33 has a lower concentration of Fe and Nd, but a higher concentration of Al, than the phase surrounding it. The spot is brighter compared to the phase around it, but from the composition it

should appear darker than heavier phases. The spot can appear brighter if the spot is elevated from the rest of the sample, it is therefore believed that this spot is a part of the matrix which has detached from the sample.

6.4.2   Sample 2K

The remaining melt was cooled and solidified inside the electromagnetic field of the coil. In the picture taken of the solidified melt, Figure 34, a colour difference between the outer and inner areas of the dross can be observed. Close to the edge, the dross has a darker gray colour, than in the center, where the dross is bright gray.

Figure 34: *Picture of the remaining melt, after cooling inside the electromagnetic field of the coil. The picture is taken from above. The dross has a different colour closer to the edge than towards the center.*

Sample 2.K was cut from the solidified piece and there were found four different phases. The composition of the phases found in sample 2K are shown in Table 14. The Fe-rich phase is only observed within the Fe-poor phase, as seen in the middle of Figure 37.

Table 14: *The composition of the different phases found in sample 2K. All numbers are in mol%. The EDS report is found in appendix F.*

Element	Nd-rich phase	Fe-rich phase	Fe-poor phase	Matrix
O	11.35	10.70	12.79	8.64
Al	71.22	70.80	79.92	91.08
Pr	0.77	0.17	0.32	0.06
Nd	16.57	2.46	4.73	0.12
Fe	0.09	15.87	2.24	0.10

Figure 35 shows where the SEM pictures in Figures 36-39 of sample 2K were taken. There is a clear
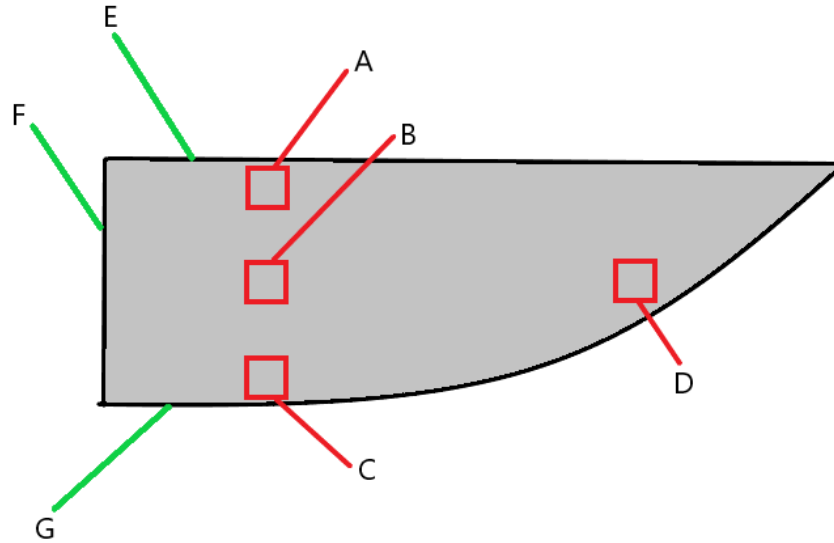
Figure 35: *An overview of where the pictures in Figure 36-39 were taken on sample 2K. The picture in Figure 36 was taken in area A, Figure 37 was taken in area B, Figure 38 was taken in area C and Figure 39 was taken in area D. Line E represents the dross, line F is close to the center of the solidified melt and line G is where the sample was in contact with the crucible.*

variation in the amount of different phases present in Figures 36-39.

Figure 36 shows the microstructure of sample 2K, close to the dross. There are some Fe-poor and Nd-rich phases, but mostly Al-rich matrix.

Figure 37 displays the microstructure of sample 2K in the middle of the sample. The amount of phases present in area B is higher than in area A, which is closer to the top of the sample. Figure 38 displays the microstructure of sample 2K in area C, close to the bottom of the sample. The amount of phases present here is higher than in area A and B. It seems that there is an increase in Fe-rich and Fe-poor phases.

Figure 39 shows the microstructure of sample 2K in area D, close to were the melt was in contact with the crucible. The amount of phases is higher than in A and B, and is roughly the same as area C.
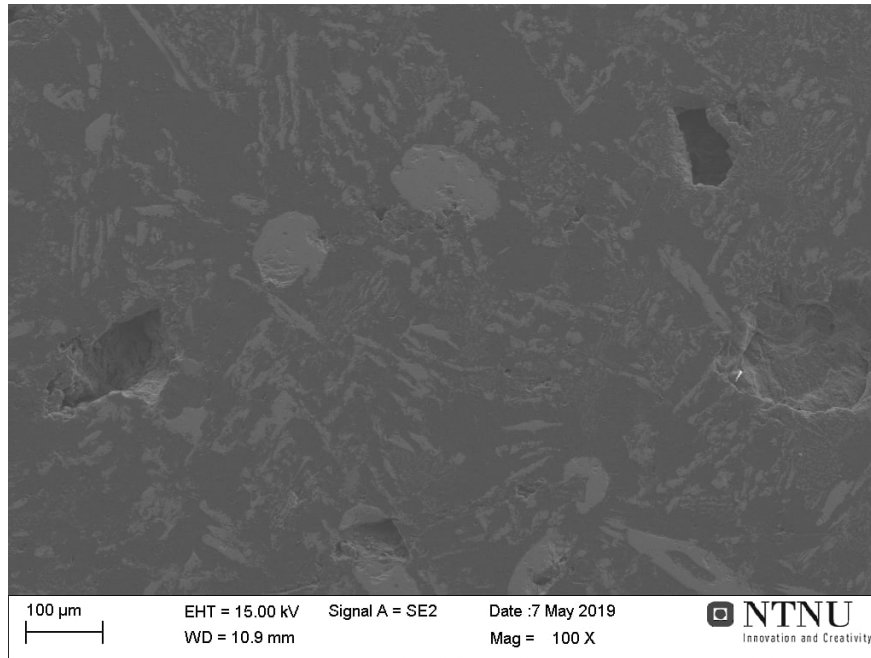
Figure 36: *SEM, SE image of sample 2K in area A, close to the top of the sample. 100x magnification*
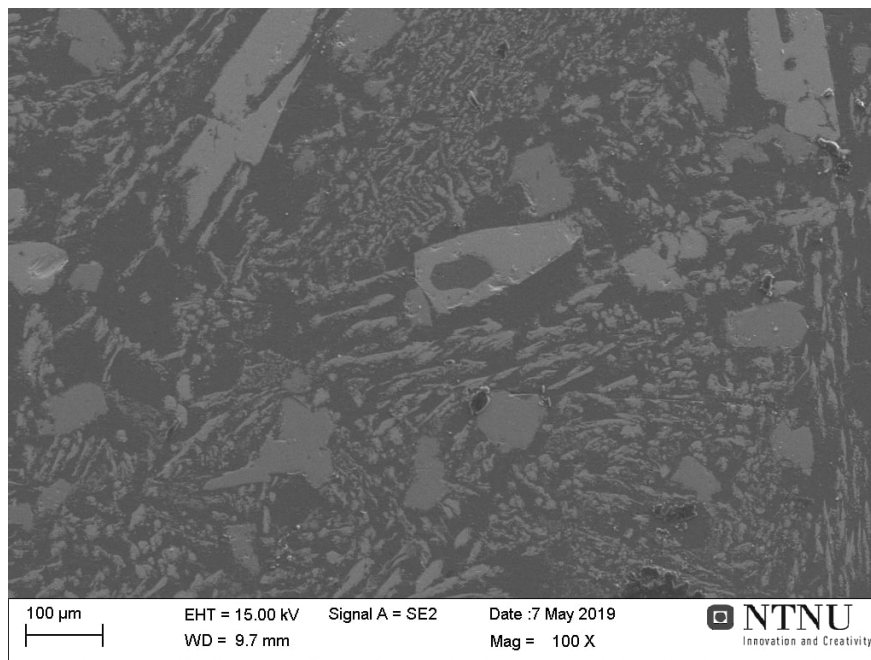
Figure 37: *SEM, SE image of sample 2K in area B, close to the middle of the sample. 100x magnification*
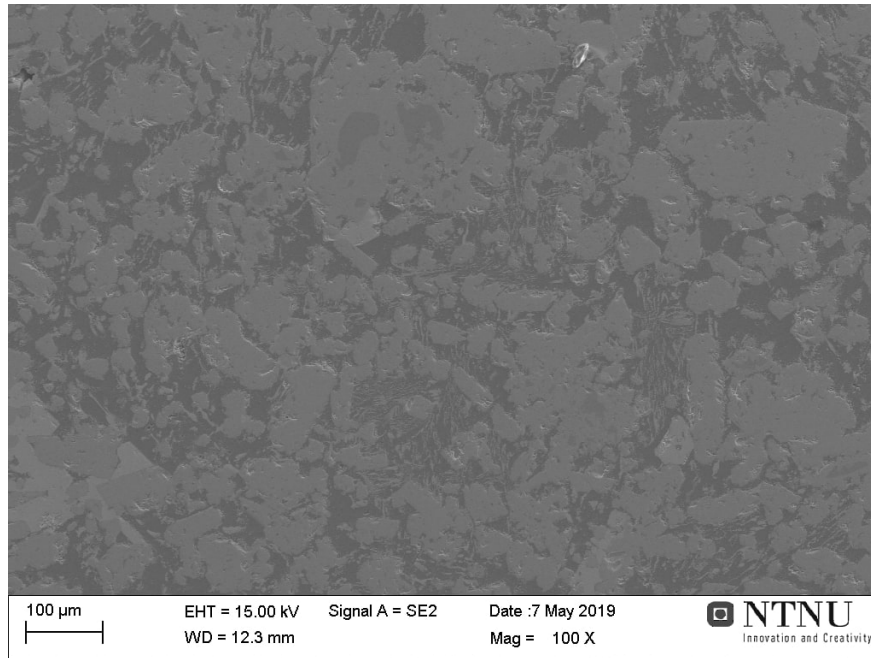
Figure 38: *SEM, SE image of sample 2K in area C, close to the bottom of the sample. 100x magnification*
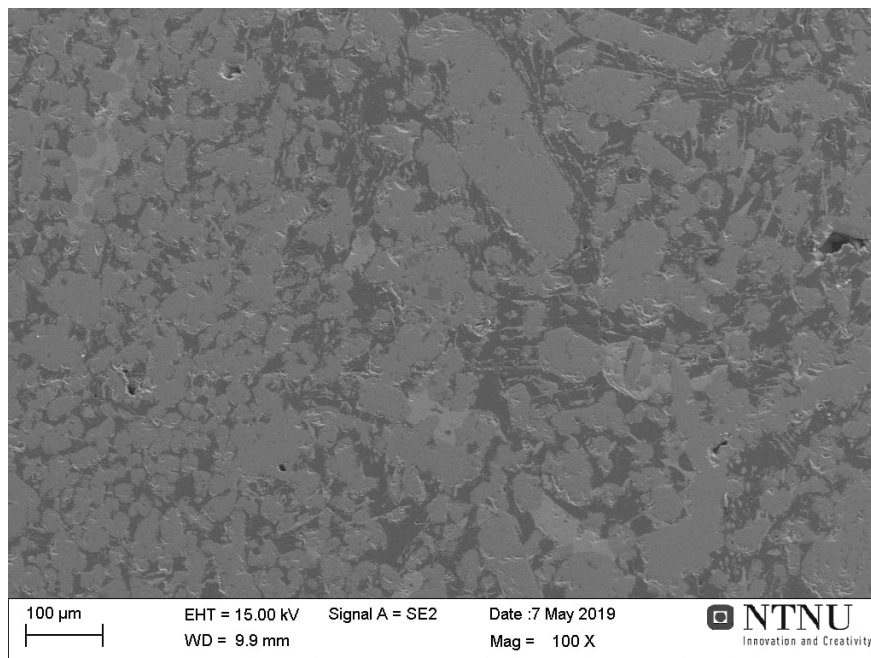
Figure 39: *SEM, SE image of sample 2K in area D, close to the crucible wall of the sample. 100x magnification*

The amount of phases is higher close to the edge of the sample. If the amount of phases was related to the cooling of the sample, there should be a difference in the amount of phases present in areas A and B from Figure 35. The amount of phases present in area A would be more similar to area C and D. There are some possibilities to why this happens:

Gravitational forces may be the cause of the higher amount of Fe-rich and Fe-poor phases close to the

bottom and edge. The Fe-poor and Fe-rich phases settle at the bottom of the crucible and the induced Lorentz forces may not be strong enough to stir the melt homogeneous.

The phase formation could be affected by the crucible wall, making the formation of the Fe-rich and Fe-poor phases easier in that area.

Magnetic separation could be a possible explanation. The Fe-rich and Fe-poor phase may have a lower conductivity than the rest of the melt, resulting in a magnetic separation of the melt. The microstructure in sample 2.1 and 2.2 is similar to the microstructure found in the middle of sample 2K. Figure 30 and 31 are at a different magnification and may not representable for the sampled area.

Because of this, a conclusion about the effect the electromagnetic field of the coil has on the melt can not be drawn.

6.5   Trial 3: 35 mol% Iron

This trial aims to confirm the phase diagrams, Figures 20-26, indicating that increasing Fe concentration enables the formation of the Laves_C15 structure at a low concentration of Nd. The comparison of trial 2: 5 mol% Fe and trial 3: 35 mol% Fe, will be done and discussed in this section.

In this trial the IF75 was used, because the muffle furnaces can not reach the required temperature of >1000 °C, to keep the metal liquid when the concentration of Fe is significantly increased. According to the phase diagram, Figure 26, the required temperature should not be higher than approximately 1150 °C. In this trial the temperature had to be increased to more than 1400 °C to keep it molten. The mushy zone extended from below 1000 °C up to 1400 °C. The phase diagram does not include all the trace elements, and the NdFeB magnets bought from Clas Ohlson can have a different composition when comparing to the earlier used NdFeB magnets, supplied by Supermagnete. It is possible that the trace elements can increase the melting temperature and form additional phases. Another explanation can be found from the equilibrium requirements of the calculated phase diagrams. If the melt is not at equilibrium, the melting temperature can be higher. It is also considered possible that there are unknown formations of intermetallic phases with high melting temperatures.

6.5.1   Sample 3.1 and 3.2

Sample 3.1 was collected when the temperature of the melt was approximately 1350 °C, 10 minutes prior from when sample 3.2 was collected and the metal was cast. The metal was cast into a copper mold. Sample 3.1 and 3.2 were taken at different times, but the microstructure is the same for both samples, as shown by Figure 40 and 41. There were no signs of NdFeB magnets or metallic Nd when the cast was cut into pieces. Its therefore believed that the Nd and the NdFeB magnets were fully dissolved in the Al and that the concentration of Fe and Nd reached respectively 35 mol% and 5 mol%.
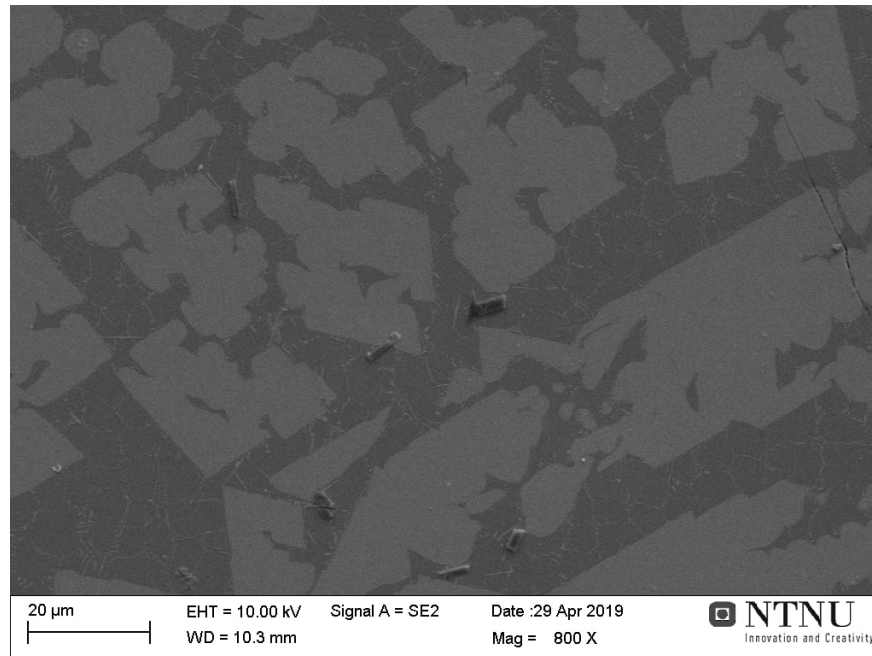
Figure 40: *SEM, SE image of sample 3.1. 800x magnification.*
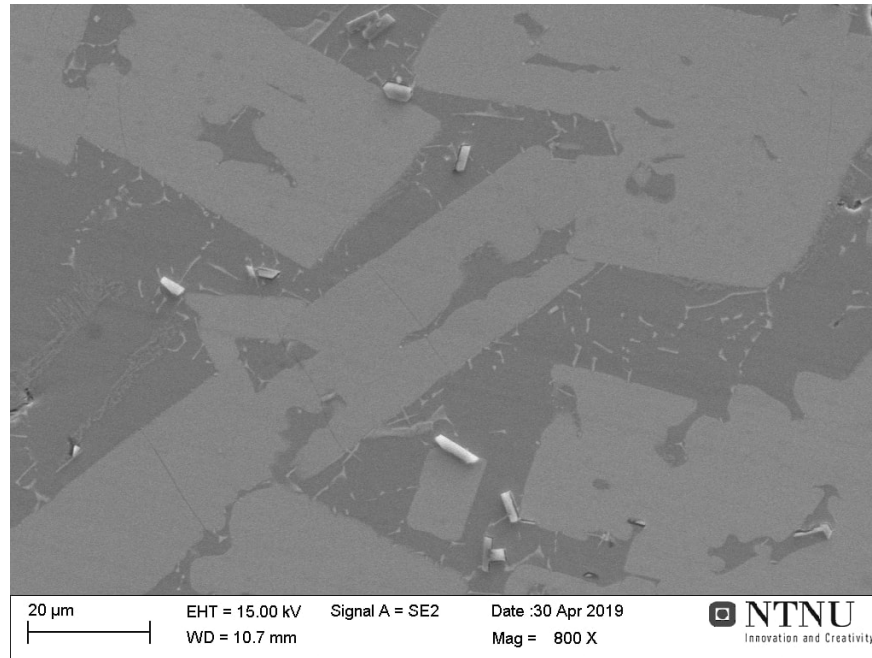
Figure 41: *SEM, SE image of sample 3.2. 800x magnification.*

Four different phases and intermetallic phases were found in sample 3.1 and 3.2, as well as some particles. The Nd-rich phase is the brightest phase, the Fe-rich phase is the larger grey phase, the matrix is the dark grey area and the rest is the script phase, small white lines within the matrix. All four phases are visible in Figure 40 and41. The composition of the four phases found in sample 3.1 are given in Table 15 and the composition of sample 3.2 are given in Table 16.

Table 15: *The composition of the different phases found in sample 3.1. All numbers are in mol%. The EDS report is found in appendix G.*

Element	Nd-rich phase	Fe-rich phase	Matrix	Script phase
O	2,01	-	-	-
Al	59,45	66,48	71,17	68,75
Pr	5,53	1,46	-	0,16
Nd	16,77	5,49	-	0,55
Fe	16,24	26,57	28,83	30,54

The concentration of Nd, Fe and Pr in the script phase, observed in sample 3.1 and 3.2 are expected to have a deviation from the actual concentration, shown in table 15 and 16, because of the size of the phase. The measured EDS spot utilizes an area larger than the script phases and probably that the EDS scan also measure some of the matrix surrounding the script phase, hereby increasing the Al concentration.

Table 16: *The composition of the different phases found in sample 3.2. All numbers are in mol%. The EDS report is found in appendix H.*

Element	Nd-rich phase	Fe-rich phase	Matrix	Script phase
Al	57,46	65,25	70,86	68,91
Pr	5,30	1,54	-	0,90
Nd	15,63	5,92	-	2,13
Fe	21,61	27,30	29,14	28,07

6.5.2 Sample 3.3

Sample 3.3 is the dross removed before sample 3.1 and 3.2 were collected. Figure 42 shows that the size of the intermetallics and phases found in sample 3.1 and 3.2 are larger close to the dross layer.
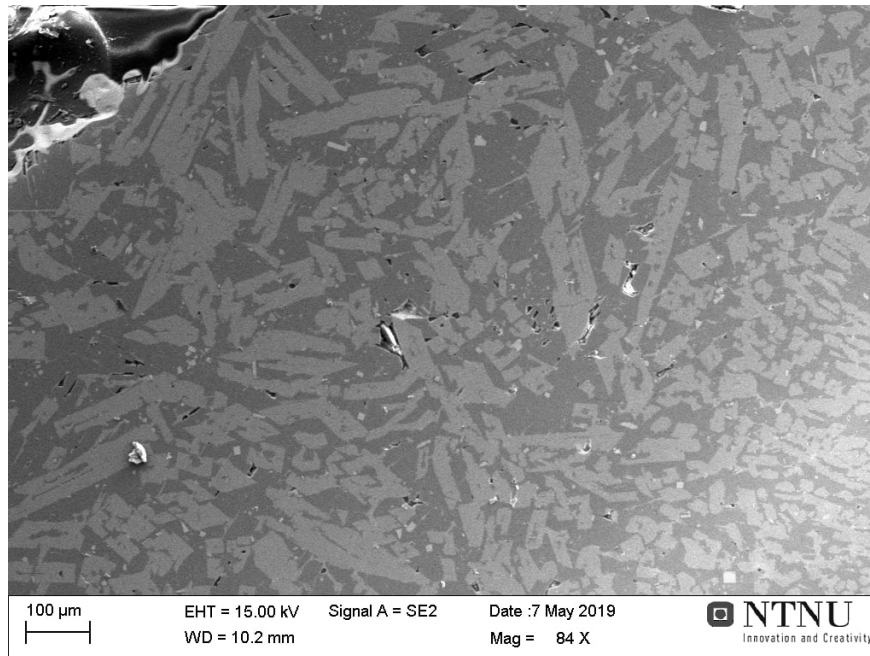
Figure 42: *SEM, SE image of sample 3.3 close to the dross layer. 84x magnification.*

Three different phases were found in sample 3.3, a Nd-rich phase, a Fe-rich phase and the matrix. Their composition is given in table 17. The Nd-rich phase is the only phase containing B. The concentration of B is high in this area of the the melt and it is possible that B is accumulating close to the dross layer.

Table 17: *The composition of the different phases found in sample 3.3. All numbers are in mol%. The EDS report is found in appendix I.*

Element	Nd-rich phase	Fe-rich phase	Matrix
B	85,44	-	-
O	4,73	9,41	6,67
Al	2,22	62,49	71,90
Pr	1,56	1,07	-
Nd	4,65	4,89	-
Fe	1,41	22,14	21,44

6.5.3 3K

Sample 3K is a sample of the cast metal, cooled at room temperature. Sample 3K is very brittle and there are cracks and holes, which were filed with epoxy during sample preparation, as shown in Figure 43. The epoxy appears dark and shiny as the epoxy does not conduct current and therefore gets charged by the electron beam of the SEM.

There is a bright phase which mainly consists of O, Al, Nd and Pr, as shown in Table 18. The bright phase is mainly oxides which do not conduct electricity, explaining the charging of the phase. The composition of the bright phase is different from the composition of the dross layer in sample 3.3, and any other phases close to the slag phase.
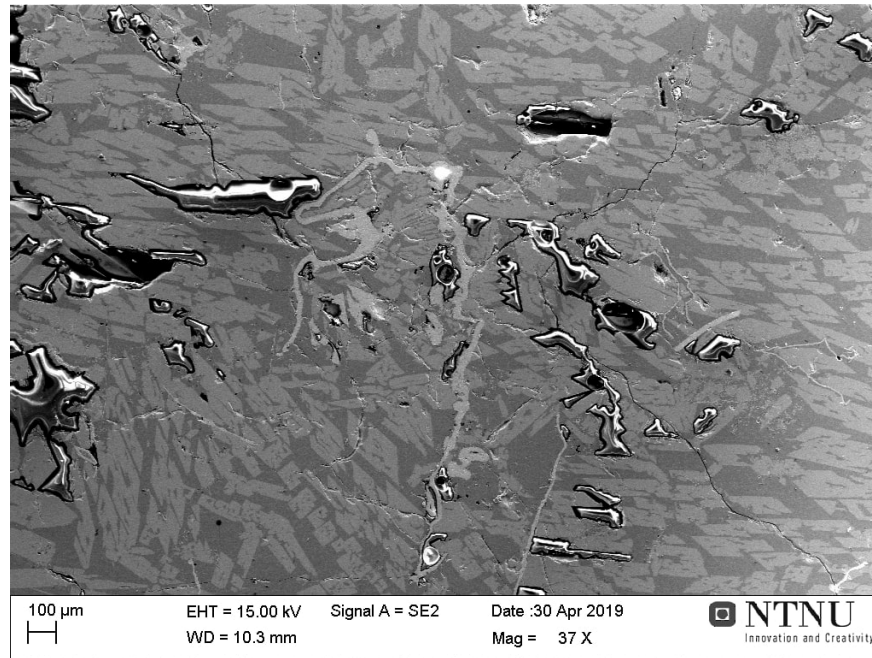
Figure 43: *SEM SE image of sample 3K at 37x magnification. The dark and shine areas are holes filled with epoxy. The bright phase in the middle of the picture is a O-, Nd- and Pr-rich phase.*

Table 18: *The composition of the different phases found in sample 3.3. All numbers are in mol%. The EDS report is found in appendix J.*

Element	Oxide phase	Matrix	Fe phase
O	58,18	-	-
Al	23,18	70,82	65,59
Pr	3,96	-	1,41
Nd	14,33	-	5,84
Fe	0,35	29,18	27,16

There is the possibility that it could be an already existing phase that has oxidized, but if the oxygen is excluded from the composition, Table 19, the phases has not the composition of the other phases found in trial 3. The phase has a high concentration of Nd and Pr, which are up-concentrated as oxides, together with oxidized Al.

Table 19: *The composition of the oxide phase, when oxygen is excluded from the EDS analysis.*

Elements	mol%
Al	55.41
Pr	9.48
Nd	34.26
Fe	0.85

6.5.4   Comparison of trial 2: 5 mol% Fe and trial 3: 35 mol% Fe

There was found no trace of the Laves_C15 structure, in either trial 2 or 3. This could be due to that the required time to reach equilibrium was not met, not giving the Laves_C15 structure enough time at elevated temperatures to form.

The main difference in the composition of the phases found in sample 2.1 and 2.2 from the phases found in 3.1 is the Fe content of the phases, and the presence of O. It seems that the samples collected at higher temperatures have oxidized more, which is to be expected. The Nd-rich phase in 2.1 has a Fe Concentration of 0.43 mol%, but in sample 3.1 the Fe concentration of the Nd-rich phase is 16.24 mol%. The Nd concentration in sample 2.1 and 3.1 is 16.95 mol% and 16.77 mol% respectively. This can be explained by the much higher Fe concentration in trial 3. The phase with the highest Nd concentration was found in sample 2.2, with a concentration of 19.86 mol%

In sample 3K, a Nd-rich oxide phase was found. This phase is not found in sample 2.1, 2.2, 2K, 3.1, 3.2 or 3.3, only in sample 3K. If the oxygen is excluded from the composition, the phase does not match any of the other phases found in sample 2.1, 2.2, 2K, 3.1, 3.2 or 3.3.

6.6   Trial 4: Dissolution of Neodymium Oxide

The goal for this trial was to see if the Nd_2O_3 would dissolve in the molten Al and if there was a possibility to substitute the magnets with the oxide powder.

The Nd_2O_3 packages did not submerge in the melt, and when they were pressed down into the melt they burst open. The Nd_2O_3 floating on the top did not seem to react with the Al at 800 °C. The temperature was then raised to 1000 °C, which did not cause any reaction. This could mean that Nd can not be recovered when it oxidizes by use of an Al bath. This makes it especially important to use a protective gas and to make sure that the added Nd is fully submerged before the Nd can oxidize. Nd-magnets are coated and there are added dopants to reduce the oxidation [17], meaning that oxidation is a problem with the magnets. If the magnets are broken or the coating is damaged there is a risk that some amount of the Nd in the magnets have been oxidized. The amount Nd that has oxidized could be considered as small, but oxidation will still impact the recovery rate of Nd negatively. If the Nd is recovered as Nd_2O_3, energy intensive processes are required to produce metallic Nd.

The magnets used in previous trials were coated with Zn or Ni. When trying to dissolve the magnets, the Ni coating was protecting the magnets which slowed down the dissolution process. Magnets used with Zn was not used in low temperature trials, but Zn has a low melting point and should not be as difficult to dissolve in Al at 800 °C. NdFeB magnets have a high melting point and are mechanically hard alloys which are not easily dissolved in Al.

The magnets was pre-treated at 350 °C to demagnetize them. According to Kyriakopous *et al.* [6] a piece of Al oxide blocked the dissolution process. If Ni oxide has the same effect on the dissolution process as Al oxide, the pre-treatment of the magnets could have increased the dissolution time significantly. As shown in Figure 44 there is some oxygen present around the Ni coating which indicates that the Ni coating has oxidized.
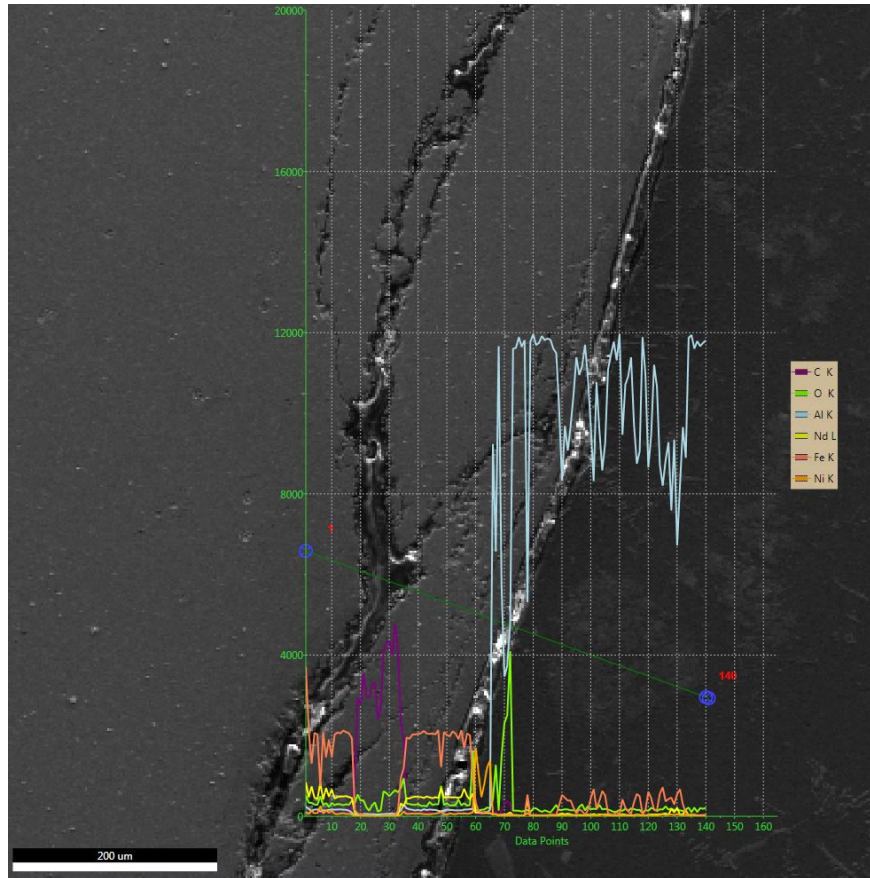
Figure 44: *EDS line scan of a NdFeB magnet which has not dissolved in the Al. On the right is the magnet and on the left is the Al matrix. The border in between the magnet and the Al is the Ni coating. The area around the coating contains oxygen which indicates that the Ni has oxidized.*

Either way, the Ni coating has some big disadvantages if Nd-magnets are recycled with molten Al, and if there are no big drawbacks by coating the Nd-magnets with Zn this should be done instead, as the Ni coating increase the dissolution time. An increase in dissolution time would increase the amount of energy the process need and in turn would give this process a higher CO_2 footprint.

6.7 Trial 5: Printed Circuit Boards

One of the main components in WEEE are the PCBs. Seeing how they behave when they are submerged in molten Al is critical for further testing with PCBs. It is also to see if the electromagnetic field of the coil had any effect on the submerging of PCB.

6.7.1 Trials with and without a Fume Hood

Two different trials were done with the submerging of PCBs in molten Al. One trial was with a fume hood in a protective atmosphere and the melt was in the electromagnetic field of the coil. The other trial was conducted without the fume hood, Ar and the electromagnetic field. The only difference between the trials was the amount of PCBs added. In the trial without the fume hood, the temperature fell quicker and the melt solidified before all of the PCB pieces could be added.

In both trials the PCBs were incinerated the instance they came in contact with the molten Al. The oxygen concentration was high enough to allow the PCBs to incinerate and the surface tension of the Al made the PCBs float on top of the melt. When pushed down in the melt, the PCBs floated back to the top and started burning again. There was observed no difference in the behavior of the PCBs with or without the electromagnetic field of the coil.

6.7.2 Submerging of Printed Circuit Boards

The amount of metal dissolved in the melt, compared to the amount of metal oxidized is not known, but it is believed that the oxidation of metal is a major problem. To reduce the amount of metal oxidized the PCBs should be submerged in the Al as quickly as possible, making the contact time with oxygen as short as possible. One of the difficulties found with submerging the PCBs in addition to the high the surface tension, was the generation of a thick oxide layer after the first PCBs were added. The oxide layer can come from the oxidation of metals, but it can also come from the pre-existing oxides found in the PCBs. About 30 % of the PCB is ceramics [9]. Either way, the thick oxide layer may be of some concern if there are to be added a lot of PCB into a small amount of Al, or if the surface of the crucible is small, compared to amount of PCB added. Another problem encountered when submerging the PCBs was that the glass fiber, found in some types of PCBs, accumulated beneath the oxide layer. This made it even more difficult to submerge the PCBs. Figure 45 and 46 shows the fiberglass found in the crucible. The Al has done limited damage to the glass fibers.
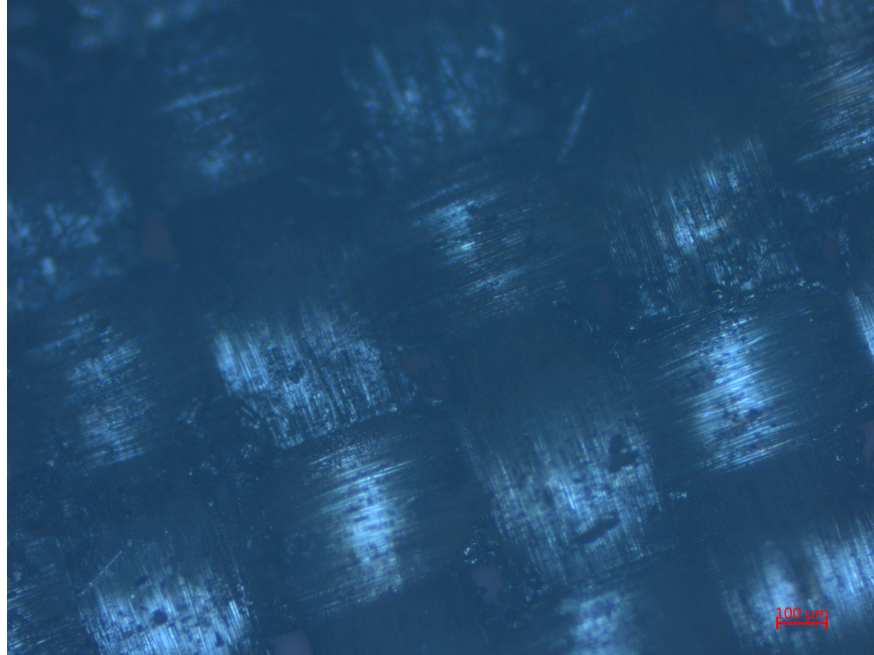
Figure 45: *Sample of glass fiber taken from the top of the crucible. The glass fiber is unharmed and there is little Al stuck to the glass fiber. The picture is taken with light microscope with 5x zoom.*
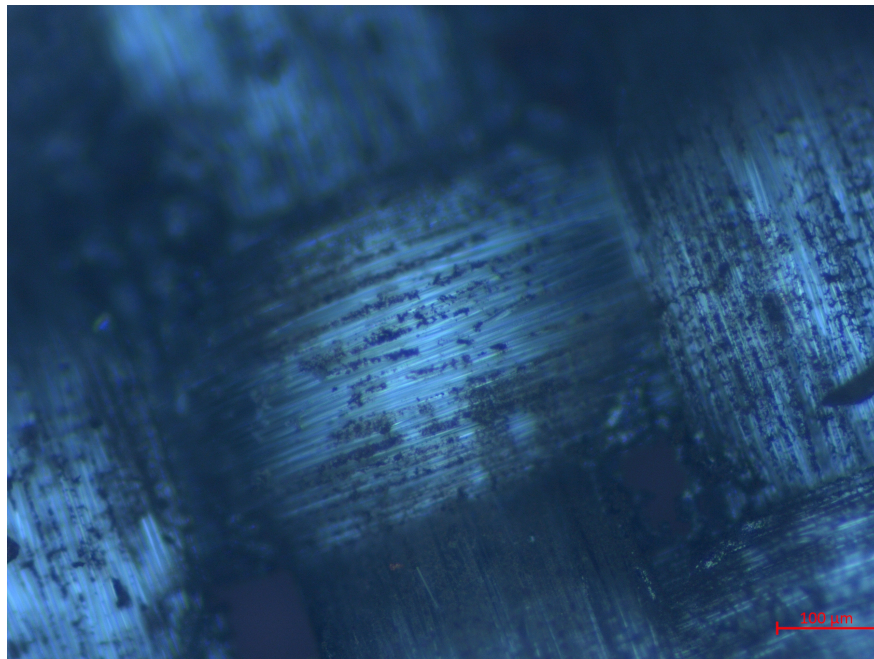
Figure 46: *Removed PCB from the second trial. The glass fiber is unharmed and there is little Al stuck to the glass fiber. The picture is taken with light microscope with 10x zoom.*

6.7.3   Dissolution of Metals

At 700 °C, the glass fibers do not dissolve or break down, but stay intact. The Cu found between the fiberglass is then protected from the Al, making the dissolution of the Cu difficult if the PCB pieces are too large. In Figure 47 there is visible Cu trapped in between the fiberglass layers.

Figure 47: *Cross section of a solidified sample with a PCB trapped in the Al. There is visible Cu between the fiberglass layers that has not dissolved because of the glass fibers.*

Most of the ECs has detached from the PCB or dissolved into the Al. Figure 48 shows a EC which has not detached or dissolved. The Al has been able to penetrate the EC, but not fully dissolved the EC. There is as well traces of organic materials trapped in the EC.

Figure 48: *Cross section of a solid sample containing a EC still connected to the PCB. There are traces of organic residue inside the EC.*

The melt was not held at high temperatures for a long time, giving only the metals with a lower melting

point then 700 °C time to dissolve. Metals with a higher temperature would need longer time to dissolve as the dissolution is governed by diffusion.

This paper doesn't go into the priming of Al or the reduction in the surface tension when it's affected by a magnetic field, but the 35 mT magnetic field generated by the coil in this trial is not sufficient enough to reduce the surface tension to such extent that the PCB sinks in the molten Al.

6.8   Trial 6: Smartphones

The goal of this trial was to see how smartphones behaved when they were submerged into molten Al, and to see if any phases contained a relatively high Nd concentration.

When the phones were submerged into the molten Al at 950 °C, the phones started to burn in a combustion reaction. When the fume hood was placed on the crucible, and Ar was used as a cover gas, there was no oxygen and the combustion reaction was replaced by pyrolysis decomposing of the organic material.

Some parts of the smartphones were stuck to the zirconia ceramic filter, Figure 49. It is mostly covers, screens and PCB remains, such as glass fiber, that are stuck to the zirconia ceramic filter. Most of the EC, organic material and metals are gone. This can explain why there are no glass fibers found in the samples, as was a problem in trial 5.

Figure 49: *The zirconia ceramic filter with remains of the smartphone and Al.*

In sample 6.K, Nd was found in a needle shaped phase, measuring $\sim 10\mu$m by $\sim 0,5\mu$m, as seen in Figure 50. EDS analysis of the phase shows that 95% of the phase composes of C, O, Bromine (Br) and Al, Table 20. The amount of Br in the phase is highly questionable as the EDS peak of Al and Br overlap each other. This means that the amount of Al could be higher than what is presented in Table 20. The phase contains 2.40 mol% Nd and 0.69 mol% Pr, which is a high concentration compared to the amount of Nd and Pr found in smartphones. The relatively high concentration of Nd and Pr present in the needle shaped phase, show that it is possible to up-concentrate Nd and Pr in molten Al, without any pre-treatment of the smartphones.
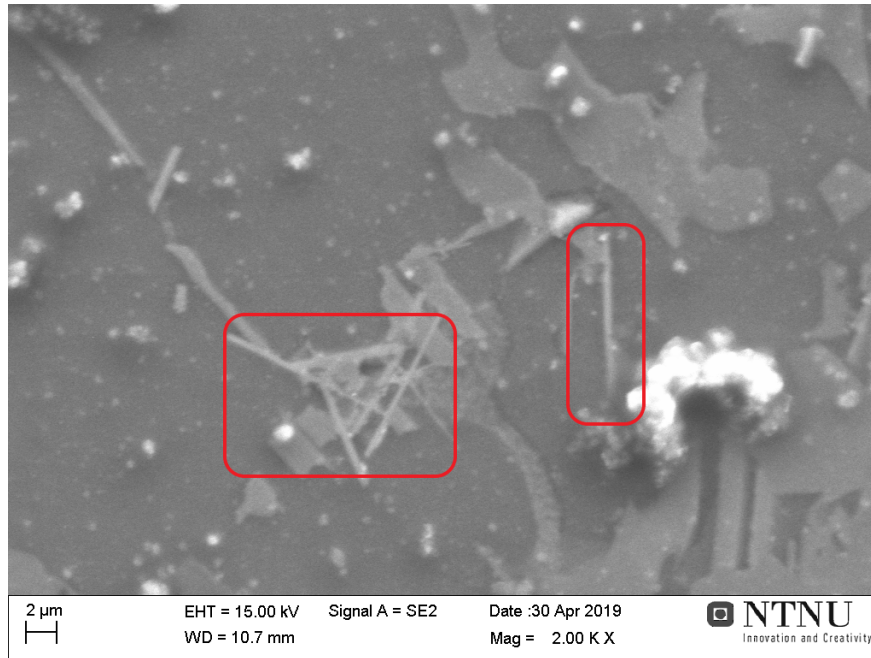
Figure 50: *SEM picture showing needle shaped phases highlighted in red*

Table 20: *Composition of the needle shaped phase. The EDS report is found in appendix K.*

Element	mol%
C	29.33
O	26.07
Br	19.60
Al	20.03
Si	6.47
Sn	1.32
Pr	0.69
Nd	2.40
Ni	2.40
Cu	4.61

7   Conclusion

According to the phase diagrams, Fe works as a catalyst for the formation of the Laves_C15 structure at low Nd concentrations. This is could not be confirmed by these trials, as there were found no Laves_C15 structure when the Fe concentration was increased.

It is possible to up-concentrate 5 mol% Nd into a phase with a concentration of 19.86 mol% Nd with liquid Al. A phase has also been found containing a high concentration of Nd and Pr oxides with low Fe concentration.

In the phase close to the dross is the only place B has been found.

A conclusion can not be drawn that the 35 mT electromagnetic field from the coil had any effect on the melt. There is a higher concentration of Fe-rich phases along the crucible wall, but it can not ensured that the concentration difference is caused by the electromagnetic field.

The 35 mT electromagnetic field is not strong enough to decrease the surface tension of Al sufficiently to submerge PCBs. This leads to oxidation of the PCBs when attempting to submerge PCBs into liquid Al.

The glass fiber found in some PCBs, can pose a problem to this method as the glass fiber accumulates on top of the melt, making the submerging of additional PCBs difficult.

The processes used for recycling of WEEE is today not suited for the recycling of REEs, as their primary focus is to extract PM and Cu. High REE concentrated fractions are treated as waste instead of a resource. The focus on REE recovery must increase.

8   Future Work

Many different adaptions and tests have been left for future work due to lack of time. If the author's had more time they would focus on these points.

It could be interesting and necessary to calculate the dissolution time of the NdFeB magnets in liquid Al. To look at the dissolution of the magnets coated with Ni and Zinc, and compare the two coatings to examine if the coating has a substantial impact on the dissolution time.

Calculating the time the system would need to reach equilibrium. This could confirm if the formation of Laves_C15 structure is a viable alternative for up-concentrating Nd, and other REEs, in molten Al. If the time to reach equilibrium is a viable option, conduct the trials with varying Fe concentration to see if it is possible to form the Laves_C15 structure at low Nd concentration.

As all REEs will form the Laves_C15 structure with Al it could be interesting to look at the effect different acids used in leaching has on the crystal. If the crystals are stable in acids it could be the way to separate the REEs from the matrix.

As it was not possible to confirm or deny the effect the electromagnetic field from the coil had on the melt, it would be necessary to recreate trial 2: 5 mol% Fe. Let the Al cool without the electromagnetic field from the coil to see if the amount of Fe-rich phases is higher along the crucible wall compared to the center of the sample.

It would be interesting to use a stronger electromagnetic field when submerging PCBs into liquid Al, to see if a stronger field can affect the surface tension.

As the next step in trying to develop a process utilizing liquid Al, it would be beneficial to see if it is possible to recycle materials which is more abundant and expensive in the PCB, like Cu and the PMs. If molten Al can not be used to recycle Cu and PMs it can not be the main process for recycling.

9   References

[1]   Santhanam Needhidasan, Melvin Samuel, and Ramalingam Chidambaram. "Electronic waste–an emerging threat to the environment of urban India". In: *Journal of Environmental Health Science and Engineering* 12.1 (2014), p. 36.

[2]   C. P Baldé et al. "Quantities, Flows and Resources". In: *The Global E-waste Monitor 2017* (2017). ISSN: 2522-7033. URL: `https://www.itu.int/en/ITU-D/Climate-Change/Documents/GEM%5C%202017/Global-E-waste%5C%20Monitor%5C%202017%5C%20.pdf`.

[3]   Jenni Ylä-Mella et al. "Overview of the WEEE Directive and its implementation in the Nordic countries: national realisations and best practices". In: *Journal of Waste Management* 2014 (2014).

[4]   Muammer Kaya. "Recovery of Metals and Nonmetals from Waste Printed Circuit Boards (PCBs) by Physical Recycling Techniques". In: *Energy Technology 2017*. Springer, 2017, pp. 433–451.

[5]   Francis O Ongondo, Ian D Williams, and Tom J Cherrett. "How are WEEE doing? A global review of the management of electrical and electronic wastes". In: *Waste management* 31.4 (2011), pp. 714–730.

[6]   A Kyriakopolous, M Lynn, and R Ghomashchi. "Reactive interaction of molten aluminum and solid nickel". In: *Journal of materials science letters* 20.18 (2001), pp. 1699–1701.

[7]   Noureddine Menad, Sylvain Guignot, and JA Van Houwelingen. "New characterisation method of electrical and electronic equipment wastes (WEEE)". In: *Waste Management* 33.3 (2013), pp. 706–713.

[8]   Jianzhi Li et al. "Printed circuit board recycling: a state-of-the-art survey". In: *IEEE transactions on electronics packaging manufacturing* 27.1 (2004), pp. 33–42.

[9]   Huaidong Wang et al. "Recovery of waste printed circuit boards through pyrometallurgical processing: a review". In: *Resources, Conservation and Recycling* 126 (2017), pp. 209–218.

[10]   Ture Damhus, RM Hartshorn, and AT Hutton. "Nomenclature of inorganic chemistry: IUPAC recommendations 2005". In: *CHEMISTRY International* (2005).

[11]   S.R. Taylor. "Abundance of chemical elements in the continental crust: a new table". In: *Geochimica et Cosmochimica Acta* 28.8 (1964), pp. 1273–1285. ISSN: 0016-7037. DOI: `https://doi.org/10.1016/0016-7037(64)90129-2`. URL: `http://www.sciencedirect.com/science/article/pii/0016703764901292`.

[12]   George G Zaimes et al. "Environmental life cycle perspective on rare earth oxide production". In: *ACS Sustainable Chemistry & Engineering* 3.2 (2015), pp. 237–244.

[13]   Thomas E Graedel et al. "What do we know about metal recycling rates?" In: *Journal of Industrial Ecology* 15.3 (2011), pp. 355–366.

[14]   Hajime Nakamura. "The current and future status of rare earth permanent magnets". In: *Scripta Materialia* 154 (2018), pp. 273–276.

[15]   Arjun K Pathak et al. "High performance Nd-Fe-B permanent magnets without critical elements". In: *Journal of Alloys and Compounds* 668 (2016), pp. 80–86.

[16]   Xiaoyue Du and TE Graedel. "Global rare earth in-use stocks in NdFeB permanent magnets". In: *Journal of Industrial Ecology* 15.6 (2011), pp. 836–843.

[17]   DS Edgley et al. "Characterisation of high temperature oxidation of Nd Fe B magnets". In: *Journal of magnetism and magnetic materials* 173.1-2 (1997), pp. 29–42.

[18]   Prashant Jadhao et al. "Greener approach for the extraction of copper metal from electronic waste". In: *Waste management* 57 (2016), pp. 102–112.

[19]   Francesco Di Maria et al. "Urban Mining: Quality and quantity of recyclable and recoverable material mechanically and physically extractable from residual waste". In: *Waste management* 33.12 (2013), pp. 2594–2599.

[20]   Jutta Gutberlet. "Cooperative urban mining in Brazil: Collective practices in selective household waste collection and recycling". In: *Waste Management* 45 (2015), pp. 22–31.

[21]   Landfill Mining. "Urban mining: Concepts, terminology, challenges". In: *Waste Management* 45 (2015), pp. 1–3.

[22]   Emile Van Eygen et al. "Resource savings by urban mining: The case of desktop and laptop computers in Belgium". In: *Resources, conservation and recycling* 107 (2016), pp. 53–64.

[23]   Nicolas Schaeffer et al. "Recovery of metals from waste electrical and electronic equipment (WEEE) using unconventional solvents based on ionic liquids". In: *Critical Reviews in Environmental Science and Technology* (2018), pp. 1–64.

[24]   Jirang Cui and Eric Forssberg. "Mechanical recycling of waste electric and electronic equipment: a review". In: *Journal of hazardous materials* 99.3 (2003), pp. 243–263.

[25]   Garima Chauhan et al. "Novel technologies and conventional processes for recovery of metals from waste electrical and electronic equipment: Challenges & opportunities–A review". In: *Journal of environmental chemical engineering* 6.1 (2018), pp. 1288–1304.

[26]   IO Ogunniyi, Matthys Karel Gerhardus Vermaak, and DR Groot. "Chemical composition and liberation characterization of printed circuit board comminution fines for beneficiation investigations". In: *Waste management* 29.7 (2009), pp. 2140–2146.

[27]   S Sander, G Schubert, and H-G Jäckel. "The fundamentals of the comminution of metals in shredders of the swing-hammer type". In: *International Journal of Mineral Processing* 74 (2004), S385–S393.

[28]   J Oberteuffer. "Magnetic separation: A review of principles, devices, and applications". In: *IEEE Transactions on Magnetics* 10.2 (1974), pp. 223–238.

[29]   Jiang Wu, Jia Li, and Zhenming Xu. "Electrostatic separation for multi-size granule of crushed printed circuit board waste using two-roll separator". In: *Journal of Hazardous materials* 159.2-3 (2008), pp. 230–234.

[30]   Masato Saeki. "Triboelectric separation of three-component plastic mixture". In: *Particulate Science and Technology* 26.5 (2008), pp. 494–506.

[31]   E Kriezis et al. "Eddy currents: theory and applications". In: *Proceedings of the IEEE* 80.10 (1992).

[32]   Masahiro Oguchi et al. "Fate of metals contained in waste electrical and electronic equipment in a municipal waste treatment process". In: *Waste Management* 32.1 (2012), pp. 96–103.

[33]   Alessandra Marra, Alessandra Cesaro, and Vincenzo Belgiorno. "Separation efficiency of valuable and critical metals in WEEE mechanical treatments". In: *Journal of Cleaner Production* 186 (2018), pp. 490–498.

[34]   J. Bachér, A. Mrotzek, and M. Wahlström. "Mechanical pre-treatment of mobile phones and its effect on the Printed Circuit Assemblies (PCAs)". In: *Waste Management* 45 (2015). Urban Mining, pp. 235–245. ISSN: 0956-053X. DOI: https://doi.org/10.1016/j.wasman.2015.06.009. URL: http://www.sciencedirect.com/science/article/pii/S0956053X15004213.

[35]   Jef R Peeters et al. "Effects of boundary conditions on the end-of-life treatment of LCD TVs". In: *CIRP Annals* 62.1 (2013), pp. 35–38.

[36]   Chenlong Duan et al. "Recovery of metals from waste printed circuit boards by a mechanical method using a water medium". In: *Journal of Hazardous Materials* 166.1 (2009), pp. 478–482.

[37]   Jirang Cui and Lifeng Zhang. "Metallurgical recovery of metals from electronic waste: a review". In: *Journal of hazardous materials* 158.2-3 (2008), pp. 228–256.

[38]   Thomas Fruergaard Astrup et al. "Life cycle assessment of thermal waste-to-energy technologies: review and recommendations". In: *Waste management* 37 (2015), pp. 104–115.

[39]   Kui Huang, Jie Guo, and Zhenming Xu. "Recycling of waste printed circuit boards: A review of current technologies and treatment status in China". In: *Journal of hazardous materials* 164.2-3 (2009), pp. 399–408.

[40]   Burçak Ebin and Mehmet Ikbal Isik. "Pyrometallurgical processes for the recovery of metals from WEEE". In: *WEEE Recycling.* Elsevier, 2016, pp. 107–137.

[41] Federica Barontini et al. "Thermal degradation and decomposition products of electronic boards containing BFRs". In: *Industrial & Engineering Chemistry Research* 44.12 (2005), pp. 4186–4199.

[42] Yu-Yang Long et al. "Flow analysis of heavy metals in a pilot-scale incinerator for residues from waste electrical and electronic equipment dismantling". In: *Journal of hazardous materials* 261 (2013), pp. 427–434.

[43] Christian Hagelüken. "Recycling of electronic scrap at Umicore's integrated metals smelter and refinery". In: *Erzmetall* 59.3 (2006), pp. 152–161.

[44] Theodore Lawrence Brown. *Chemistry: the central science.* Pearson Education, 2009.

[45] Masakatsu Hasegawa. "Ellingham diagram". In: *Treatise on Process Metallurgy.* Elsevier, 2014, pp. 507–516.

[46] Yongxiang Yang et al. "REE recovery from end-of-life NdFeB permanent magnet scrap: a critical review". In: *Journal of Sustainable Metallurgy* 3.1 (2017), pp. 122–149.

[47] T.W. Ellis, F.A. Schmidt, and L.L. Jones. "Methods and opportunities in the recycling of rare earth based materials". In: (Oct. 1994).

[48] Toru H Okabe and Sakae Shirayama. *Method and apparatus for recovery of rare earth element.* US Patent App. 12/934,112. Feb. 2011.

[49] Mehmet Ali Recai Önal et al. "Recycling of NdFeB magnets using sulfation, selective roasting, and water leaching". In: *Journal of Sustainable Metallurgy* 1.3 (2015), pp. 199–215.

[50] Osamu Takeda, Toru H Okabe, and Yoshiaki Umetsu. "Recovery of neodymium from a mixture of magnet scrap and other scrap". In: *Journal of Alloys and Compounds* 408 (2006), pp. 387–390.

[51] Timothy W Ellis and Frederick A Schmidt. *Recycling of rare earth metals from rare earth-transition metal alloy scrap by liquid metal extraction.* Tech. rep. Ames Laboratory (AMES), Ames, IA; Iowa State University, Ames, IA (US), 1995.

[52] O Takeda, TH Okabe, and Y Umetsu. "Phase equilibrium of the system Ag–Fe–Nd, and Nd extraction from magnet scraps using molten silver". In: *Journal of alloys and compounds* 379.1-2 (2004), pp. 305–313.

[53] Zhongsheng Hua et al. "Selective extraction of rare earth elements from NdFeB scrap by molten chlorides". In: *ACS Sustainable Chemistry & Engineering* 2.11 (2014), pp. 2536–2543.

[54] Lars K Jakobsson et al. "Recovery of rare earth elements from the ferrous fraction of electronic waste". In: *REWAS 2016.* Springer, 2016, pp. 89–93.

[55] Yuyang Bian et al. "Recovery of rare earth elements from NdFeB magnet by VIM-HMS method". In: *ACS Sustainable Chemistry & Engineering* 4.3 (2016), pp. 810–818.

[56] Diane Bell. "Vapor Phase Removal of Rare Earth Oxides for the Use with Spent LWR Fuel Recycling". PhD thesis. Montana Tech of The University of Montana, 2012.

[57] J-c Lee et al. "Extraction of neodymium from Nd-Fe-B magnet scraps by sulfuric acid". In: *Journal of the Korean Institute of Metals and Materials(South Korea)* 36.6 (1998), pp. 967–972.

[58] K Koyama, A Kitajima, and M Tanaka. "Selective leaching of rare-earth elements from an Nd-Fe-B magnet". In: *Kidorui* 54 (2009), pp. 36–37.

[59] Toru H Okabe et al. "Direct extraction and recovery of neodymium metal from magnet scrap". In: *Materials Transactions* 44.4 (2003), pp. 798–801.

[60] ZS Hua et al. "Extraction of rare earth elements from NdFeB scrap by AlF3–NaF melts". In: *Materials Science and Technology* 31.8 (2015), pp. 1007–1010.

[61] T. Saito et al. "The extraction of Nd from waste Nd–Fe–B alloys by the glass slag method". In: *Journal of Alloys and Compounds* 353.1 (2003), pp. 189–193. ISSN: 0925-8388. DOI: https://doi.org/10.1016/S0925-8388(02)01202-1. URL: http://www.sciencedirect.com/science/article/pii/S0925838802012021.

[62] Tetsuji Saito, Hironori Sato, and Tetsuichi Motegi. "Recovery of rare earths from sludges containing rare-earth elements". In: *Journal of Alloys and Compounds* 425.1 (2006), pp. 145–147. ISSN: 0925-8388. DOI: https://doi.org/10.1016/j.jallcom.2006.01.011. URL: http://www.sciencedirect.com/science/article/pii/S0925838806000296.

[63] Yongxiang Yang, Shoshan ABRAHAMI, and Yanping XIAO. "Recovery of rare earth elements from EOL permanent magnets with slag extraction". In: *Proceedings of the 3rd International Slag Valorisation Symposium*. 2013, pp. 249–252.

[64] Alfred Richard Burkin. *Chemical hydrometallurgy: theory and principles*. Vol. 1. World Scientific, 2001.

[65] Huan Li, Jacques Eksteen, and Elsayed Oraby. "Hydrometallurgical recovery of metals from waste printed circuit boards (WPCBs): Current status and perspectives–A review". In: *Resources, Conservation and Recycling* 139 (2018), pp. 122–139.

[66] A Tuncuk et al. "Aqueous metal recovery techniques from e-scrap: hydrometallurgy in recycling". In: *Minerals engineering* 25.1 (2012), pp. 28–37.

[67] NN Adhapure et al. "Use of large pieces of printed circuit boards for bioleaching to avoid 'precipitate contamination problem'and to simplify overall metal recovery". In: *MethodsX* 1 (2014), pp. 181–186.

[68] U Jadhav and H Hocheng. "Hydrometallurgical recovery of metals from large printed circuit board pieces". In: *Scientific reports* 5 (2015), p. 14574.

[69] MG Aylmore. "Alternative lixiviants to cyanide for leaching gold ores". In: *Gold Ore Processing*. Elsevier, 2016, pp. 447–484.

[70] D Feng and JSJ Van Deventer. "Thiosulphate leaching of gold in the presence of ethylenediaminetetraacetic acid (EDTA)". In: *Minerals Engineering* 23.2 (2010), pp. 143–150.

[71] Ellen Molleman and David Dreisinger. "The treatment of copper–gold ores by ammonium thiosulfate leaching". In: *Hydrometallurgy* 66.1-3 (2002), pp. 1–21.

[72] PMH Petter, Hugo M Veit, and Andréa M Bernardes. "Evaluation of gold and silver leaching from printed circuit board of cellphones". In: *Waste management* 34.2 (2014), pp. 475–482.

[73] Angela Cristina Kasper and Hugo Marcelo Veit. "Gold Recovery from Printed Circuit Boards of Mobile Phones Scraps Using a Leaching Solution Alternative to Cyanide". In: *Brazilian Journal of Chemical Engineering* 35.3 (2018), pp. 931–942.

[74] S Ubaldini et al. "An innovative thiourea gold leaching process". In: *Hydrometallurgy* 48.1 (1998), pp. 113–124.

[75] Li Jing-ying, Xu Xiu-Li, and Liu Wen-quan. "Thiourea leaching gold and silver from the printed circuit boards of waste mobile phones". In: *Waste management* 32.6 (2012), pp. 1209–1212.

[76] Jinshan Li and Jan D Miller. "A review of gold leaching in acid thiourea solutions". In: *Mineral Processing and Extractive Metallurgy Review* 27.3 (2006), pp. 177–214.

[77] Peter P Sheng and Thomas H Etsell. "Recovery of gold from computer circuit board scrap using aqua regia". In: *Waste management & research* 25.4 (2007), pp. 380–383.

[78] A Davis, T Tran, and DR Young. "Solution chemistry of iodide leaching of gold". In: *Hydrometallurgy* 32.2 (1993), pp. 143–159.

[79] Abhishek Kumar Awasthi and Jinhui Li. "An overview of the potential of eco-friendly hybrid strategy for metal recycling from WEEE". In: *Resources, Conservation and Recycling* 126 (2017), pp. 228–239.

[80] Saltanat Sabitovna Konyratbekova, Aliya Baikonurova, and Ata Akcil. "Non-cyanide leaching processes in gold hydrometallurgy and iodine-iodide applications: a review". In: *Mineral Processing and Extractive Metallurgy Review* 36.3 (2015), pp. 198–212.

[81] Flávia PC Silvas et al. "Printed circuit board recycling: physical processing and copper extraction by selective leaching". In: *Waste management* 46 (2015), pp. 503–510.

[82] Ching-Hwa Lee et al. "Selective leaching process for neodymium recovery from scrap Nd-Fe-B magnet". In: *Metallurgical and Materials Transactions A* 44.13 (2013), pp. 5825–5833.

[83]   SS Behera et al. "Ultrasound and Microwave assisted leaching of neodymium from waste magnet using organic solvent". In: *Hydrometallurgy* 185 (2019), pp. 61–70.

[84]   Young Jun Park and Derek J Fray. "Recovery of high purity precious metals from printed circuit boards". In: *Journal of Hazardous materials* 164.2-3 (2009), pp. 1152–1158.

[85]   Jinhui Li et al. "Recovery of valuable materials from waste liquid crystal display panel". In: *Waste Management* 29.7 (2009), pp. 2033–2039.

[86]   Chenna Rao Borra et al. "Leaching of rare earths from bauxite residue (red mud)". In: *Minerals Engineering* 76 (2015), pp. 20–27.

[87]   Takeshi Itakura, Ryo Sasai, and Hideaki Itoh. "Resource recovery from Nd–Fe–B sintered magnet by hydrothermal treatment". In: *Journal of Alloys and Compounds* 408 (2006), pp. 1382–1385.

[88]   S Ndlovu. "Biohydrometallurgy for sustainable development in the African minerals industry". In: *Hydrometallurgy* 91.1-4 (2008), pp. 20–27.

[89]   Marek Kolenčık et al. "Leaching of zinc, cadmium, lead and copper from electronic scrap using organic acids and the Aspergillus niger strain". In: *Fresenius Environ Bull* 22.12a (2013), pp. 3673–3679.

[90]   Jingwei Wang et al. "Bioleaching of metals from printed wire boards by Acidithiobacillus ferrooxidans and Acidithiobacillus thiooxidans and their mixture". In: *Journal of Hazardous Materials* 172.2 (2009), pp. 1100–1105. ISSN: 0304-3894. DOI: https://doi.org/10.1016/j.jhazmat.2009.07.102. URL: http://www.sciencedirect.com/science/article/pii/S0304389409012382.

[91]   Klaus Bosecker. "Bioleaching: metal solubilization by microorganisms". In: *FEMS Microbiology reviews* 20.3-4 (1997), pp. 591–604.

[92]   K Harneit et al. "Adhesion to metal sulfide surfaces by cells of Acidithiobacillus ferrooxidans, Acidithiobacillus thiooxidans and Leptospirillum ferrooxidans". In: *Hydrometallurgy* 83.1-4 (2006), pp. 245–254.

[93]   Alessandra Marra et al. "Bioleaching of metals from WEEE shredding dust". In: *Journal of environmental management* 210 (2018), pp. 180–190.

[94]   James A Brierley. "A perspective on developments in biohydrometallurgy". In: *Hydrometallurgy* 94.1-4 (2008), pp. 2–7.

[95]   Nengwu Zhu et al. "Bioleaching of metal concentrates of waste printed circuit boards by mixed culture of acidophilic bacteria". In: *Journal of hazardous materials* 192.2 (2011), pp. 614–619.

[96]   Yuankun Yang et al. "Bioleaching waste printed circuit boards by Acidithiobacillus ferrooxidans and its kinetics aspect". In: *Journal of biotechnology* 173 (2014), pp. 24–30.

[97]   Yun Xiang et al. "Bioleaching of copper from waste printed circuit boards by bacterial consortium enriched from acid mine drainage". In: *Journal of hazardous materials* 184.1-3 (2010), pp. 812–818.

[98]   Moon-Sung Choi et al. "Microbial recovery of copper from printed circuit boards of waste computer by Acidithiobacillus ferrooxidans". In: *Journal of Environmental Science and Health, Part A* 39.11-12 (2004), pp. 2973–2982.

[99]   MI Muravyov et al. "Leaching of rare earth elements from coal ashes using acidophilic chemolithotrophic microbial communities". In: *Microbiology* 84.2 (2015), pp. 194–201.

[100] Garima Chauhan, KK Pant, and KDP Nigam. "Chelation technology: a promising green approach for resource management and waste minimization". In: *Environmental Science: Processes & Impacts* 17.1 (2015), pp. 12–40.

[101] Koteswara R Vuyyuru et al. "Recovery of nickel from spent industrial catalysts using chelating agents". In: *Industrial & Engineering Chemistry Research* 49.5 (2010), pp. 2014–2024.

[102] Dorota Kołodyńska. "Iminodisuccinic acid as a new complexing agent for removal of heavy metal ions from industrial effluents". In: *Chemical Engineering Journal* 152.1 (2009), pp. 277–288.

[103] Michael J Page, Karin Soldenhoff, and Mark D Ogden. "Comparative study of the application of chelating resins for rare earth recovery". In: *Hydrometallurgy* 169 (2017), pp. 275–281.

[104] Garima Chauhan, Kamal K Pant, and Krishna DP Nigam. "Extraction of nickel from spent catalyst using biodegradable chelating agent EDDS". In: *Industrial & Engineering Chemistry Research* 51.31 (2012), pp. 10354–10363.

[105] Holly Thomas, Timothy P Reinhardt, and Brittany Segneri. "Low temperature geothermal mineral recovery program". In: *Proceedings of the 40th Workshop on Geothermal Reservoir Engineering, Stanford University, Stanford, CA, USA.* 2015, pp. 26–28.

[106] Ji Chen. *Application of ionic liquids on rare earth green separation and utilization.* Springer, 2016.

[107] Martyn J Earle and Kenneth R Seddon. "Ionic liquids. Green solvents for the future". In: *Pure and applied chemistry* 72.7 (2000), pp. 1391–1398.

[108] Kazunori Nakashima et al. "Ionic liquids as a novel solvent for lanthanide extraction". In: *Analytical Sciences* 19.8 (2003), pp. 1097–1098.

[109] Fukiko Kubota et al. "Application of ionic liquids to extraction separation of rare earth metals with an effective diglycol amic acid extractant". In: *Journal of chemical engineering of Japan* (2011), pp. 1102280146–1102280146.

[110] Jesik Park et al. "Application of ionic liquids in hydrometallurgy". In: *International journal of molecular sciences* 15.9 (2014), pp. 15320–15343.

[111] Terence Makanyire, Sergio Sanchez-Segado, and Animesh Jha. "Separation and recovery of critical metal ions using ionic liquids". In: *Advances in Manufacturing* 4.1 (2016), pp. 33–46.

[112] Jerome O Nriagu. "Cupellation: The oldest quantitative chemical process". In: *Journal of Chemical Education* 62.8 (1985), p. 668.

[113] Fakhri Ibraheem. "Modified pyro-metallurgical technology for recovery of impurities from crude lead using chalk powder". In: Dec. 2012, pp. 293–303. ISBN: 9781845647582. DOI: 10.2495/PMR120261.

[114] Hans Lukas, Suzana G Fries, and Bo Sundman. *Computational thermodynamics: the Calphad method.* Cambridge university press, 2007.

[115] Johan C van Dyk, S Melzer, and A Sobiecki. "Mineral matter transformation during Sasol-Lurgi fixed bed dry bottom gasification–utilization of HT-XRD and FactSage modelling". In: *Minerals Engineering* 19.10 (2006), pp. 1126–1135.

[116] Ch W Bale et al. "FactSage thermochemical software and databases". In: *Calphad* 26.2 (2002), pp. 189–228.

[117] Hiroaki Okamoto and Thaddeus B Massalski. "Correct and incorrect phase diagram features". In: *Methods for Phase Diagram Determination.* Elsevier, 2007, pp. 51–107.

[118] Xiaoma Tao et al. "Ab initio calculation of the total energy and elastic properties of Laves phase C15 Al2RE (RE= Sc, Y, La, Ce–Lu)". In: *Computational Materials Science* 44.2 (2008), pp. 392–399.

[119] Liling Jin et al. "ARTICLE 1: THERMODYNAMIC EVALUATION AND OPTIMIZATION OF AL–LA, AL–CE, AL–PR, AL–ND AND AL–SM SYSTEMS USING THE MODIFIED QUASICHEMICAL MODEL FOR LIQUIDS Published in CALPHAD, 35 (2011), 30-41." In: *THERMODYNAMIC MODELING OF ALUMINUM-MAGNESIUM-RARE EARTH SYSTEMS* 35 (2012), p. 45.

[120] N Nereson, C Olsen, and G Arnold. "Magnetic properties of DyAl2 and NdAl2". In: *Journal of Applied Physics* 37.12 (1966), pp. 4575–4580.

[121] Rafał Michalski and Jakub Zygadło. "Predictions of thermomagnetic properties of Laves phase compounds: TbAl2, GdAl2 and SmAl2 performed with ATOMIC MATTERS MFA computation system". In: *Journal of Magnetism and Magnetic Materials* 452 (2018), pp. 415–426.

[122] A Bouayad et al. "Kinetic interactions between solid iron and molten aluminium". In: *Materials Science and Engineering: A* 363.1-2 (2003), pp. 53–61.

[123] HR Shahverdi et al. "Kinetics of interfacial reaction between solid iron and molten aluminium". In: *Journal of materials science* 37.5 (2002), pp. 1061–1066.

[124] T Engh. "Principles of metal refining". In: *Oxford University Press, Walton St, Oxford OX 2 6 DP, UK, 1992. 473* (1992).

[125]   Ivan Egry, Georg Lohoefer, and Gerd Jacobs. "Surface tension of liquid metals: results from measurements on ground and in space". In: *Physical review letters* 75.22 (1995), p. 4043.

[126]   Robert Fritzsch. *The influence of a electromagnetic field from a singel phase low frequency induction coil has on the wetting behaviour of aluminium*. Mar. 2019.

[127]   Pascale Gillon. "Uses of intense dc magnetic fields in materials processing". In: *Materials Science and Engineering: A* 287.2 (2000), pp. 146–152.

[128]   Robert Fritzsch et al. "Electromagnetic Priming of Ceramic Foam Filters (CFF) for Liquid Aluminum Filtration". In: *Light Metals 2013*. Springer, 2016, pp. 973–979.

[129]   Mark William Kennedy. "Removal of Inclusions from Liquid Aluminium using Electromagnetically Modified Filtration". In: (2013).

[130]   Daniel Leenov and Alexander Kolin. "Theory of electromagnetophoresis. I. Magnetohydrodynamic forces experienced by spherical and symmetrically oriented cylindrical particles". In: *The Journal of Chemical Physics* 22.4 (1954), pp. 683–688.

[131]   Valery Rudnev. "COIL END EFFECT". In: *Heat Treating Progress* (May 2006).

[132]   Hugo Royen and Uwe Fortkamp. "Rare Earth Elements-Purification, Separation and Recycling". In: (2016).

10 Appendices

10.1 Table of Appendix

NTNU ▢ HSE	Hazardous activity identification process	Prepared by HSE section	Number HMSRV2601	Date 22.03.2011	
		Approved by The Rector	Page	Replaces 01.12.2006	

Unit: *(Institute)*   **IMA**   **Date:**   18.05.2019

Line manager:

Participants in the identification process (incl. function)
(supervisor, student, co-supervisor, others)   Eystein vada, Eskil Christensen, Superviser: Robert Fritzsch

Short description of the main activity/main process: Bachelor project for student Eystein Vada & Eskil Christensen. Project title

Is the project work purely theoretical? (YES/NO)   NO

Answer "YES" implies that **supervisor is assured that no activities requiring risk assessment are involved in the work**. *If YES, skip rest of the form.*

Is the project work safe to perform outside normal work hours (8-17)? (YES/NO) NO

Responsible supervisor: Robert Fritzsch   *Students:* Eskil Christens Eystein Vada

ID nr.	Activity/process	Respons-ible person	Existing documentation	Existing safety measures	Laws, regulations etc.	Comment
1	Cuting Aluminium and samples	Eskil Eystein		Safety goggles, make sure the lid on the saw is closed		
2	Melting of Aluminium and adding material in the melt	Eskil Eystein		protective glasses, Helmet, safety trousers, safety jacket, safety shoes, gloves, shoe covers	Work needs to be done by at least two.	Use tongs to add material, first time its done under supervision of supervisor
3	Taking samples with quartz glass tube	Eskil Eystein		protective glasses, Helmet, safety trousers, safety jacket, safety shoes, gloves		The process was rehearsed before it was used on molten aluminium

I

4	Casting of aluminium below 1000 K	Eskil Eystein		protective glasses, Helmet, safety trousers, safety jacket, safety shoes, gloves, shoe covers	Needs to be at least two persons in the room	Clean the space before casting, make sure there are no water in the casting area, ready the molds before taking the crucible out of the furnac, first time its done under supervision of supervisor
5	Molding the samples with epoxy	Eskil Eystein		Nitrile gloves, protective glasses	Working in a fume hood, HSE course	
6	Polishing the samples	Eskil Eystein		Nitrile gloves, protective glasses	HSE course	Check fingers regularly
7	Transporting crucible with molten metal	Eskil Eystein		protective glasses, Helmet, safety trousers, safety jacket, safety shoes, gloves, shoe covers, apron	Needs to be at least two in the room	Clean the space before transportation, make sure there are no water in the area, use corect tools
8	Using electromagnetic coil	Eskil Eystein Robert		Coil is "live" when the plug is in the socket, working on the opposite side of the cables, All cables are coverd with insulation	used under supervison of superviser	Take it slow, no need to rush
9	Puting printed circuit boards into molten aluminium	Eskil Eystein Robert		protective glasses, Helmet, safety trousers, safety jacket, safety shoes, gloves, shoe covers, using a steinless steel lid on the crucible that is connected to the fume hood	Done under supervision of superviser.	Available gas masks with filters
10	Using the IF75	Eskil Eystein Robert		protective glasses, Helmet, safety trousers, safety jacket, safety shoes, gloves, shoe covers,	HSE round before use, Allways one person watchin water temperature and water preasure	Done under supervison by supervisor

II

11	Adding iron and Nd magnets to molten aluminium in the IF75. Temperatures up to 1673 K.	Eskil Eystein Robert		protective glasses, Helmet, safety trousers, safety jacket, safety shoes, gloves, shoe covers, using a steinless steel lid on the crucible that's conectet to the fume extractor	HSE round before use, Allways one person watching water temperature and water pressure	Done under Supervison by superviser, all material is added with tongs
12	Adding phones to molten aluminium in the IF75. Temperatures up to 1673K	Eskil Eystein Robert		protective glasses, Helmet, safety trousers, safety jacket, safety shoes, gloves, shoe covers, using a steinless steel lid on the crucible that is connected to the fume extractor, phones taped to a Zirconia ceramic filter to prevent aluminium to splash outside of the crucible and allow gases to pass through		Done under Supervison by supervisor
13	Casting Aluminium alloy at 1673 K	Eskil Eystein Robert		protective glasses, Helmet, safety trousers, safety jacket, safety shoes, gloves, shoe, aluminium covers		Done under Supervison by supervisor. Cleaning the space before casting.
14	Quenching samples in water	Eskil Eystein		protective glasses, Helmet, safety trousers, safety jacket, safety shoes, gloves, shoe, aluminium covers		Cup of water is placed inside a casting mould to prevent fire and leakage.

III

NTNU	Risk assessment	Prepared by	Nummer	Date	
		HSE section	HMSRV2603	04.02.2011	
⬤		Approved by	Page	Replaces	
HMS /KS		The Rector		09.02.2010	

Unit: *(Institute)* _____ **Date:** _____

Line manager:

Participants in the identification process (incl. function)

(supervisor, student, co-supervisor, others) _____

Risk assessment of: Bachelor project for student Eystein Vada & Eskil Christensen. Project title

Signatures: *Responsible supervisor:* _____   *Students*
                                                                                          :

ID nr.	Activity from the identification process form	Potential undesirable incident/strain	Likeli-hood: (1-5)	Consequence:				Risk value (human)	Comments/status Suggested measures
				Human (A-E)	Enviroment (A-E)	Economy/ material (A-E)			
1	Cuting Aluminium and samples	Cut, bruise	1	A	A	A		A1	
2	Melting of Aluminium and adding material in the melt	Burns, splashing of aluminium	1	B	A	A		B1	
3	Taking samples with quartz glass tube	Burns, splashing of aluminium	2	A	A	A		A2	
4	Casting of aluminium below 1000 K	Burns, splashing of aluminium	2	A	A	A		A2	
5	Molding the samples with epoxy	Contact with dangerous substances	1	A	A	A		A1	
6	poleshing the samples	Bruises	2	A	A	A		A2	

IV

7	Using electromagnetic coil	Electric shock	3	B	A	A		**B3**	Done in pars, looking after one aother, Bether electric isolated.
8	Transporting crucible with molten metal	Burns, splashing of aluminium	3	A	A	B		**A3**	
9	Puting printed circuit cards into molten aluminium	Burns, splashing of aluminium, explosions	3	A	A	A		**A3**	
10	Using IF75	Explosions	1	B	A	C		**B1**	It has an automatic shutdown
11	Adding iron and Nd magnets to molten aluminium in the IF75. Temperatures up to 1673 K.	Burns, splashing of aluminium	2	B	A	A		**B2**	
12	Adding phones to molten aluminium in the IF75. Temperatures up to 1673K	Burns, splashing og aluminium explosions, toxic gas	4	B	A	A		**B4**	Two "lids", closed system with the steel lid on top. To reduce the consequence gas mask should be available to everyone
13	Casting Aluminium alloy at 1673 K	Burns, splashing of aluminium	2	C	A	A		**C2**	Full protective gir is used, but more experience would help
14	Quenching samples in water	Cuts, burns, splashing of aluminium, splintering of quartz glass	2	B	A	A		**B2**	Very small amounts, full protective gear is used

V

Less Common Metals - a subsidiary of

Great Western
MINERALS GROUP

Certificate of Conformance

Customer:	Dept of Materials Science & Engineering NTNU
Order:	E-mail dated 12/02/2014
LCM Job/Batch No.	J7283 / FP9290

Description: NdFeB Alloy broken lump

SPECIFICATION	RESULTS			Method
Neodymium	Neodymium		28.03%	ICP-OES
Praseodymium	Praseodymium		0.04%	ICP-OES
Boron	Boron		1.08%	ICP-OES
Gallium	Gallium		0.28%	ICP-OES
Aluminium	Aluminium		0.08%	ICP-OES
Niobium	Niobium		0.29%	ICP-OES
Iron	Iron		Balance	
Impurities:	Impurities:			
Cobalt	Cobalt	<	0.002%	ICP-OES
Chromium	Chromium		0.005%	ICP-OES
Copper	Copper		0.010%	ICP-OES
Magnesium	Magnesium	<	0.001%	ICP-OES
Manganese	Manganese		0.032%	ICP-OES
Silicon	Silicon		0.030%	ICP-OES
Carbon	Carbon		0.017%	FUSION GAS ANALYSIS
Oxygen	Oxygen		0.015%	FUSION GAS ANALYSIS
Nitrogen	Nitrogen	<	0.001%	FUSION GAS ANALYSIS

Comments:

Certified that the materials described above comply with the requirements of the stated order:

Signed: Date: 03·04·2014

EDAX TEAM

Eystein Vada

Author: student
Creation: 03/22/2019 9:39:03 AM

Sample Name: Test 2

Area 9
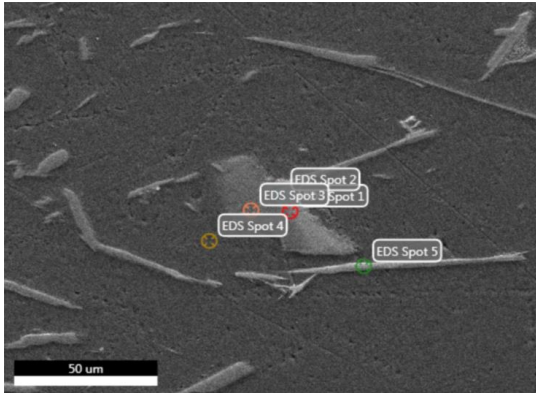
Notes:

EDAX TEAM

EDS Spot 1

kV: 15	Mag:585	Takeoff: 30.7	Live Time(s): 17.6	Amp Time(µs):1.92	Resolution:(eV)127.3

EDS Spot 1 - Det 1

Lsec: 17.6   2.473K Cnts   1.190 keV   Det: Octane Pro A
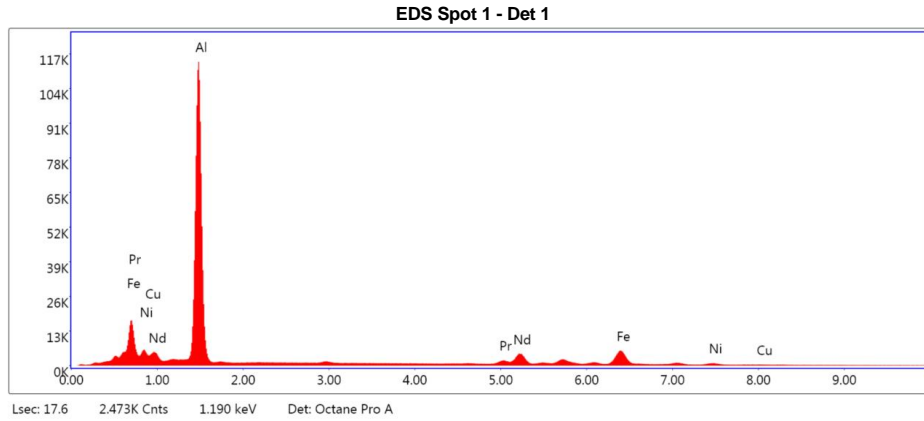
eZAF Smart Quant Results

Element	Weight %	Atomic %	Net Int.	Error %	Kratio	Z	A	F
AlK	55.99	80.17	53755.50	5.80	0.3510	1.1159	0.5611	1.0014
PrL	5.50	1.51	918.91	8.63	0.0438	0.7592	1.0390	1.0097
NdL	19.31	5.17	2982.42	3.58	0.1514	0.7494	1.0396	1.0065
FeK	15.91	11.01	4172.94	3.28	0.1503	0.9604	0.9684	1.0156
NiK	2.75	1.81	491.43	9.14	0.0261	0.9681	0.9607	1.0215
CuK	0.54	0.33	72.77	38.31	0.0050	0.9177	0.9699	1.0296

EDAX TEAM

EDS Spot 2

| kV: 15 | Mag:585 | Takeoff: 30.7 | Live Time(s): 17.6 | Amp Time(µs):1.92 | Resolution:(eV)127.3 |

EDS Spot 2 - Det 1

Lsec: 17.6   2.488K Cnts   1.190 keV   Det: Octane Pro A
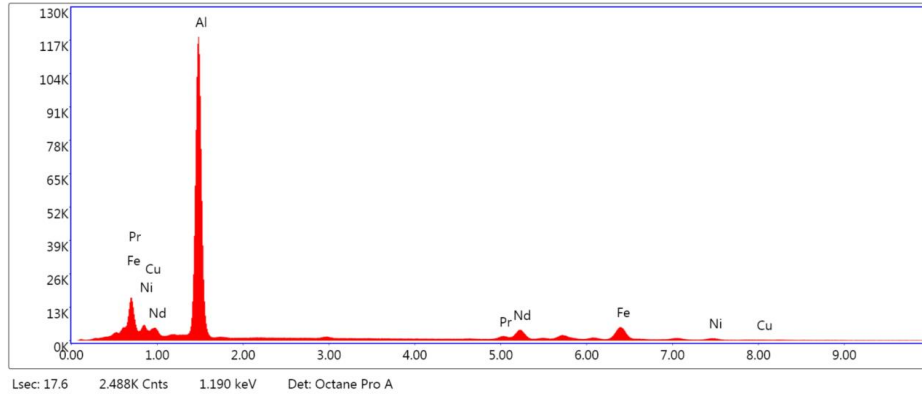
eZAF Smart Quant Results

Element	Weight %	Atomic %	Net Int.	Error %	Kratio	Z	A	F
AlK	57.99	81.34	55856.78	5.66	0.3703	1.1095	0.5748	1.0014
PrL	5.11	1.37	836.05	9.17	0.0405	0.7542	1.0396	1.0096
NdL	18.27	4.79	2762.81	3.77	0.1424	0.7444	1.0402	1.0065
FeK	15.41	10.44	3962.39	3.31	0.1449	0.9539	0.9700	1.0163
NiK	2.88	1.85	503.62	8.88	0.0272	0.9612	0.9628	1.0221
CuK	0.34	0.20	45.28	67.84	0.0031	0.9110	0.9716	1.0306

EDAX TEAM

EDS Spot 3

| kV: 15 | Mag:585 | Takeoff: 30.7 | Live Time(s): 17.2 | Amp Time(µs):1.92 | Resolution:(eV)127.3 |

EDS Spot 3 - Det 1

Lsec: 17.2   1.650K Cnts   1.190 keV   Det: Octane Pro A
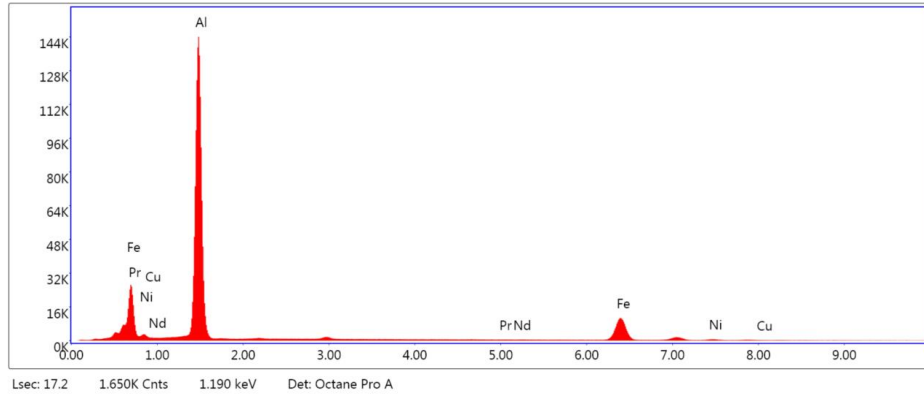
eZAF Smart Quant Results

Element	Weight %	Atomic %	Net Int.	Error %	Kratio	Z	A	F
AlK	62.94	77.97	69822.90	4.58	0.4524	1.0542	0.6813	1.0007
PrL	0.04	0.01	6.12	65.84	0.0003	0.7112	1.0522	1.0192
NdL	0.13	0.03	19.45	58.86	0.0010	0.7017	1.0524	1.0226
FeK	34.46	20.62	8783.78	2.64	0.3138	0.8980	0.9962	1.0181
NiK	2.07	1.18	353.20	10.70	0.0186	0.9024	0.9744	1.0238
CuK	0.37	0.19	46.91	58.93	0.0032	0.8538	0.9811	1.0325

X

EDAX TEAM

EDS Spot 4

| kV: 15 | Mag:585 | Takeoff: 30.7 | Live Time(s): 13.1 | Amp Time(µs):1.92 | Resolution:(eV)127.3 |

EDS Spot 4 - Det 1

Lsec: 13.1   1.863K Cnts   1.190 keV   Det: Octane Pro A
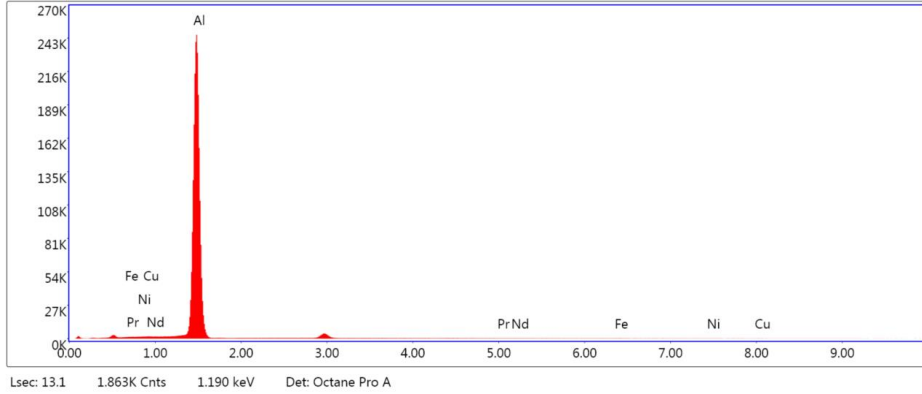
eZAF Smart Quant Results

Element	Weight %	Atomic %	Net Int.	Error %	Kratio	Z	A	F
AlK	99.47	99.80	159396.80	1.44	0.9882	1.0010	0.9924	1.0000
PrL	0.03	0.01	4.13	90.58	0.0002	0.6709	1.0483	0.9985
NdL	0.13	0.02	18.21	64.24	0.0009	0.6616	1.0491	0.9988
FeK	0.17	0.08	46.03	52.50	0.0016	0.8459	0.9946	1.0696
NiK	0.09	0.04	16.27	70.63	0.0008	0.8482	1.0005	1.1084
CuK	0.11	0.05	15.69	67.61	0.0010	0.8016	1.0021	1.1401

XI

EDAX TEAM

EDS Spot 5

| kV: 15 | Mag:585 | Takeoff: 30.7 | Live Time(s): 17.6 | Amp Time(µs):1.92 | Resolution:(eV)127.3 |

EDS Spot 5 - Det 1

Lsec: 17.6   2.628K Cnts   1.190 keV   Det: Octane Pro A
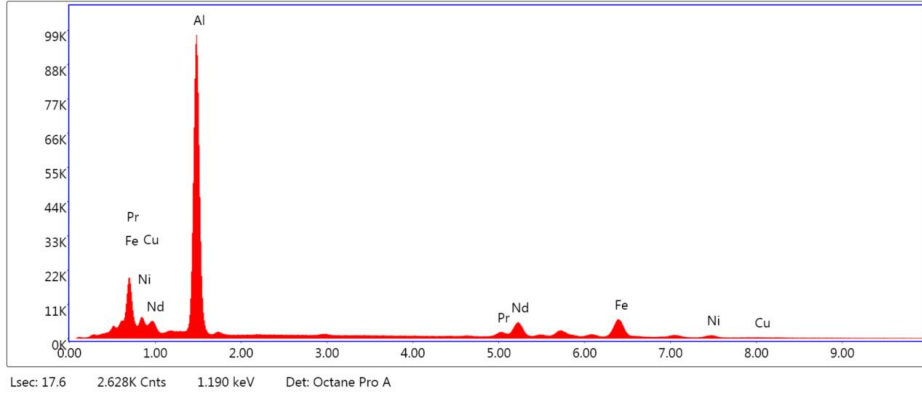
eZAF Smart Quant Results

Element	Weight %	Atomic %	Net Int.	Error %	Kratio	Z	A	F
AlK	50.01	76.23	46226.71	6.18	0.2975	1.1343	0.5236	1.0016
PrL	6.30	1.84	1087.57	7.05	0.0511	0.7735	1.0375	1.0104
NdL	22.30	6.36	3556.37	3.38	0.1780	0.7636	1.0380	1.0066
FeK	17.38	12.80	4691.37	3.30	0.1665	0.9790	0.9642	1.0147
NiK	3.33	2.34	611.67	7.71	0.0321	0.9879	0.9550	1.0196
CuK	0.68	0.44	93.63	32.19	0.0063	0.9369	0.9653	1.0271

EDAX TEAM

6

Author: guest
Creation: 04/15/2019 7:56:30 PM

Sample Name: 6

Area 1
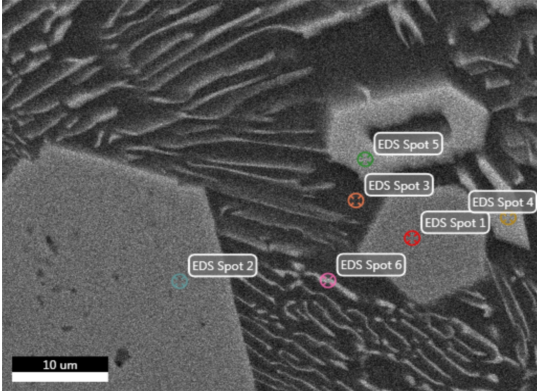
Notes:

EDAX TEAM

EDS Spot 1

| kV: | 20 | Mag: 1971 | Takeoff: 28.2 | Live Time(s): 28.1 | Amp Time(µs): 1.92 | Resolution:(eV) 127.3 |

EDS Spot 1 - Det 1

Lsec: 28.1   156 Cnts   6.660 keV   Det: Octane Pro A

eZAF Smart Quant Results

Element	Weight %	Atomic %	Net Int.	Error %	Kratio	Z	A	F
AlK	53.55	78.62	4429.84	7.27	0.2383	1.1109	0.4000	1.0016
PrL	0.84	0.24	24.59	41.03	0.0072	0.7939	1.0600	1.0123
NdL	25.78	7.08	712.56	3.81	0.2167	0.7857	1.0625	1.0069
FeK	19.83	14.06	1001.84	3.00	0.1825	0.9722	0.9374	1.0102

EDAX TEAM

EDS Spot 2

| kV: 20 | Mag: 1971 | Takeoff: 28.2 | Live Time(s): 28.1 | Amp Time(µs): 1.92 | Resolution:(eV) 127.3 |

EDS Spot 2 - Det 1

Lsec: 28.1   153 Cnts   6.660 keV   Det: Octane Pro A
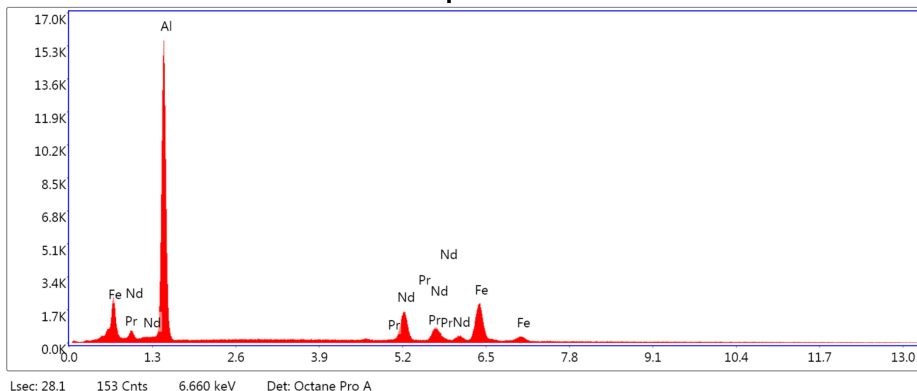
eZAF Smart Quant Results

Element	Weight %	Atomic %	Net Int.	Error %	Kratio	Z	A	F
AlK	53.71	78.72	4444.96	7.25	0.2396	1.1104	0.4011	1.0016
PrL	0.74	0.21	21.68	42.60	0.0063	0.7936	1.0600	1.0124
NdL	25.76	7.06	710.35	3.82	0.2164	0.7853	1.0626	1.0069
FeK	19.78	14.01	997.73	3.01	0.1821	0.9718	0.9376	1.0102

EDAX TEAM

EDS Spot 3

| kV: 20 | Mag: 1971 | Takeoff: 28.2 | Live Time(s): 27.4 | Amp Time(μs): 1.92 | Resolution:(eV) 127.3 |

EDS Spot 3 - Det 1

Lsec: 27.4   55 Cnts   6.660 keV   Det: Octane Pro A
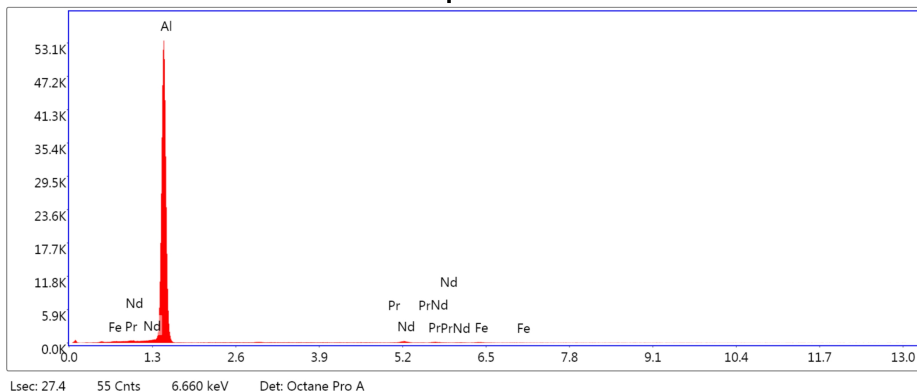
eZAF Smart Quant Results

Element	Weight %	Atomic %	Net Int.	Error %	Kratio	Z	A	F
AlK	94.25	98.59	15890.21	2.58	0.8152	1.0147	0.8521	1.0003
PrL	0.39	0.08	10.74	55.80	0.0030	0.7173	1.0716	1.0002
NdL	4.44	0.87	116.73	11.39	0.0339	0.7095	1.0742	0.9994
FeK	0.92	0.46	47.20	16.40	0.0082	0.8768	0.9781	1.0411

XVI

EDAX TEAM

EDS Spot 4

| kV: 20 | Mag: 1971 | Takeoff: 28.2 | Live Time(s): 28 | Amp Time(μs): 1.92 | Resolution:(eV) 127.3 |

EDS Spot 4 - Det 1

Lsec: 28.0   254 Cnts   6.660 keV   Det: Octane Pro A
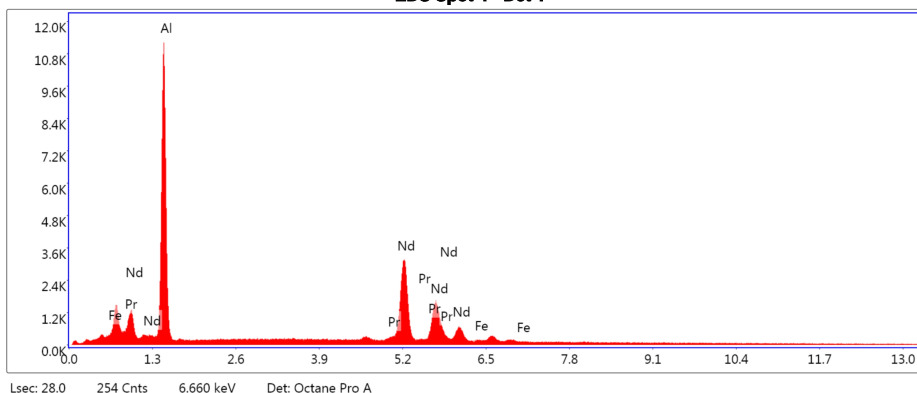
eZAF Smart Quant Results

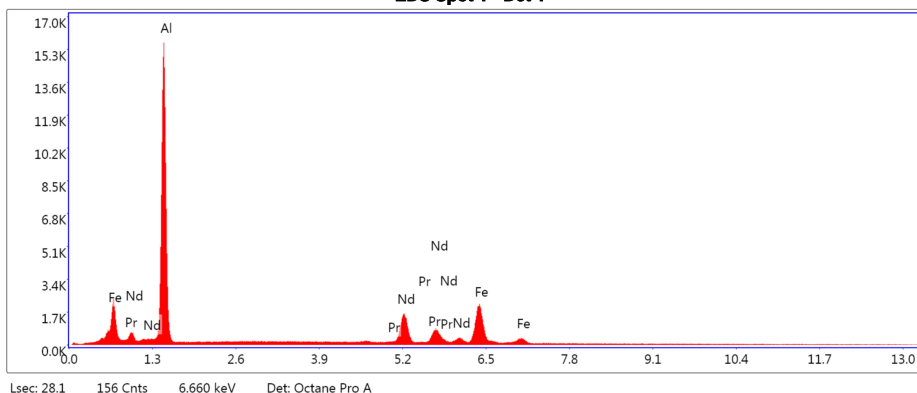| Element	Weight %	Atomic %	Net Int.	Error %	Kratio	Z	A	F
AlK	46.39	81.99	3178.69	8.20	0.1717	1.1770	0.3138	1.0023
PrL	1.86	0.63	56.02	24.02	0.0164	0.8467	1.0347	1.0087
NdL	51.25	16.95	1460.40	2.56	0.4459	0.8383	1.0385	0.9995
FeK	0.51	0.43	25.74	33.01	0.0047	1.0384	0.8851	1.0096

EDAX TEAM

EDS Spot 5

| kV: 20 | Mag: 1971 | Takeoff: 28.2 | Live Time(s): 28.1 | Amp Time(µs): 1.92 | Resolution:(eV) 127.3 |

EDS Spot 5 - Det 1

Lsec: 28.1   251 Cnts   6.660 keV   Det: Octane Pro A
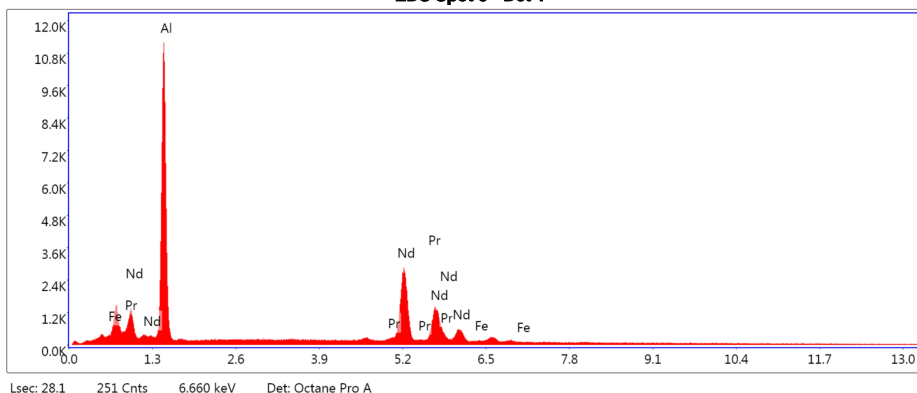
eZAF Smart Quant Results

Element	Weight %	Atomic %	Net Int.	Error %	Kratio	Z	A	F
AlK	48.81	83.40	3226.25	8.08	0.1861	1.1678	0.3258	1.0022
PrL	1.87	0.61	52.39	25.10	0.0164	0.8395	1.0365	1.0083
NdL	48.89	15.63	1295.15	2.66	0.4223	0.8311	1.0402	0.9994
FeK	0.44	0.36	20.66	39.04	0.0040	1.0293	0.8895	1.0099

XVIII

EDAX TEAM

EDS Spot 6

| kV: 20 | Mag: 1971 | Takeoff: 28.2 | Live Time(s): 27.8 | Amp Time(µs): 1.92 | Resolution:(eV) 127.3 |

EDS Spot 6 - Det 1

Lsec: 27.8   118 Cnts   6.660 keV   Det: Octane Pro A
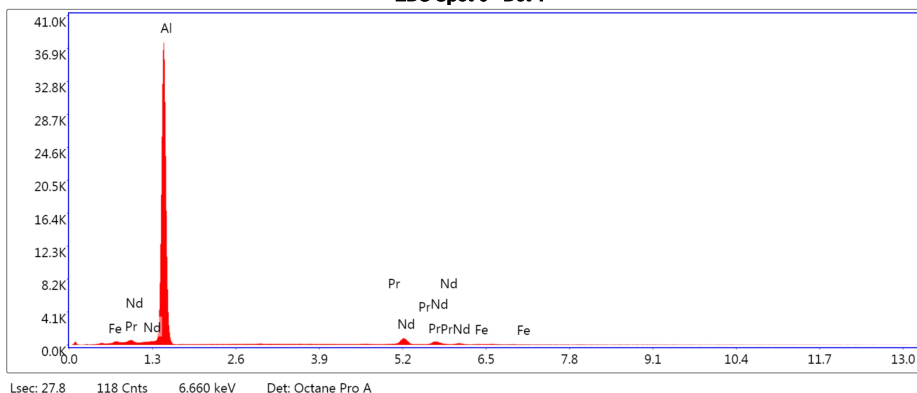
eZAF Smart Quant Results

Element	Weight %	Atomic %	Net Int.	Error %	Kratio	Z	A	F
AlK	85.51	96.80	10996.16	4.42	0.5986	1.0420	0.6713	1.0008
PrL	0.59	0.13	15.63	46.78	0.0046	0.7393	1.0643	1.0018
NdL	13.51	2.86	342.27	5.91	0.1053	0.7313	1.0672	0.9988
FeK	0.39	0.22	19.05	34.85	0.0035	0.9040	0.9596	1.0246

XIX

EDAX TEAM

Eystein

Author: guest
Creation: 04/30/2019 7:53:38 PM

Sample Name: 8K

Area 2

Notes:

XX
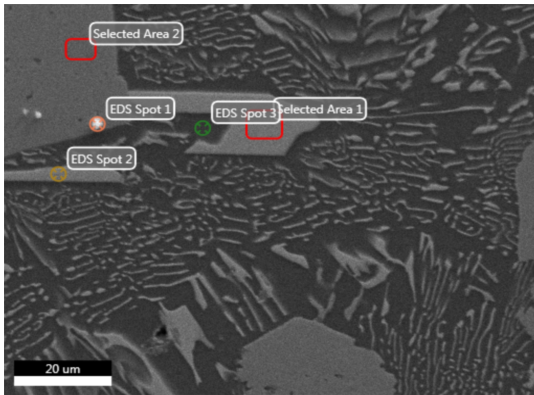
EDAX TEAM

Selected Area 1

| kV: 15 | Mag: 1000 | Takeoff: 30.5 | Live Time(s): 30.3 | Amp Time(µs): 1.92 | Resolution:(eV) 127.3 |

Selected Area 1 - Det 1

Lsec: 30.3   2.437K Cnts   0.300 keV   Det: Octane Pro A
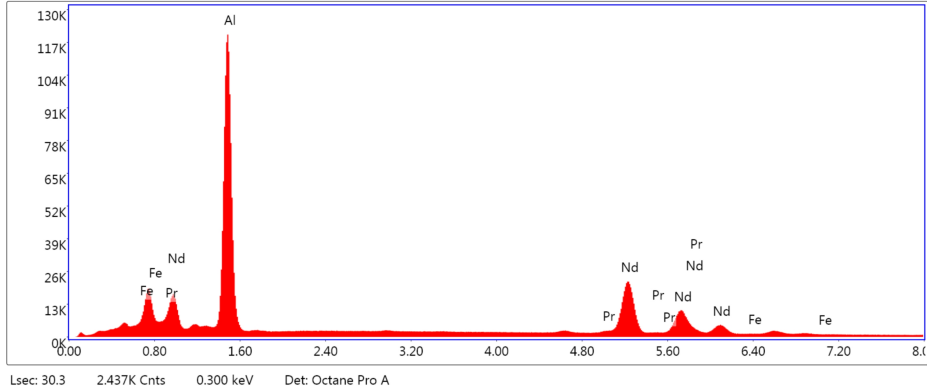
eZAF Smart Quant Results

Element	Weight %	Atomic %	Net Int.	Error %	Kratio	Z	A	F
AlK	41.84	79.25	33067.83	7.14	0.2183	1.2197	0.4269	1.0022
PrL	2.13	0.77	383.60	12.40	0.0185	0.8404	1.0212	1.0092
NdL	55.81	19.77	9235.05	2.53	0.4739	0.8304	1.0233	0.9995
FeK	0.22	0.20	61.47	46.98	0.0022	1.0669	0.9295	1.0090

XXI

EDAX TEAM

Selected Area 2

| kV: 15 | Mag: 1000 | Takeoff: 30.5 | Live Time(s): 30.1 | Amp Time(µs): 1.92 | Resolution:(eV) 127.3 |

Selected Area 2 - Det 1

Lsec: 30.1   1.796K Cnts   0.300 keV   Det: Octane Pro A
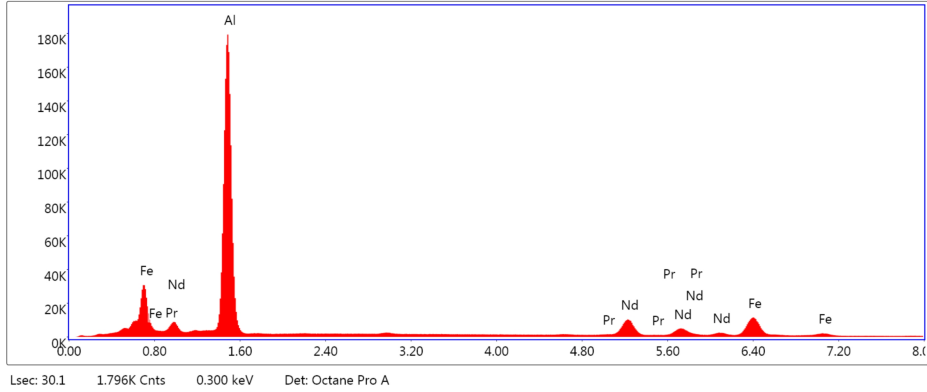
eZAF Smart Quant Results

Element	Weight %	Atomic %	Net Int.	Error %	Kratio	Z	A	F
AlK	52.81	78.34	49151.67	5.99	0.3222	1.1281	0.5399	1.0015
PrL	1.16	0.33	195.95	18.87	0.0094	0.7686	1.0382	1.0117
NdL	26.54	7.36	4132.38	3.02	0.2106	0.7588	1.0392	1.0062
FeK	19.48	13.96	5113.77	3.02	0.1847	0.9726	0.9651	1.0100

XXII

EDAX TEAM

EDS Spot 1

kV: 15	Mag: 1000	Takeoff: 30.5	Live Time(s): 30.4	Amp Time(µs): 1.92	Resolution:(eV) 127.3

EDS Spot 1 - Det 1

Lsec: 30.4   1.702K Cnts   0.300 keV   Det: Octane Pro A
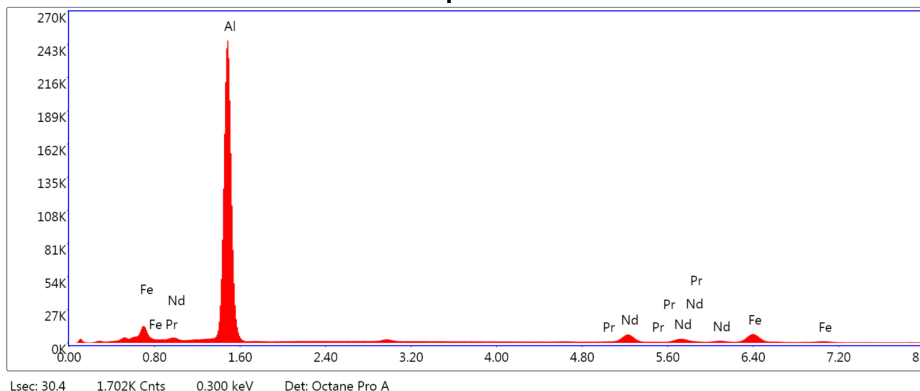
eZAF Smart Quant Results

Element	Weight %	Atomic %	Net Int.	Error %	Kratio	Z	A	F
AlK	67.02	87.04	67410.42	5.04	0.4631	1.0885	0.6341	1.0012
PrL	1.29	0.32	199.58	12.75	0.0100	0.7380	1.0409	1.0087
NdL	18.86	4.58	2692.85	3.30	0.1438	0.7283	1.0418	1.0049
FeK	12.84	8.06	3121.68	3.16	0.1182	0.9328	0.9733	1.0140

EDAX TEAM

EDS Spot 2

| kV: | 15 | Mag: 1000 | Takeoff: 30.5 | Live Time(s): 30.5 | Amp Time(µs): 1.92 | Resolution:(eV) 127.3 |

EDS Spot 2 - Det 1

Lsec: 30.5   2.242K Cnts   0.300 keV   Det: Octane Pro A
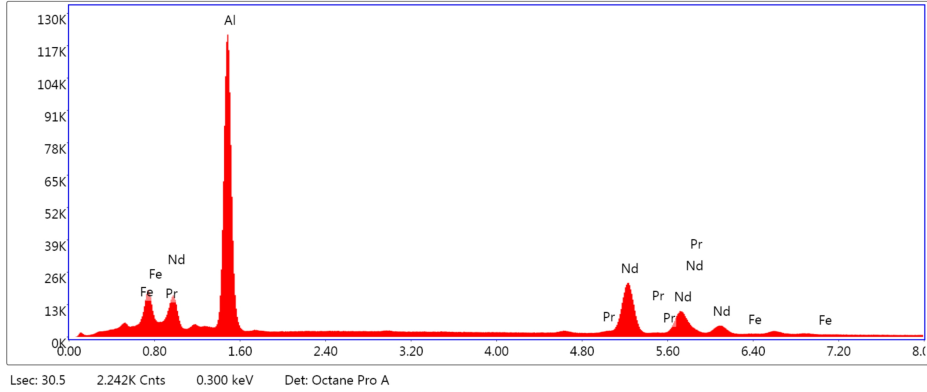
eZAF Smart Quant Results

Element	Weight %	Atomic %	Net Int.	Error %	Kratio	Z	A	F
AlK	42.19	79.42	33059.87	7.12	0.2209	1.2178	0.4291	1.0022
PrL	2.24	0.81	396.82	10.78	0.0193	0.8388	1.0215	1.0091
NdL	55.21	19.44	9012.91	2.54	0.4681	0.8289	1.0235	0.9995
FeK	0.36	0.33	98.69	26.75	0.0036	1.0649	0.9301	1.0090

XXIV

EDAX TEAM

EDS Spot 3

kV: 15	Mag: 1000	Takeoff: 30.5	Live Time(s): 30.3	Amp Time(µs): 1.92	Resolution:(eV) 127.3

EDS Spot 3 - Det 1

Lsec: 30.3   2.293K Cnts   0.300 keV   Det: Octane Pro A
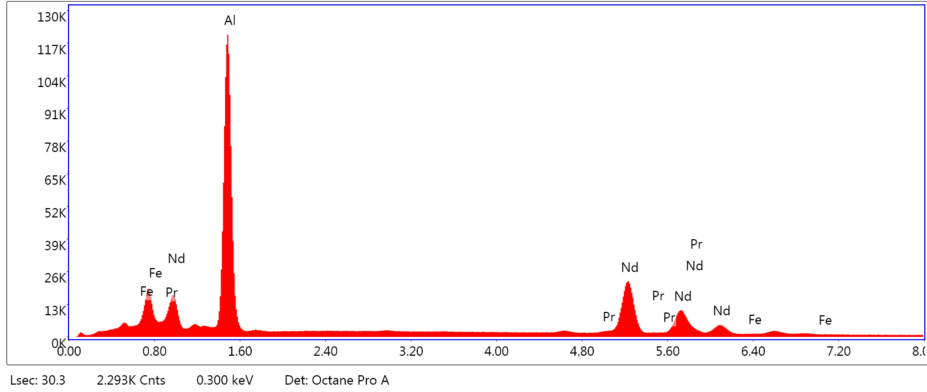
eZAF Smart Quant Results

Element	Weight %	Atomic %	Net Int.	Error %	Kratio	Z	A	F
AlK	41.60	79.08	32869.35	7.15	0.2166	1.2208	0.4257	1.0022
PrL	2.31	0.84	416.43	10.76	0.0200	0.8412	1.0211	1.0091
NdL	55.86	19.86	9266.31	2.52	0.4747	0.8312	1.0232	0.9995
FeK	0.23	0.21	64.24	46.56	0.0023	1.0679	0.9292	1.0090

XXV

EDAX TEAM

Eystein

Author: guest
Creation: 04/29/2019 6:46:01 PM

Sample Name: 7 1

Area 3
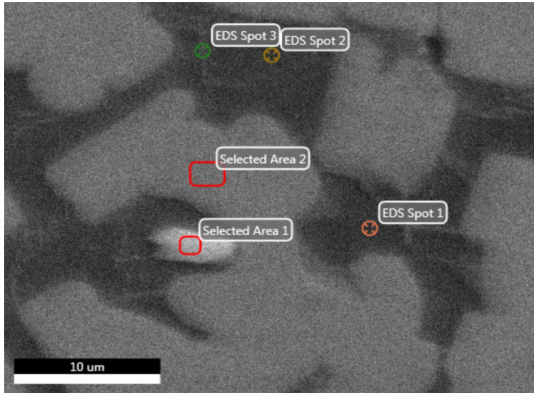
Notes:

EDAX TEAM

Selected Area 1

kV: 20	Mag: 3000	Takeoff: 31.1	Live Time(s): 35.1	Amp Time(µs): 1.92	Resolution:(eV) 127.3

Selected Area 1 - Det 1

Lsec: 35.1   0 Cnts   0.000 keV   Det: Octane Pro A
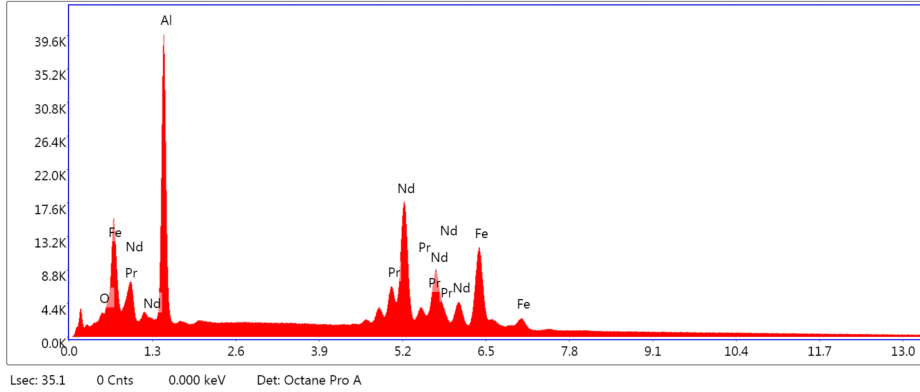
eZAF Smart Quant Results

Element	Weight %	Atomic %	Net Int.	Error %	Kratio	Z	A	F
O K	0.56	2.01	181.59	11.98	0.0027	1.3479	0.3614	1.0000
AlK	27.94	59.45	9442.72	8.34	0.0962	1.2124	0.2832	1.0026
PrL	13.57	5.53	2224.53	2.98	0.1239	0.8744	1.0342	1.0098
NdL	42.13	16.77	6518.72	2.01	0.3789	0.8658	1.0352	1.0035
FeK	15.80	16.24	4326.96	3.00	0.1521	1.0730	0.8909	1.0073

EDAX TEAM

Selected Area 2

| kV: | 20 | Mag: 3000 | Takeoff: 31.1 | Live Time(s): 34.7 | Amp Time(µs): 1.92 | Resolution:(eV) 127.3 |

Selected Area 2 - Det 1

Lsec: 34.7   0 Cnts   0.000 keV   Det: Octane Pro A
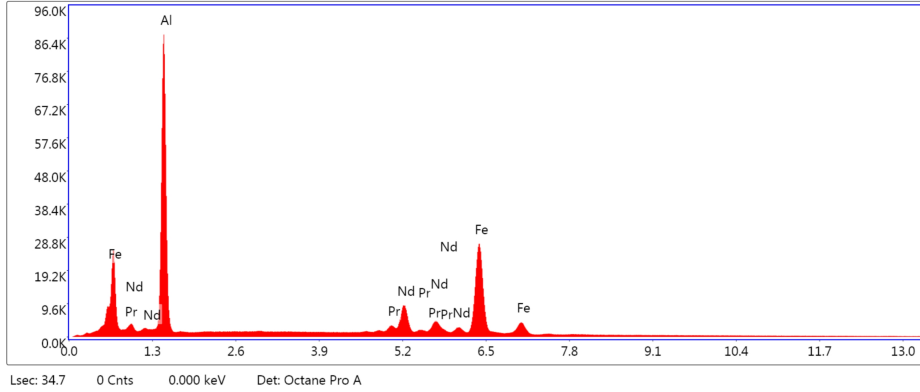
eZAF Smart Quant Results

Element	Weight %	Atomic %	Net Int.	Error %	Kratio	Z	A	F
AlK	41.95	66.48	20677.15	7.25	0.1809	1.1227	0.3833	1.0017
PrL	4.82	1.46	872.05	6.19	0.0417	0.8029	1.0610	1.0155
NdL	18.52	5.49	3169.39	2.65	0.1582	0.7946	1.0620	1.0122
FeK	34.70	26.57	10819.37	2.11	0.3266	0.9833	0.9498	1.0077

XXVIII

EDAX TEAM

EDS Spot 1

kV: 20	Mag: 3000	Takeoff: 31.1	Live Time(s): 34.6	Amp Time(µs): 1.92	Resolution:(eV) 127.3

EDS Spot 1 - Det 1

Lsec: 34.6   0 Cnts   0.000 keV   Det: Octane Pro A
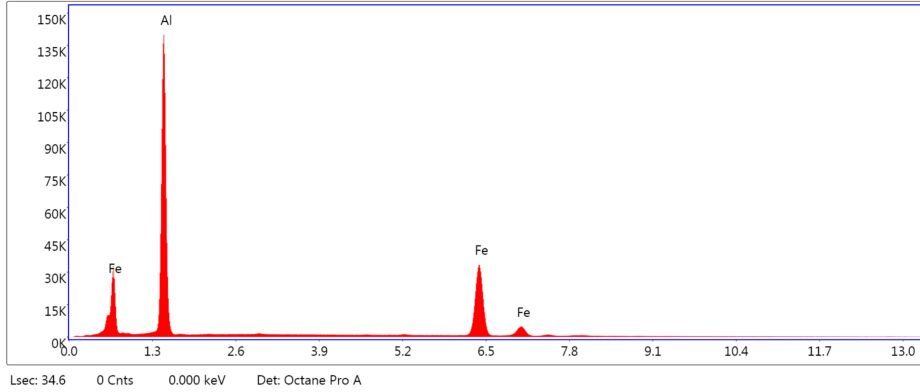
eZAF Smart Quant Results

Element	Weight %	Atomic %	Net Int.	Error %	Kratio	Z	A	F
AlK	54.39	71.17	33342.38	5.93	0.2960	1.0604	0.5128	1.0009
FeK	45.61	28.83	13747.74	1.63	0.4211	0.9209	0.9936	1.0092

EDAX TEAM

EDS Spot 2

| kV: 20 | Mag: 3000 | Takeoff: 31.1 | Live Time(s): 34.6 | Amp Time(µs): 1.92 | Resolution:(eV) 127.3 |

EDS Spot 2 - Det 1

Lsec: 34.6   0 Cnts   0.000 keV   Det: Octane Pro A
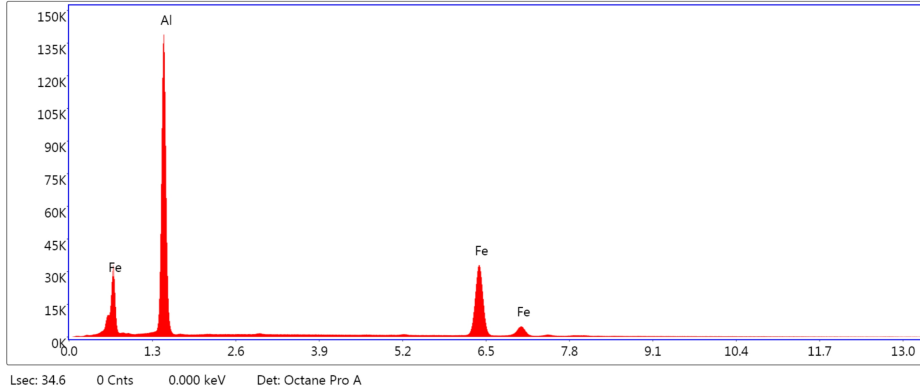
eZAF Smart Quant Results

Element	Weight %	Atomic %	Net Int.	Error %	Kratio	Z	A	F
AlK	54.78	71.49	33077.91	5.91	0.2993	1.0598	0.5152	1.0009
FeK	45.22	28.51	13361.81	1.64	0.4173	0.9204	0.9936	1.0093

XXX

EDAX TEAM

EDS Spot 3

| kV: | 20 | Mag: 3000 | Takeoff: 31.1 | Live Time(s): 34.9 | Amp Time(µs): 1.92 | Resolution:(eV) 127.3 |

EDS Spot 3 - Det 1

Lsec: 34.9   0 Cnts   0.000 keV   Det: Octane Pro A
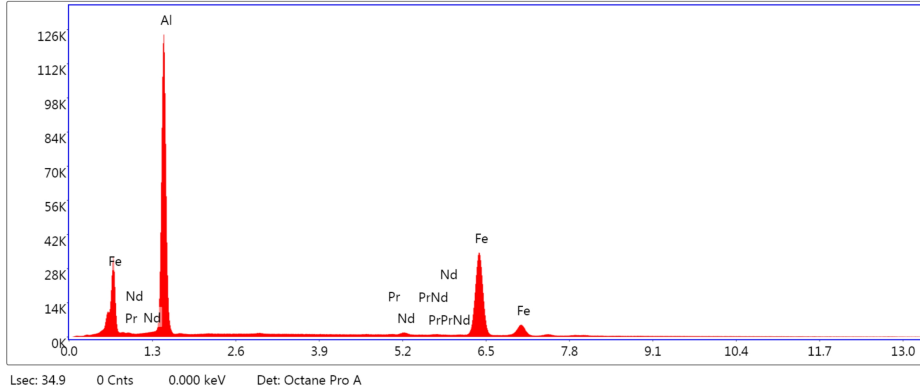
eZAF Smart Quant Results

Element	Weight %	Atomic %	Net Int.	Error %	Kratio	Z	A	F
AlK	50.64	68.75	29298.96	6.25	0.2610	1.0707	0.4810	1.0010
PrL	0.61	0.16	105.13	25.03	0.0051	0.7611	1.0781	1.0226
NdL	2.18	0.55	357.05	12.14	0.0182	0.7530	1.0788	1.0249
FeK	46.56	30.54	14053.45	1.67	0.4321	0.9312	0.9886	1.0083

EDAX TEAM

Eystein

Author: guest
Creation: 04/30/2019 4:01:55 PM

Sample Name: 7 2

Area 1
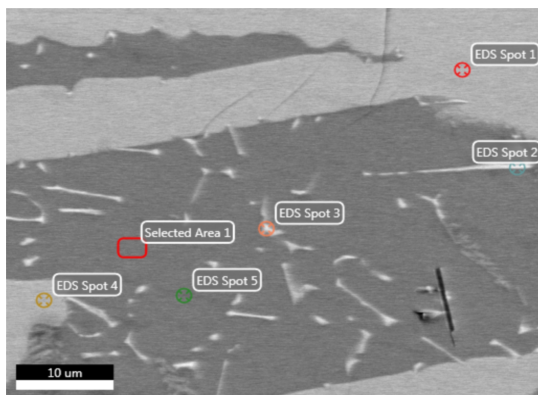
Notes:

EDAX TEAM

EDS Spot 1

| kV: 15 | Mag: 2000 | Takeoff: 31.5 | Live Time(s): 30.6 | Amp Time(µs): 1.92 | Resolution:(eV) 127.3 |

EDS Spot 1 - Det 1

Lsec: 30.6   1.799K Cnts   0.300 keV   Det: Octane Pro A
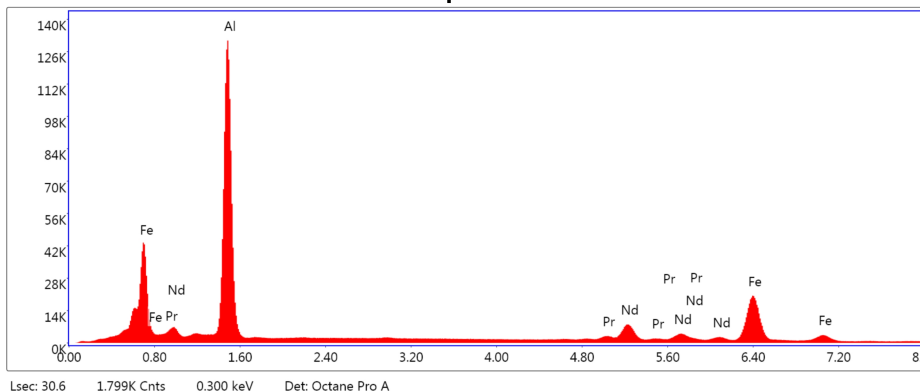
eZAF Smart Quant Results

Element	Weight %	Atomic %	Net Int.	Error %	Kratio	Z	A	F
AlK	40.42	65.25	35092.00	6.34	0.2341	1.1422	0.5061	1.0017
PrL	4.97	1.54	838.95	6.74	0.0409	0.7793	1.0403	1.0147
NdL	19.60	5.92	3055.93	3.31	0.1587	0.7694	1.0406	1.0112
FeK	35.00	27.30	9148.29	2.78	0.3375	0.9866	0.9701	1.0075

XXXIII

EDAX TEAM

EDS Spot 2

kV: 15	Mag: 2000	Takeoff: 31.5	Live Time(s): 32.5	Amp Time(μs): 1.92	Resolution:(eV) 127.3

EDS Spot 2 - Det 1

Lsec: 32.5   1.987K Cnts   0.300 keV   Det: Octane Pro A
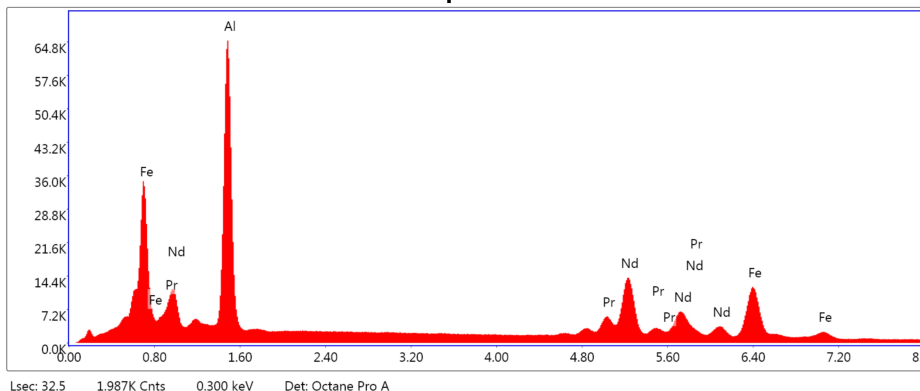
eZAF Smart Quant Results

Element	Weight %	Atomic %	Net Int.	Error %	Kratio	Z	A	F
AlK	26.93	57.46	16606.37	7.41	0.1346	1.2328	0.4046	1.0023
PrL	12.97	5.30	1930.43	4.01	0.1144	0.8504	1.0259	1.0105
NdL	39.14	15.63	5373.16	2.78	0.3392	0.8404	1.0263	1.0046
FeK	20.96	21.61	4772.31	3.34	0.2140	1.0802	0.9386	1.0069

EDAX TEAM

EDS Spot 3

kV: 15	Mag: 2000	Takeoff: 31.5	Live Time(s): 30.6	Amp Time(µs): 1.92	Resolution:(eV) 127.3

EDS Spot 3 - Det 1

Lsec: 30.6   1.472K Cnts   0.300 keV   Det: Octane Pro A
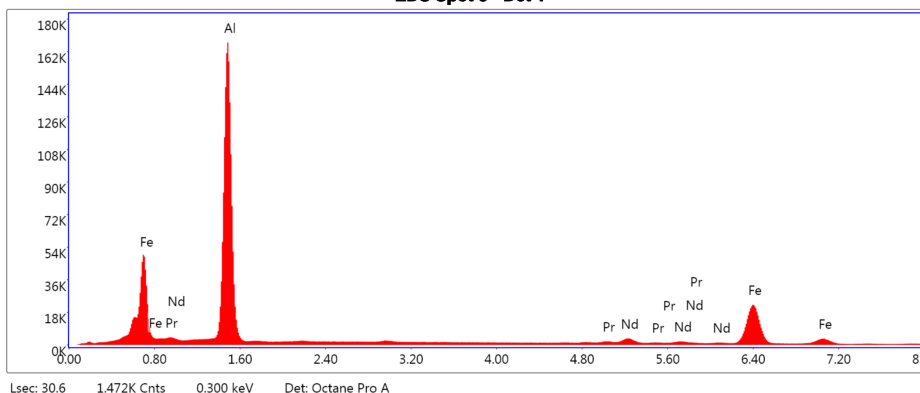
eZAF Smart Quant Results

Element	Weight %	Atomic %	Net Int.	Error %	Kratio	Z	A	F
AlK	48.16	68.91	45042.91	5.65	0.3049	1.1001	0.5746	1.0012
PrL	3.27	0.90	525.37	8.80	0.0260	0.7465	1.0469	1.0172
NdL	7.96	2.13	1185.48	4.89	0.0625	0.7368	1.0470	1.0170
FeK	40.60	28.07	10164.95	2.62	0.3806	0.9438	0.9848	1.0083

EDAX TEAM

EDS Spot 4

kV: 15	Mag: 2000	Takeoff: 31.5	Live Time(s): 30.7	Amp Time(µs): 1.92	Resolution:(eV) 127.3

EDS Spot 4 - Det 1

Lsec: 30.7   1.713K Cnts   0.300 keV   Det: Octane Pro A
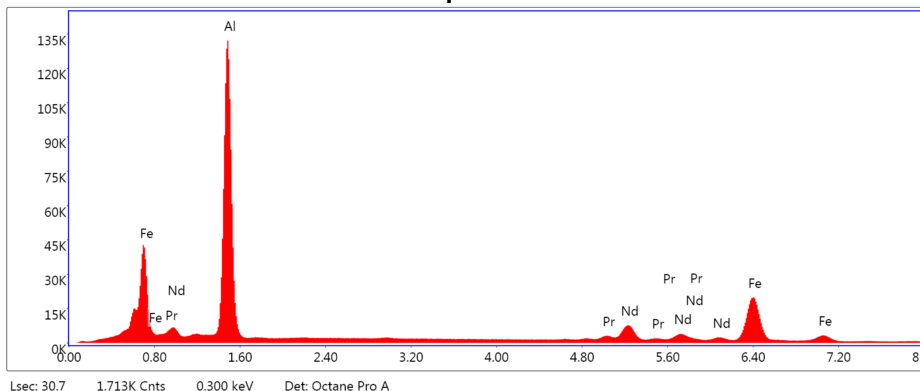
eZAF Smart Quant Results

Element	Weight %	Atomic %	Net Int.	Error %	Kratio	Z	A	F
AlK	40.96	65.78	35168.61	6.32	0.2381	1.1410	0.5085	1.0017
PrL	5.26	1.62	873.88	6.88	0.0432	0.7783	1.0404	1.0145
NdL	19.19	5.76	2943.89	3.40	0.1552	0.7685	1.0406	1.0112
FeK	34.58	26.83	8896.98	2.79	0.3332	0.9854	0.9702	1.0076

EDAX TEAM

EDS Spot 5

| kV: 15 | Mag: 2000 | Takeoff: 31.5 | Live Time(s): 29.7 | Amp Time(μs): 1.92 | Resolution:(eV) 127.3 |

EDS Spot 5 - Det 1

Lsec: 29.7   1.455K Cnts   0.300 keV   Det: Octane Pro A
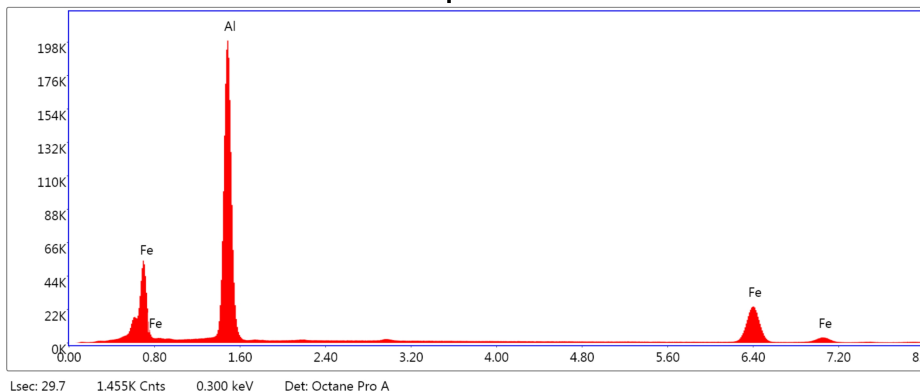
eZAF Smart Quant Results

Element	Weight %	Atomic %	Net Int.	Error %	Kratio	Z	A	F
AlK	54.01	70.86	55305.27	4.99	0.3690	1.0677	0.6393	1.0008
FeK	45.99	29.14	11422.11	2.46	0.4216	0.9112	0.9970	1.0091

EDAX TEAM

Selected Area 1

| kV: 15 | Mag: 2000 | Takeoff: 31.5 | Live Time(s): 29.7 | Amp Time(µs): 1.92 | Resolution:(eV) 127.3 |

Selected Area 1 - Det 1

Lsec: 29.7   1.325K Cnts   0.300 keV   Det: Octane Pro A
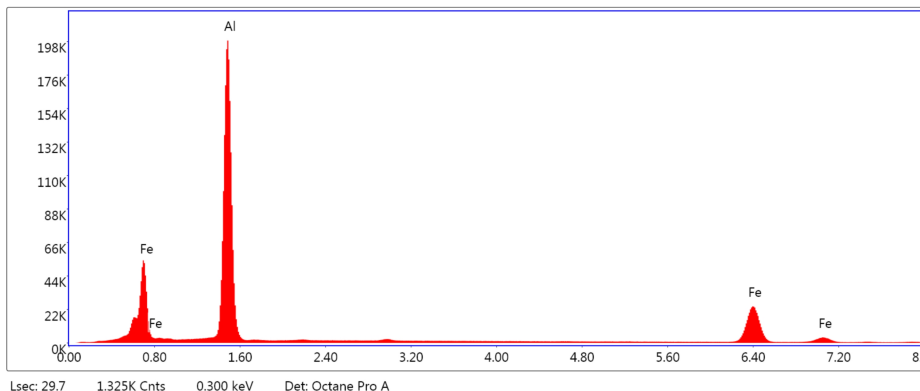
eZAF Smart Quant Results

Element	Weight %	Atomic %	Net Int.	Error %	Kratio	Z	A	F
AlK	53.88	70.75	55144.31	5.00	0.3678	1.0679	0.6386	1.0008
FeK	46.12	29.25	11462.65	2.46	0.4229	0.9114	0.9970	1.0090

XXXVIII

EDAX TEAM

6

Author: guest
Creation: 05/07/2019 10:27:46 AM

Sample Name: 7 3

Area 2
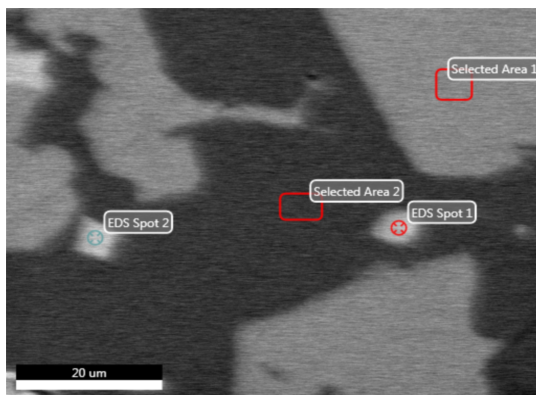
Notes:

EDAX TEAM

EDS Spot 1

| kV: 15 | Mag: 1500 | Takeoff: 33.6 | Live Time(s): 16.3 | Amp Time(μs): 1.92 | Resolution:(eV) 128 |

EDS Spot 1 - Det 1

Lsec: 16.3   0 Cnts   0.000 keV   Det: Apollo X-SDD
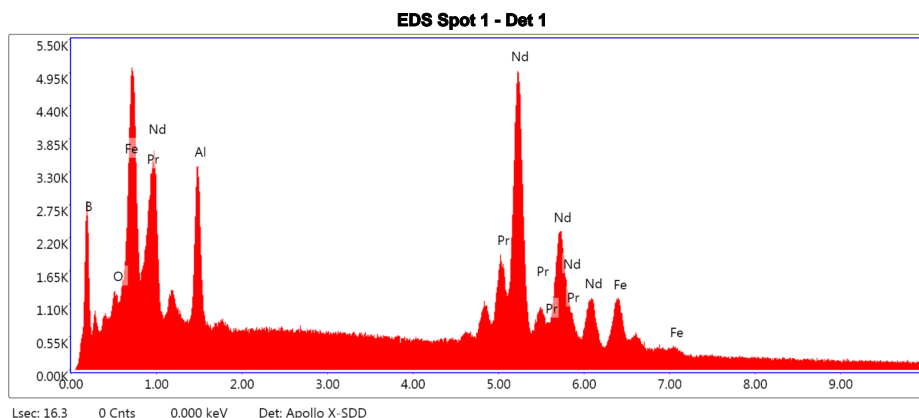
eZAF Smart Quant Results

Element	Weight %	Atomic %	Net Int.	Error %	Kratio	Z	A	F
B K	45.53	85.44	1332.56	6.51	0.2951	1.2015	0.5393	1.0000
O K	3.73	4.73	988.05	9.46	0.0133	1.2092	0.2948	1.0000
AlK	2.95	2.22	1619.56	8.28	0.0131	1.0773	0.4118	1.0031
PrL	10.84	1.56	1437.90	5.61	0.0860	0.7351	1.0700	1.0092
NdL	33.07	4.65	3992.72	3.49	0.2566	0.7257	1.0674	1.0016
FeK	3.88	1.41	737.56	6.34	0.0345	0.9300	0.9479	1.0088

EDAX TEAM

EDS Spot 2

| kV: 15 | Mag: 1500 | Takeoff: 33.6 | Live Time(s): 16.3 | Amp Time(μs): 1.92 | Resolution:(eV) 128 |

EDS Spot 2 - Det 1

Lsec: 16.3   0 Cnts   0.000 keV   Det: Apollo X-SDD
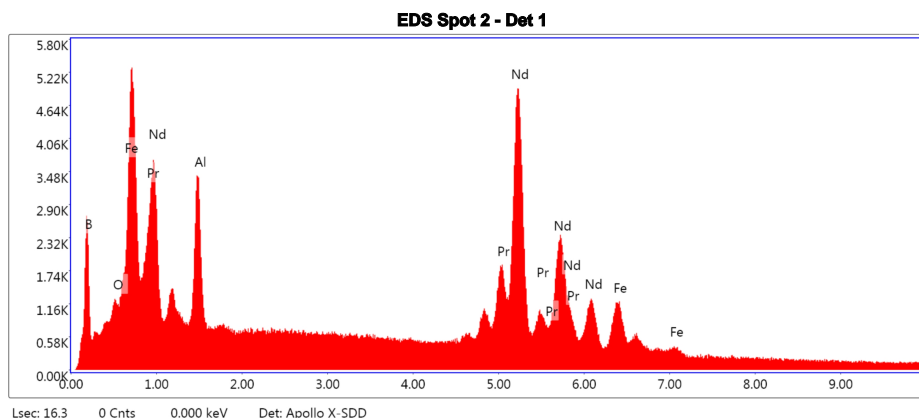
eZAF Smart Quant Results

Element	Weight %	Atomic %	Net Int.	Error %	Kratio	Z	A	F
B K	44.96	85.17	1248.46	6.65	0.2861	1.2041	0.5285	1.0000
O K	3.62	4.63	932.89	9.49	0.0130	1.2119	0.2960	1.0000
AlK	3.15	2.39	1666.93	8.18	0.0140	1.0798	0.4096	1.0031
PrL	10.53	1.53	1352.07	5.91	0.0837	0.7370	1.0694	1.0093
NdL	33.67	4.78	3935.54	3.48	0.2618	0.7275	1.0669	1.0017
FeK	4.07	1.49	748.22	6.25	0.0363	0.9325	0.9472	1.0087

EDAX TEAM

Selected Area 1

| kV: 15 | Mag: 1500 | Takeoff: 33.6 | Live Time(s): 15.6 | Amp Time(µs): 1.92 | Resolution:(eV) 128 |

Selected Area 1 - Det 1

Lsec: 15.6   0 Cnts   0.000 keV   Det: Apollo X-SDD
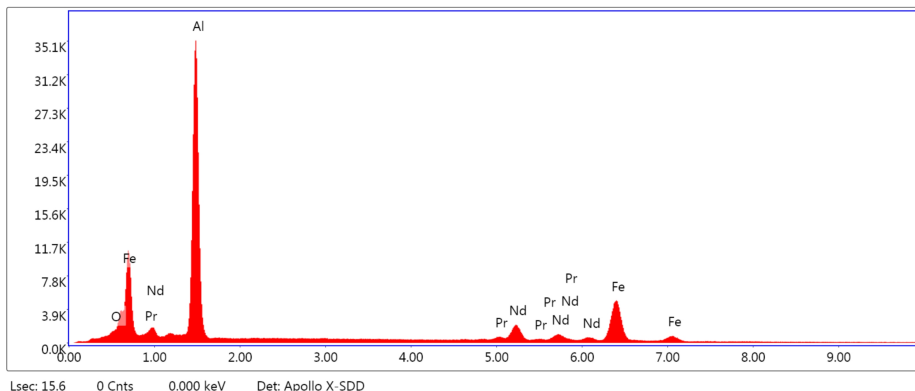
eZAF Smart Quant Results

Element	Weight %	Atomic %	Net Int.	Error %	Kratio	Z	A	F
O K	3.83	9.41	902.95	8.79	0.0176	1.2566	0.3663	1.0000
AlK	42.91	62.49	18575.76	6.95	0.2185	1.1182	0.4547	1.0016
PrL	3.85	1.07	361.88	13.13	0.0314	0.7613	1.0570	1.0144
NdL	17.93	4.89	1543.62	5.04	0.1441	0.7515	1.0573	1.0111
FeK	31.47	22.14	4340.81	3.16	0.2951	0.9632	0.9654	1.0085

EDAX TEAM

Selected Area 2

kV: 15	Mag: 1500	Takeoff: 33.6	Live Time(s): 15.2	Amp Time(µs): 1.92	Resolution:(eV) 128

Selected Area 2 - Det 1

Lsec: 15.2   0 Cnts   0.000 keV   Det: Apollo X-SDD
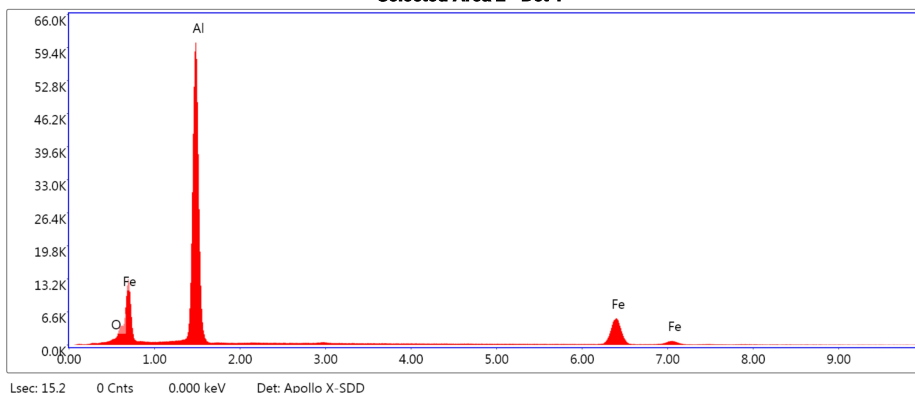
eZAF Smart Quant Results

Element	Weight %	Atomic %	Net Int.	Error %	Kratio	Z	A	F
O K	3.29	6.67	652.77	9.35	0.0128	1.1825	0.3303	1.0000
AlK	59.80	71.90	32674.38	5.27	0.3871	1.0485	0.6169	1.0007
FeK	36.91	21.44	4854.91	2.79	0.3324	0.8929	0.9964	1.0124

XLIII

EDAX TEAM

Eystein

Author: guest
Creation: 04/30/2019 5:05:34 PM

Sample Name: the real 7K

Area 2
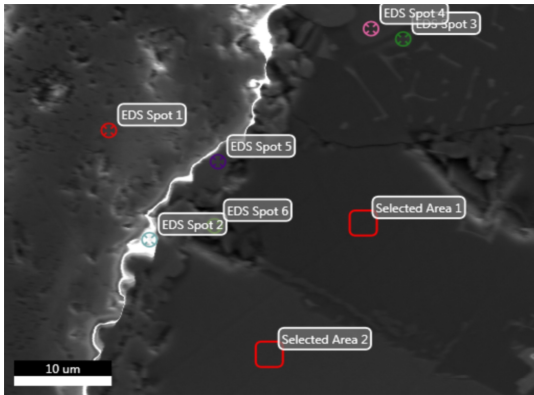
Notes:

EDAX TEAM

EDS Spot 1

kV: 15	Mag: 2000	Takeoff: 31.7	Live Time(s): 31.1	Amp Time(µs): 1.92	Resolution:(eV) 127.3

EDS Spot 1 - Det 1

Lsec: 31.1   3.761K Cnts   0.300 keV   Det: Octane Pro A
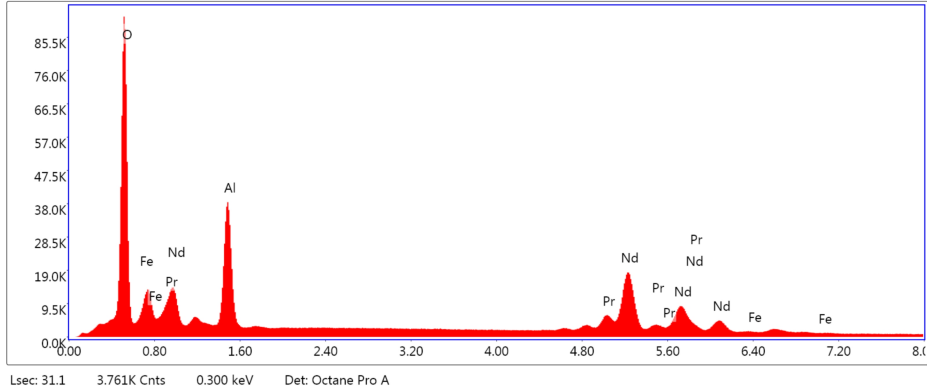
eZAF Smart Quant Results

Element	Weight %	Atomic %	Net Int.	Error %	Kratio	Z	A	F
O K	22.16	58.18	19321.92	6.03	0.1575	1.3385	0.5310	1.0000
AlK	14.89	23.18	9915.82	7.59	0.0703	1.1947	0.3939	1.0027
PrL	13.29	3.96	2189.84	3.95	0.1135	0.8240	1.0284	1.0078
NdL	49.20	14.33	7462.05	2.63	0.4120	0.8143	1.0284	1.0000
FeK	0.46	0.35	116.31	23.39	0.0046	1.0463	0.9325	1.0084

EDAX TEAM

EDS Spot 2

kV: 15	Mag: 2000	Takeoff: 31.7	Live Time(s): 30.8	Amp Time(µs): 1.92	Resolution:(eV) 127.3

EDS Spot 2 - Det 1

Lsec: 30.8   3.652K Cnts   0.300 keV   Det: Octane Pro A
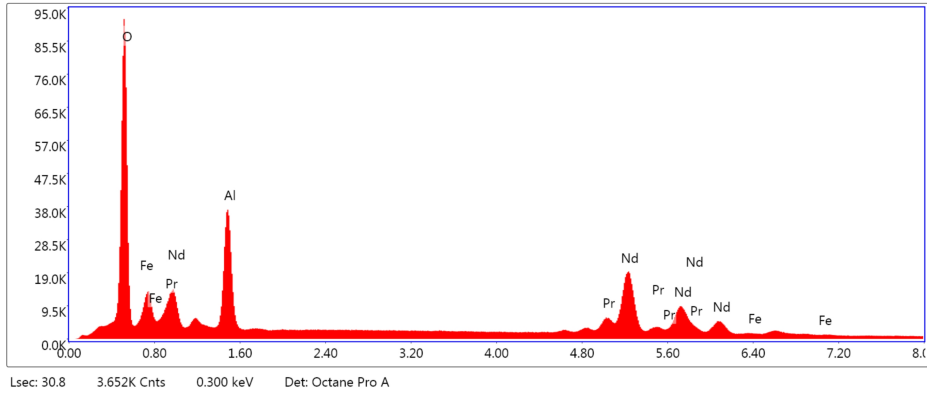
eZAF Smart Quant Results

Element	Weight %	Atomic %	Net Int.	Error %	Kratio	Z	A	F
O K	21.69	57.94	19519.69	6.03	0.1549	1.3440	0.5313	1.0000
AlK	14.35	22.73	9764.38	7.63	0.0673	1.1997	0.3901	1.0028
PrL	12.40	3.76	2109.54	4.00	0.1064	0.8279	1.0278	1.0082
NdL	50.94	15.09	7972.06	2.60	0.4283	0.8181	1.0279	1.0001
FeK	0.61	0.47	158.92	17.15	0.0061	1.0513	0.9314	1.0083

XLVI

EDAX TEAM

Selected Area 1

| kV: 15 | Mag: 2000 | Takeoff: 31.7 | Live Time(s): 29.4 | Amp Time(µs): 1.92 | Resolution:(eV) 127.3 |

Selected Area 1 - Det 1

Lsec: 29.4   1.567K Cnts   0.300 keV   Det: Octane Pro A
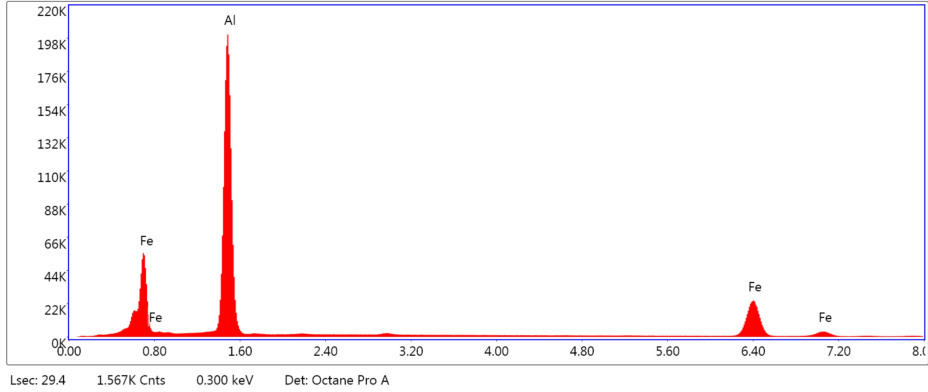
eZAF Smart Quant Results

Element	Weight %	Atomic %	Net Int.	Error %	Kratio	Z	A	F
AlK	53.97	70.82	55929.48	4.98	0.3694	1.0678	0.6403	1.0008
FeK	46.03	29.18	11543.90	2.46	0.4220	0.9112	0.9971	1.0090

XLVII

EDAX TEAM

Selected Area 2

| kV: 15 | Mag: 2000 | Takeoff: 31.7 | Live Time(s): 30.4 | Amp Time(µs): 1.92 | Resolution:(eV) 127.3 |

Selected Area 2 - Det 1

Lsec: 30.4   2.075K Cnts   0.300 keV   Det: Octane Pro A
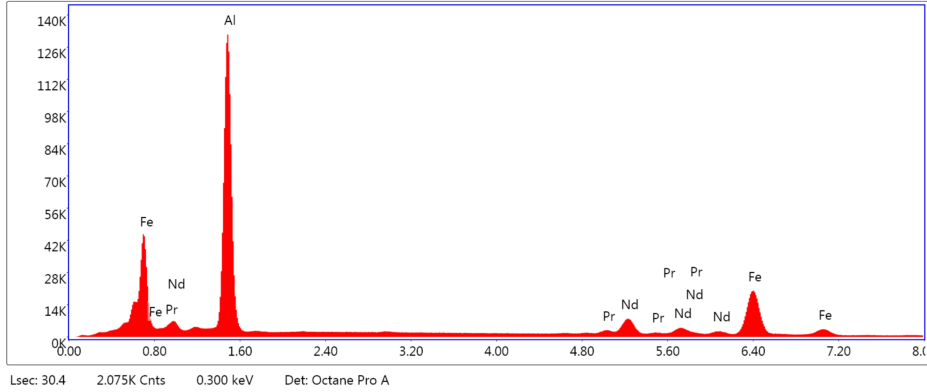
eZAF Smart Quant Results

Element	Weight %	Atomic %	Net Int.	Error %	Kratio	Z	A	F
AlK	40.89	65.59	35674.14	6.30	0.2384	1.1402	0.5105	1.0016
PrL	4.58	1.41	770.19	7.95	0.0376	0.7778	1.0404	1.0149
NdL	19.47	5.84	3022.86	3.37	0.1574	0.7679	1.0407	1.0114
FeK	35.05	27.16	9125.57	2.80	0.3376	0.9846	0.9708	1.0075

EDAX TEAM

EDS Spot 3

kV: 15	Mag: 2000	Takeoff: 31.7	Live Time(s): 29.5	Amp Time(µs): 1.92	Resolution:(eV) 127.3

EDS Spot 3 - Det 1

Lsec: 29.5   1.613K Cnts   0.300 keV   Det: Octane Pro A
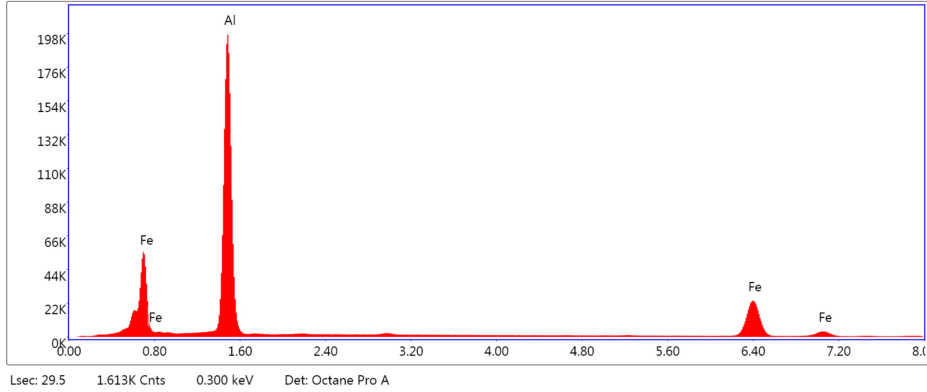
eZAF Smart Quant Results

Element	Weight %	Atomic %	Net Int.	Error %	Kratio	Z	A	F
AlK	53.91	70.77	55085.44	4.99	0.3687	1.0679	0.6400	1.0008
FeK	46.09	29.23	11406.78	2.46	0.4226	0.9113	0.9971	1.0090

EDAX TEAM

EDS Spot 4

| kV: 15 | Mag: 2000 | Takeoff: 31.7 | Live Time(s): 30.9 | Amp Time(µs): 1.92 | Resolution:(eV) 127.3 |

EDS Spot 4 - Det 1

Lsec: 30.9   1.767K Cnts   0.300 keV   Det: Octane Pro A
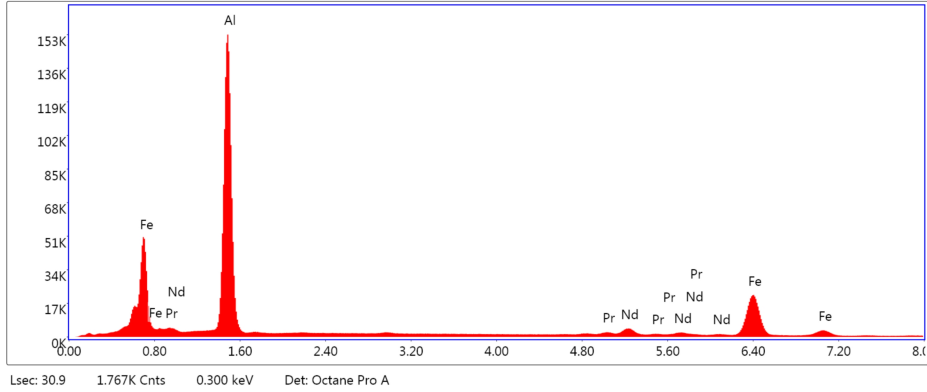
eZAF Smart Quant Results

Element	Weight %	Atomic %	Net Int.	Error %	Kratio	Z	A	F
AlK	46.29	68.08	40942.05	5.81	0.2874	1.1098	0.5586	1.0013
PrL	4.23	1.19	659.67	7.54	0.0339	0.7541	1.0452	1.0163
NdL	10.16	2.79	1467.92	4.57	0.0803	0.7443	1.0452	1.0154
FeK	39.32	27.94	9549.31	2.67	0.3710	0.9537	0.9815	1.0080

L

EDAX TEAM

EDS Spot 5

kV: 15	Mag: 2000	Takeoff: 31.7	Live Time(s): 30.8	Amp Time(µs): 1.92	Resolution:(eV) 127.3

EDS Spot 5 - Det 1

Lsec: 30.8   4.705K Cnts   0.300 keV   Det: Octane Pro A
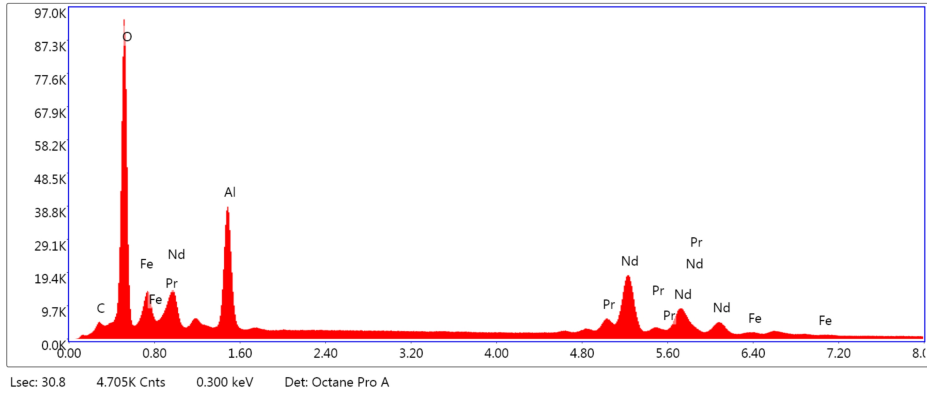
eZAF Smart Quant Results

Element	Weight %	Atomic %	Net Int.	Error %	Kratio	Z	A	F
C K	3.25	10.32	946.35	8.89	0.0147	1.3723	0.3297	1.0000
O K	22.45	53.51	20004.73	6.29	0.1491	1.3142	0.5053	1.0000
AlK	13.89	19.63	10223.22	7.48	0.0662	1.1729	0.4054	1.0027
PrL	11.56	3.13	2050.74	4.08	0.0971	0.8076	1.0319	1.0083
NdL	47.66	12.60	7776.76	2.64	0.3924	0.7979	1.0317	1.0002
FeK	1.19	0.81	320.69	10.07	0.0115	1.0248	0.9373	1.0085

EDAX TEAM

EDS Spot 6

| kV: 15 | Mag: 2000 | Takeoff: 31.7 | Live Time(s): 30.1 | Amp Time(µs): 1.92 | Resolution:(eV) 127.3 |

EDS Spot 6 - Det 1

Lsec: 30.1   2.028K Cnts   0.300 keV   Det: Octane Pro A
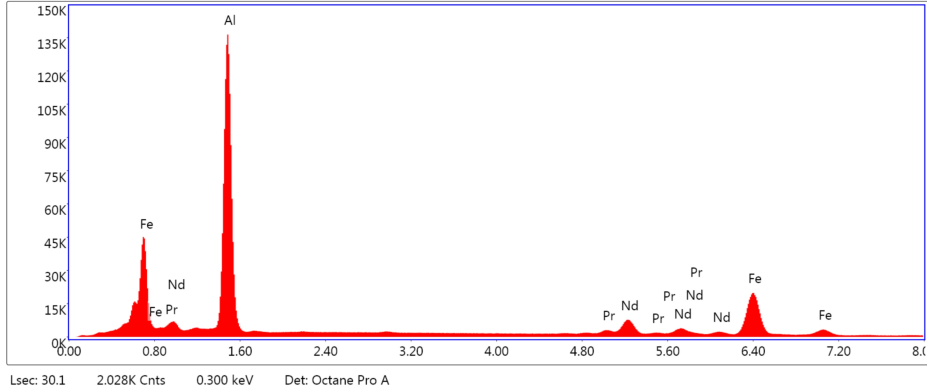
eZAF Smart Quant Results

Element	Weight %	Atomic %	Net Int.	Error %	Kratio	Z	A	F
AlK	41.76	66.48	36997.93	6.26	0.2449	1.1385	0.5142	1.0016
PrL	5.11	1.56	865.00	7.11	0.0419	0.7764	1.0403	1.0145
NdL	18.86	5.62	2950.68	3.41	0.1522	0.7666	1.0406	1.0112
FeK	34.27	26.35	8993.19	2.79	0.3295	0.9829	0.9709	1.0077

EDAX TEAM

Eystein

Author: guest
Creation: 04/30/2019 2:59:31 PM

Sample Name: 8K

Area 2
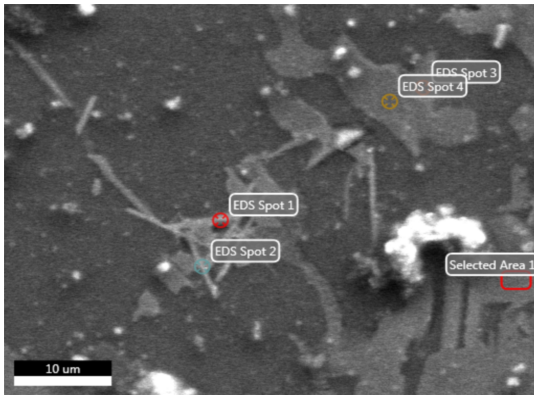
Notes:

EDAX TEAM

EDS Spot 1

kV: 15	Mag: 2000	Takeoff: 31.5	Live Time(s): 47.4	Amp Time(μs): 1.92	Resolution:(eV) 127.3

EDS Spot 1 - Det 1

Lsec: 47.4   1.267K Cnts   0.300 keV   Det: Octane Pro A
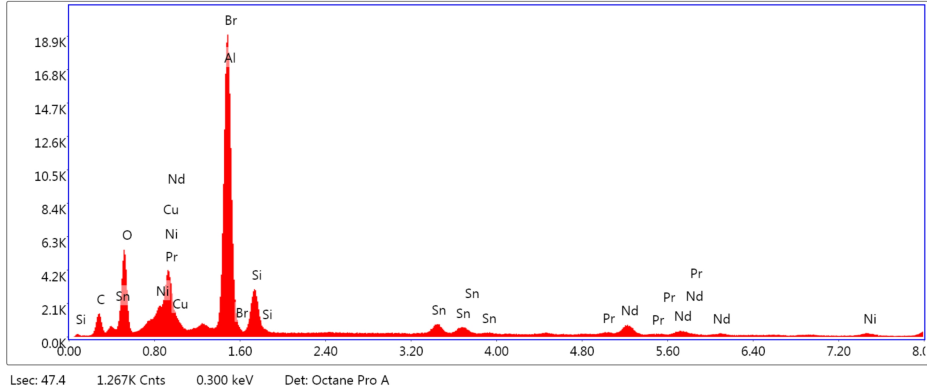
eZAF Smart Quant Results

Element	Weight %	Atomic %	Net Int.	Error %	Kratio	Z	A	F
C K	11.45	29.33	145.95	11.35	0.0225	1.2741	0.1542	1.0000
O K	13.56	26.07	672.66	8.83	0.0496	1.2194	0.3000	1.0000
BrL	19.60	7.55	1084.83	4.53	0.1246	0.8513	0.7467	0.9999
AlK	17.56	20.03	1757.05	5.83	0.1124	1.0854	0.5888	1.0014
SiK	5.90	6.47	496.00	7.38	0.0331	1.1094	0.5047	1.0019
SnL	5.08	1.32	150.01	6.53	0.0395	0.7773	0.9975	1.0041
PrL	3.17	0.69	52.16	16.49	0.0244	0.7392	1.0346	1.0067
NdL	11.24	2.40	171.45	6.74	0.0854	0.7297	1.0358	1.0051
NiK	2.92	1.53	54.30	12.04	0.0284	0.9426	0.9822	1.0507
CuK	9.52	4.61	131.34	6.43	0.0878	0.8935	0.9871	1.0460

EDAX TEAM

EDS Spot 2

| kV: 15 | Mag: 2000 | Takeoff: 31.5 | Live Time(s): 47.9 | Amp Time(µs): 1.92 | Resolution:(eV) 127.3 |

EDS Spot 2 - Det 1

Lsec: 47.9   1.074K Cnts   0.300 keV   Det: Octane Pro A
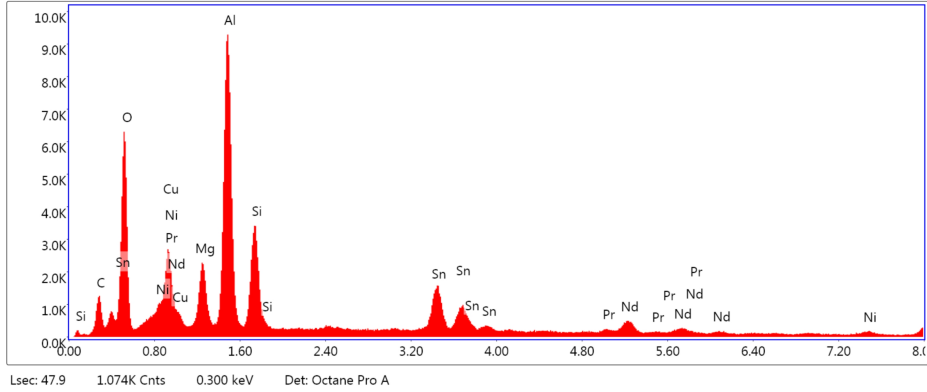
eZAF Smart Quant Results

Element	Weight %	Atomic %	Net Int.	Error %	Kratio	Z	A	F
C K	9.17	21.52	109.92	11.67	0.0216	1.2393	0.1901	1.0000
O K	17.11	30.15	785.82	8.15	0.0739	1.1855	0.3643	1.0000
MgK	5.01	5.81	321.77	7.77	0.0257	1.0945	0.4678	1.0021
AlK	21.94	22.93	1572.77	6.22	0.1283	1.0539	0.5535	1.0024
SiK	7.95	7.98	565.78	6.71	0.0482	1.0770	0.5604	1.0035
SnL	14.26	3.39	327.60	4.30	0.1100	0.7534	1.0216	1.0029
PrL	2.22	0.44	27.53	28.67	0.0164	0.7153	1.0281	1.0043
NdL	8.96	1.75	102.95	11.66	0.0654	0.7060	1.0301	1.0036
NiK	2.63	1.26	36.86	16.27	0.0246	0.9102	0.9832	1.0448
CuK	10.75	4.77	111.22	6.82	0.0948	0.8621	0.9881	1.0357

EDAX TEAM

EDS Spot 3

| kV: 15 | Mag: 2000 | Takeoff: 31.5 | Live Time(s): 47.4 | Amp Time(µs): 1.92 | Resolution:(eV) 127.3 |

EDS Spot 3 - Det 1

Lsec: 47.4   846 Cnts   0.300 keV   Det: Octane Pro A
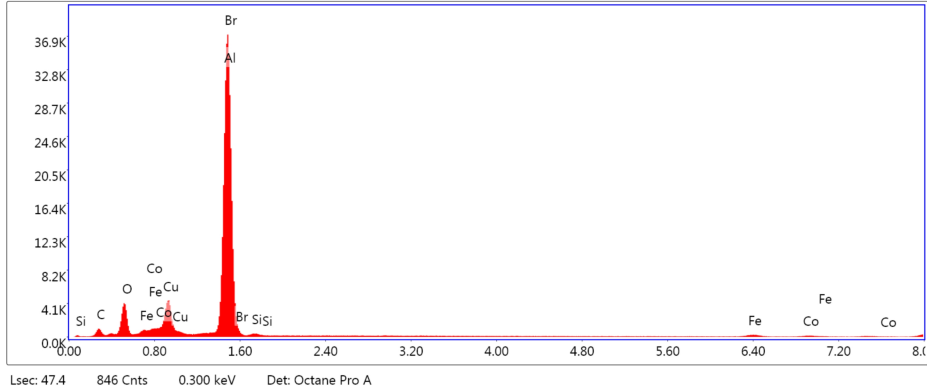
eZAF Smart Quant Results

Element	Weight %	Atomic %	Net Int.	Error %	Kratio	Z	A	F
C K	10.12	23.00	87.60	12.59	0.0144	1.2190	0.1168	1.0000
O K	12.46	21.27	525.80	9.04	0.0414	1.1650	0.2850	1.0000
BrL	20.63	7.05	1262.01	2.55	0.1547	0.8107	0.9251	0.9997
AlK	40.70	41.19	4543.34	4.17	0.3101	1.0337	0.7369	1.0005
SiK	0.68	0.66	49.09	13.28	0.0035	1.0560	0.4871	1.0007
FeK	2.48	1.21	62.98	9.61	0.0238	0.8818	0.9954	1.0934
CoK	1.54	0.71	32.24	10.19	0.0147	0.8597	0.9983	1.1162
CuK	11.40	4.90	143.28	5.78	0.1022	0.8387	0.9997	1.0696

EDAX TEAM

EDS Spot 4

| kV: 15 | Mag: 2000 | Takeoff: 31.5 | Live Time(s): 47.7 | Amp Time(µs): 1.92 | Resolution:(eV) 127.3 |

EDS Spot 4 - Det 1

Lsec: 47.7   1.309K Cnts   0.300 keV   Det: Octane Pro A
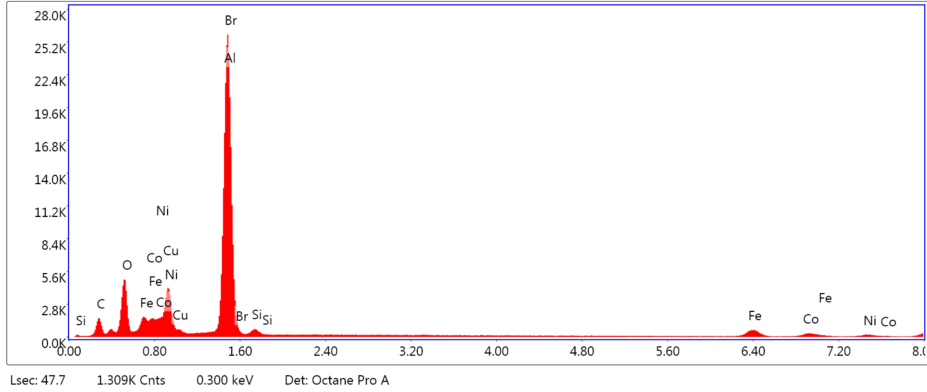
eZAF Smart Quant Results

Element	Weight %	Atomic %	Net Int.	Error %	Kratio	Z	A	F
C K	15.51	32.40	160.23	11.39	0.0261	1.1969	0.1408	1.0000
O K	14.81	23.21	642.07	8.86	0.0501	1.1436	0.2960	1.0000
BrL	13.86	4.35	780.69	3.47	0.0949	0.7954	0.8612	0.9996
AlK	31.65	29.43	3241.53	4.77	0.2196	1.0142	0.6835	1.0007
SiK	1.06	0.95	82.65	11.10	0.0058	1.0360	0.5304	1.0010
FeK	6.39	2.87	159.70	5.00	0.0598	0.8642	0.9990	1.0848
CoK	3.61	1.54	73.09	8.56	0.0331	0.8424	1.0007	1.0898
NiK	2.74	1.17	45.97	11.98	0.0254	0.8682	0.9978	1.0721
CuK	10.36	4.09	125.89	5.95	0.0891	0.8214	0.9975	1.0496

EDAX TEAM

Selected Area 1

kV:	15	Mag: 2000	Takeoff: 31.5	Live Time(s): 47.7	Amp Time(µs): 1.92	Resolution:(eV) 127.3

Selected Area 1 - Det 1

Lsec: 47.7   1.835K Cnts   0.300 keV   Det: Octane Pro A
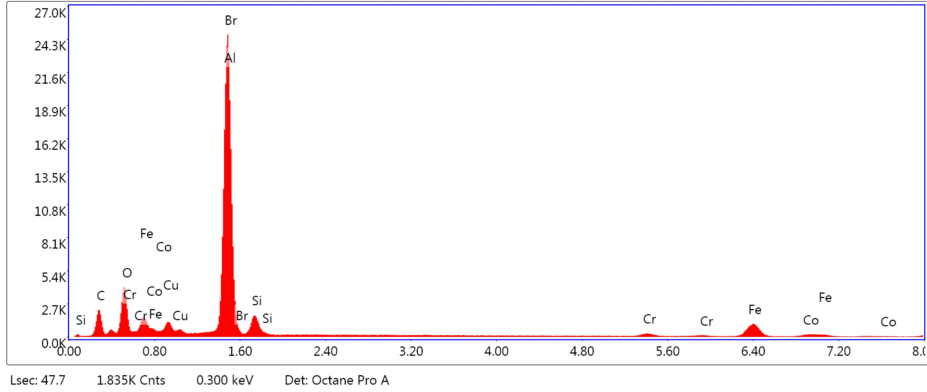
eZAF Smart Quant Results

Element	Weight %	Atomic %	Net Int.	Error %	Kratio	Z	A	F
C K	22.09	42.13	233.42	11.06	0.0387	1.1724	0.1492	1.0000
O K	12.33	17.65	481.49	9.44	0.0382	1.1195	0.2765	1.0000
BrL	10.95	3.14	633.50	3.04	0.0782	0.7779	0.9183	0.9998
AlK	30.72	26.08	3233.82	4.31	0.2223	0.9919	0.7290	1.0009
SiK	3.41	2.78	274.91	7.33	0.0197	1.0130	0.5702	1.0012
CrK	1.64	0.72	55.56	7.86	0.0150	0.8513	0.9935	1.0818
FeK	12.81	5.25	296.85	3.86	0.1129	0.8433	0.9993	1.0459
CoK	2.45	0.95	46.05	9.51	0.0212	0.8217	1.0004	1.0543
CuK	3.61	1.30	42.35	11.69	0.0304	0.8006	0.9951	1.0595

Recycling of waste electrical and electronic equipment, a path to a sustainable future

Eystein Vada and Eskil Christensen

Abstract— **WEEE is the fastest growing wast stream in the world, making it one of the dawning problem along with today's problem with global warming and micro plastic. Existing recycling processes are not good enough to handle the increasing use of REEs in WEEE and there is a need for better processes.**

INTRODUCTION

Have you ever wondered where your old phones, computers, microwave, TV and fridge end up after you have tossed it away? Have you ever heard the term e-waste or WEEE (Waste Electric and Electronic Equipment)? Maybe you haven't, but you will soon. As micro plastic and global warming is recognized as one of the biggest problems in the 21st century, WEEE is one of the dawning problems. As of today WEEE is the fastest growing waste stream in the world and there is no sign that the amount of WEEE will decrease, rather the opposite. In 2016, the world generated a shockingly 44.7 million tons of WEEE [1]! This is equivalent to 223 500 fully grown blue whales (that's about 10 times higher than the actual world population), 124,7 empire state buildings or 5.8 kg/person. Even worse, it's suspected that this number in reality is much higher.

> ### Rare earth elements
>
> Rare Earth Elements, or REEs, are a group of elements defined as the fifteen lanthanides (Lanthanum, Cerium, Praseodymium, Neodymium, Promethium, Samarium, Europium, Gadolinium, Terbium, Dysprosium, Holmium, Erbium, Thulium, Ytterbium, Lutetium), Yttrium and Scandium.

WHAT IS EEE AND WEEE?

What is defined as electrical and electronic equipment (EEE)? well, the EU defines EEE as; " *electrical and electronic equipment ,or EEE means equipment which is dependent on electric currents or electromagnetic fields in order to work properly and equipment for the generation, transfer and measurement of such currents and fields and designed for use with a voltage rating not exceeding 1 000 volts for alternating current and 1 500 volts for direct current*" and waste is defined as; "*waste means any substance or object which the holder discards or intends or is required to discard*" So, WEEE is basically defined as everything that uses electricity that you don't want.

THE USE OF RARE EARTH ELEMENTS IN EEE

As the demand for faster, better and yet smaller electronics grows the use of Rare Earth Elements (REEs) increases. REEs have the certain unique abilities that makes them vital in today's EEE [4].

Yttrium, terbium, europium are essential in televisions, computer screens or other devices which has a display. Praseodymium is used to create strong alloys used in aircraft engines. Gadolinium is used in X-rays and MRI scanning systems. Neodymium, which is the most used REE, is primarily used in permanent magnets. These magnets are used in loudspeakers, electric motors, hard drives, wind turbines, electric car motors and many more [5]. Scientist's have not yet found a way to replace the REEs with more easily obtainable materials, so until then, REEs play a role in the technology around us.

> ### REEs are not that rare
>
> The rarest rare earth, thulium, with atomic number 69, is 125 times more common than gold. And the least-rare rare earth, cerium, with atomic number 58, is 15,000 times more abundant than gold. The name comes from it's tendency to not be highly concentrated in a few local deposits, but rather finely dispersed in the earth's crust.

ENVIRONMENTAL IMPACT OF WEEE

WEEE is considered as hazardous waste and can, at worst, pose serious threats to life nearby. In many countries, laws are in place that ensure the proper handling of WEEE. However, in some countries WEEE is mostly handled informally, meaning that the waste is stripped of it's most valuable components (copper wire and gold containing components), leaving hazardous materials in the environment. These materials can pollute ground water and acidify the soil. To make matters worse, for liberation of the valuable materials from WEEE, a common practice is to burn off the polymers found in casings, printed circuit boards and insulation. In turn, dangerous fumes, such as brominated flame retardants, dioxins and mercury, are released into the air. This creates major hazards for people living around places where informal WEEE recycling takes place [3].

THE UMICORE PROCESS

So what happens with your your old smartphone, television and washing machine? Well, that depends if you live in a country which reuses components or recover metals from
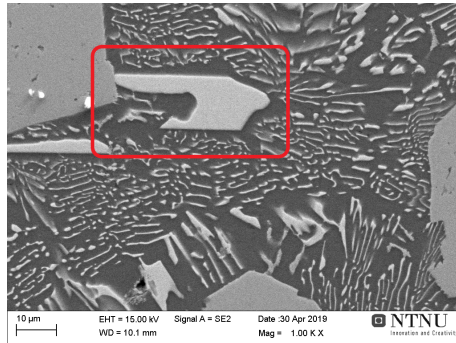
Fig. 1.   Electron microscopy image of neodymium-rich phase

the WEEE. Umicore, a global materials technology company, have developed a process for the recycling of WEEE. Through a series of furnaces and chemical treatments, the Umicore process manages to recover Cu, Au, Ag, Pt, Pd, Rh, Ru, Ir, In, Se, Te, Pb, Sn, Sb and Bi. Waist from the Umicore process, containing REEs, are used ends up as filler concrete.

RECYCLING OF REE

Although there are processes to recycle REEs, its estimated that <1% of REEs used are recycled [2]. There are several reasons why the recycling rates of REEs are so low:

- The low concentration of REEs in products making it ineffective to recycle.
- The wide variation of applications containing REEs
- The difficulty in separating individual REEs

There is also the the question of money. Is the recycling of REEs really worth it economically? As it stands today the processes today are to expensive to make the recovery of REEs an option.

RECYCLING OF WEEE WITH ALUMINIUM

Our bachelor thesis is the start of research around the possibility to utilize aluminium the same way the Umicore process uses copper. Aluminium is a cheaper metal than copper and the required temperature to melt aluminium is lower than for copper, making the process less energy demanding. We have been looking into the recovery of neodymium from magnets and smartphones, by submerging magnets and smartphones in molten aluminium, this is shown in figure 2. It's possible to achieve a phase that has a higher concentration of neodymium than the starting concentration, this is shown in figure 1.

The next step will be to see if its possible to separate out this phase and further up-concentrate it. This is a small but important step towards the recycling of WEEE and a sustainable future where the recycling of metals will be more important than ever before.

Fig. 2.   Photo of an experiment with smartphones in liquid aluminium

REFERENCES

[1] C. P Balde et al. "Quantities, Flows and Resources". In: *The Global E-waste Monitor 2017* (2017). ISSN: 2522-7033. URL: https://www.itu.int/en/ITU-D/Climate-Change/Documents/GEM%5C%202017/Global-E-waste%5C%20Monitor%5C%202017%5C%20.pdf.

[2] Simon M Jowitt et al. "Recycling of the rare earth elements". In: *Current Opinion in Green and Sustainable Chemistry* 13 (2018), pp. 1–7.

[3] Francis O Ongondo, Ian D Williams, and Tom J Cherrett. "How are WEEE doing? A global review of the management of electrical and electronic wastes". In: *Waste management* 31.4 (2011), pp. 714–730.

[4] Bradley S Van Gosen et al. *The rare-earth elements: vital to modern technologies and lifestyles.* Tech. rep. US Geological Survey, 2014.

[5] *What are 'rare earths' used for?*